

Mutant-selective AKT inhibition through lysine targeting and neo-zinc chelation

<https://doi.org/10.1038/s41586-024-08176-4>

Received: 17 November 2023

Accepted: 8 October 2024

Published online: 6 November 2024

 Check for updates

Gregory B. Craven¹, Hang Chu², Jessica D. Sun², Jordan D. Carelli², Brittany Coyne², Hao Chen¹, Ying Chen¹, Xiaolei Ma², Subhamoy Das², Wayne Kong², Adam D. Zajdlik², Kin S. Yang², Solomon H. Reisberg², Peter A. Thompson², J. Russell Lipford² & Jack Taunton¹✉

Somatic alterations in the oncogenic kinase AKT1 have been identified in a broad spectrum of solid tumours. The most common AKT1 alteration replaces Glu17 with Lys (E17K) in the regulatory pleckstrin homology domain¹, resulting in constitutive membrane localization and activation of oncogenic signalling. In clinical studies, pan-AKT inhibitors have been found to cause dose-limiting hyperglycaemia^{2–6}, which has motivated the search for mutant-selective inhibitors. We exploited the E17K mutation to design allosteric, lysine-targeted salicylaldehyde inhibitors with selectivity for AKT1 (E17K) over wild-type AKT paralogues, a major challenge given the presence of three conserved lysines near the allosteric site. Crystallographic analysis of the covalent inhibitor complex unexpectedly revealed an adventitious tetrahedral zinc ion that coordinates two proximal cysteines in the kinase activation loop while simultaneously engaging the E17K-imine conjugate. The salicylaldimine complex with AKT1 (E17K), but not that with wild-type AKT1, recruits endogenous Zn²⁺ in cells, resulting in sustained inhibition. A salicylaldehyde-based inhibitor was efficacious in AKT1 (E17K) tumour xenograft models at doses that did not induce hyperglycaemia. Our study demonstrates the potential to achieve exquisite residence-time-based selectivity for AKT1 (E17K) by targeting the mutant lysine together with Zn²⁺ chelation by the resulting salicylaldimine adduct.

AKT1 occupies a central node in the PI3K–AKT–mTOR signalling pathway, which drives cell proliferation and survival. In unstimulated cells, AKT1 localizes to the cytoplasm in an autoinhibited state owing to an interaction between its pleckstrin homology and kinase domains⁷. Upstream activation of PI3K generates phosphatidylinositol-(3,4,5)-trisphosphate (PIP₃), which serves as the primary ligand for the pleckstrin homology domain, relieving kinase autoinhibition while recruiting AKT1 to the plasma membrane⁸. Subsequent phosphorylation of AKT1 at Thr308 and Ser473 further activates the kinase domain and downstream signalling. This pathway is frequently upregulated in cancer by somatic genetic alterations and is an important target of current drug discovery efforts⁹. The most common oncogenic AKT1 alteration is Glu17 to Lys (E17K)¹. Inversion of the electrostatic charge at this position leads to increased binding affinity for phosphatidylinositol-(4,5)-bisphosphate (PIP₂), a relatively abundant membrane phospholipid, thereby stimulating pathological hyperactivation of AKT1 (E17K)^{10,11}. The somatic AKT1 E17K mutation occurs in cancers of the breast (6–8%)^{1,12}, endometrium (4%)¹³ and meninges (12–31%)^{14,15} and in other solid tumours at lower frequencies (<2%). In addition, AKT1 (E17K) mutations have emerged as a secondary resistance mechanism in breast cancer patients treated with PI3Kα inhibitors¹⁶. Although ubiquitous heterozygous expression of AKT1 (E17K) is embryonically lethal¹⁷, somatic mosaic mutations can give rise to progressive tissue overgrowth disorder Proteus syndrome¹⁸.

Clinical-stage AKT inhibitors bind to either the kinase active site or an allosteric pocket formed at the interface of the kinase and pleckstrin homology domains. Within the AKT family (AKT1, AKT2, AKT3), these binding sites are nearly identical. Consequently, few parologue-selective AKT inhibitors have been reported. An orthosteric pan-AKT inhibitor, capivasertib, was recently approved in combination with fulvestrant for metastatic hormone-receptor-positive breast cancer¹⁹. Moreover, both capivasertib and ipatasertib have shown modest efficacy in small-cohort studies of patients harbouring AKT1 (E17K)-mutant tumours^{2–5}. Despite these advances, hyperglycaemia has been a dose-limiting toxicity of all pan-AKT inhibitors tested so far. This side effect has been attributed to AKT2 inhibition on the basis of genetic evidence from mice and humans^{20–22}. By contrast, AKT1 is genetically dispensable with respect to glucose homeostasis^{23–25}. Hyperglycaemia and other side effects have necessitated dose reductions of capivasertib⁶, potentially resulting in suboptimal levels of AKT1 (E17K) inhibition. Accordingly, there is an unmet need for AKT1 (E17K)-targeted drugs that minimally affect AKT2. Although covalent mutant-allele-specific inhibitors have been developed for KRAS (G12C)^{26–28}, this strategy has not been applied to any oncogenic lysine mutant to our knowledge. Here, we use structure-based design to develop reversible salicylaldehyde inhibitors that covalently engage the mutant lysine of AKT1 (E17K). These inhibitors form an E17K-dependent zinc chelate, which results in prolonged target engagement in cells

¹Department of Cellular and Molecular Pharmacology, University of California, San Francisco, San Francisco, CA, USA. ²Terremoto Biosciences, San Francisco, CA, USA.
✉e-mail: jack.taunton@ucsf.edu

and unprecedented residence-time-based selectivity over wild-type (WT) AKT paralogues.

The E17K mutation resides within the highly charged phosphoinositide binding groove of the pleckstrin homology domain, which is remote from the kinase ATP binding site. By modelling the E17K mutation into the crystal structure of AKT1 in complex with the clinical allosteric inhibitor ARQ092 (ref. 29), we observed that the mutant lysine could extend to within approximately 8 Å of the bound inhibitor (Fig. 1a). This suggested the possibility of trapping the ε-amine of Lys17 with an electrophilic salicylaldehyde linked to a scaffold that occupies the allosteric pocket. However, we noted three further lysines (Lys179, Lys276 and Lys297) within 7–10 Å of the allosteric pocket. Collectively, these lysines pose a major selectivity challenge, as they are conserved in all three AKT paralogues (AKT1, AKT2, AKT3) and could potentially form a covalent adduct with a salicylaldehyde-based inhibitor. Moreover, allosteric AKT inhibitors generally bind with lower affinity to AKT1 (E17K) than to WT AKT1 (sixfold lower in the case of ARQ092: AKT1 (WT), $K_d = 8.6$ nM; AKT1 (E17K), $K_d = 42$ nM)³⁰, which further compounds the challenge of achieving selectivity for the E17K mutant.

Guided by computational modelling, we functionalized the imidazopyridine core found in ARQ092 with different linkers to a salicylaldehyde, generating compounds **1–3** (Fig. 1b). We treated purified recombinant AKT1 (E17K or WT; 1 μM) with a fixed concentration of each compound (5 μM, 15 min) and quantified covalent adduct formation after brief exposure to NaBH₄, which converts reversible imines to stable amines suitable for analysis by intact-protein mass spectrometry (Fig. 1c). Treatment with benzamide-linked salicylaldehyde **1** produced an equilibrium mixture of 89% covalently modified and 11% unmodified AKT1 (E17K). WT AKT1 was also covalently modified under these conditions, albeit to a lesser extent (41% modification at equilibrium). Preformed covalent complexes of salicylaldehyde **1** bound to either E17K or WT AKT1 rapidly dissociated (dissociation half-time ($t_{1/2}$) < 5 min) after the addition of a tenfold molar excess of ARQ092, confirming the specificity of the interaction but also implying a suboptimal covalent binding geometry (Fig. 1d). Extending the linker by one methylene unit (compound **2**) markedly increased the residence time for AKT1 (E17K) relative to AKT1 (WT) ($t_{1/2} = 71$ min and 6.8 min, respectively) and increased the extent of covalent modification to 100% (Fig. 1c,d).

Replacing the amide linker with a secondary amine to give compound **3** further increased the dissociation half-time for AKT1 (E17K), resulting in a residence-time-based E17K/WT selectivity ratio of 11.4 (Fig. 1d). Differential scanning fluorimetry (DSF) measurements in the presence of compound **3** revealed enhanced thermal stabilization of AKT1 (E17K) relative to WT AKT1. By contrast, ARQ092 preferentially stabilized WT AKT1 (Fig. 1e). Compound **3** showed even greater selectivity for AKT1 (E17K) over AKT2 in terms of both residence time and thermal stabilization (Extended Data Fig. 1a–c). This selectivity trend was further corroborated by biochemical kinase assays, in which compound **3** inhibited AKT1 (E17K) (half-maximal inhibitory concentration = 0.6 nM; 10 μM ATP) with 28-fold and 103-fold selectivity over AKT1 (WT) and AKT2 (WT), respectively (Extended Data Fig. 1d).

Liquid chromatography and tandem mass spectrometry (LC–MS/MS) analysis of tryptic peptides derived from the NaBH₄-reduced complex of AKT1 (E17K) and compound **3** confirmed that Lys17 is the predominant site of covalent modification, whereas compound **3** modified mainly Lys297 in WT AKT1 (Extended Data Fig. 1e,f). Although Lys297 was disordered in the structure of AKT1 bound to ARQ092, modelling suggested that the ε-amine could also extend into the allosteric pocket (Fig. 1a). The preferential covalent engagement of Lys17 in the presence of Lys297, together with the increased residence time and thermal stability of the covalent AKT1 (E17K) complex compared to WT AKT1 (Fig. 1d,e), suggests that the corresponding imine adduct with Lys17 is more stable with respect to hydrolysis.

To demonstrate cellular AKT1 engagement, we first performed a thermal shift assay³¹ in BEAS-2B lung epithelial cells stably overexpressing FLAG–AKT1 (E17K), FLAG–AKT1 (WT) or FLAG–AKT2 (WT). In cells, compound **3** stabilized AKT1 (E17K) (change in melting temperature (ΔT_m) = 18.8 °C; Fig. 2a) to an even greater extent than the purified protein in buffer (ΔT_m = 15.0 °C; Fig. 1e). The selectivity of compound **3** for AKT1 (E17K) over WT AKT1 and AKT2, as determined by thermal stabilization, was also enhanced in cells (Fig. 2a and Extended Data Fig. 2) relative to buffer solution (Fig. 1e and Extended Data Fig. 1c). As expected, and in contrast to compound **3**, ARQ092 preferentially stabilized WT AKT1 and AKT2 over AKT1 (E17K) in cells (Fig. 2a and Extended Data Fig. 2c).

We synthesized the salicylaldehyde probe **3-alkyne** to directly assess covalent target engagement in cells (Fig. 2b and Extended Data Fig. 3a). The alkyne moiety enables visualization or affinity enrichment of probe-modified proteins through copper-catalysed click conjugation to a fluorophore-azide or biotin-azide reagent³². Cells expressing FLAG–AKT constructs were treated with **3-alkyne** (2 μM) for 45 min, and, after cell lysis, the imine adducts were reduced with NaBH₄, subjected to click conjugation with rhodamine (TAMRA)-azide and analysed by in-gel fluorescence. Consistent with the results of intact-protein mass spectrometry, **3-alkyne** rapidly modified AKT1 (E17K) and WT AKT1/2 ($t_{1/2} < 5$ min, Extended Data Fig. 3b) in a manner that was prevented by ARQ092 pretreatment (Fig. 2c). Even without a washout step to accentuate residence-time-based discrimination, **3-alkyne** dose-dependently modified AKT1 (E17K) (half-maximal effective concentration (EC_{50}) = 28 nM) with 2.4-fold increased potency over WT AKT1 and a striking 140-fold increased potency over AKT2 (Fig. 2d and Extended Data Fig. 3c). The observed selectivity for E17K over WT AKT1 was time dependent and further enhanced under washout conditions (Fig. 2e and Extended Data Fig. 3d–f). After treatment with **3-alkyne**, cells were washed into medium containing the potent competitor ARQ092 (5 μM), and the decrease in **3-alkyne**-modified FLAG–AKT was quantified over time. Dissociation of **3-alkyne** from WT AKT1 and AKT2 occurred with half-times of 45 and 10 min, respectively, whereas covalent modification of AKT1 (E17K) decreased by less than 10% during the 3 h chase period (Fig. 2e). These results indicate that the residence-time-based selectivity for AKT1 (E17K) over WT AKT1 was even greater in cells than with the purified proteins (Fig. 1d), mirroring the enhanced thermal stability conferred by compound **3** on cells (Figs. 1e and 2a). We consider the mechanistic basis of these unexpected observations below (Fig. 5).

We used LAPC4-CR prostate cancer cells³³, which are heterozygous for E17K-mutant AKT1 (Extended Data Fig. 4a,b), to identify the endogenous targets of **3-alkyne**. Cells were treated with **3-alkyne** (1 μM) or dimethyl sulfoxide (DMSO) in triplicate, and, following cell lysis, the imine adducts were reduced with NaBH₄. After click conjugation to biotin-picolyl azide, modified proteins were enriched with neutravidin agarose, eluted and probed for AKT1 and AKT2 by immunoblotting. Consistent with the results in FLAG–AKT-overexpressing cells, endogenous AKT1 was strongly enriched by **3-alkyne** in LAPC4-CR cells, whereas AKT2 was barely detected (Fig. 3a). A quantitative chemoproteomics approach was then used to identify the main cellular targets of **3-alkyne** in an unbiased manner. After click conjugation and enrichment with neutravidin agarose beads, we performed on-bead trypsinization, TMT6 labelling and LC–MS/MS analysis (Fig. 3b and Supplementary Table 1). AKT1 was by far the most enriched protein from LAPC4-CR cells (**3-alkyne** versus DMSO fold change = 17.4; $P = 9.67 \times 10^{-7}$). AKT2 was also specifically enriched by **3-alkyne** versus DMSO (fold change = 3.5; $P = 1.26 \times 10^{-3}$) but at a low fractional occupancy according to the immunoblotting results (Fig. 3a). For technical reasons, we were not able to identify a unique AKT1 peptide containing Glu17 or Lys17 by LC–MS/MS analysis. Nevertheless, our unbiased chemoproteomic results indicate that **3-alkyne**

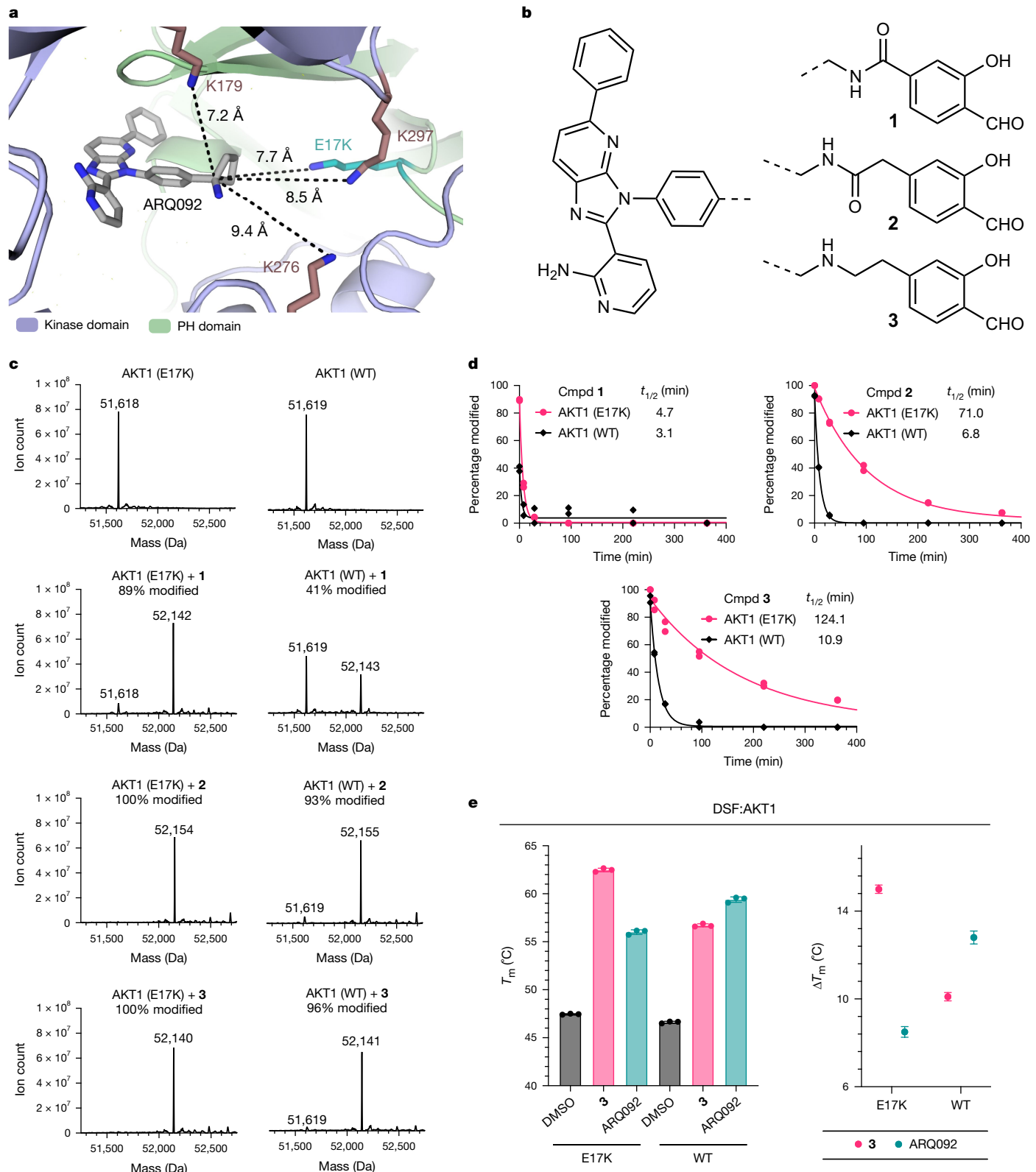


Fig. 1 | Structure-based design and biochemical characterization of reversible covalent AKT1 (E17K) inhibitors. **a**, Model of AKT1 (E17K) in complex with ARQ092 (based on PDB 5KCV), highlighting proximal lysines.

b, Chemical structures of salicylaldehydes **1–3**. **c**, Deconvoluted intact-protein mass spectra of AKT1 (E17K or WT) (1 μ M) treated with vehicle or **1–3** (5 μ M, 37 °C, 15 min) and then reduced with NaBH₄ (10 mM, 5 min). **d**, Dissociation of preformed AKT1–ligand complexes (1 μ M AKT1, 5 μ M ligand) was initiated by the addition of excess ARQ092 (50 μ M) with continuous incubation at 37 °C. At the indicated

time points, the percentage of covalently modified AKT1 was determined by intact-protein mass spectrometry after quenching with NaBH₄ (10 mM, 5 min). Duplicate measurements for each time point were plotted, and dissociation half-times were determined using an exponential decay function. **e**, The T_m of AKT1 (E17K or WT) (2 μ M) treated with DMSO, **3** (10 μ M) or ARQ092 (10 μ M) was assessed by DSF (mean \pm s.d., $n = 3$). Missing error bars indicate that the error was too small to be visualized. ΔT_m was calculated relative to the DMSO control for each protein (mean \pm s.d.). Cmpd, compound; PH, pleckstrin homology.

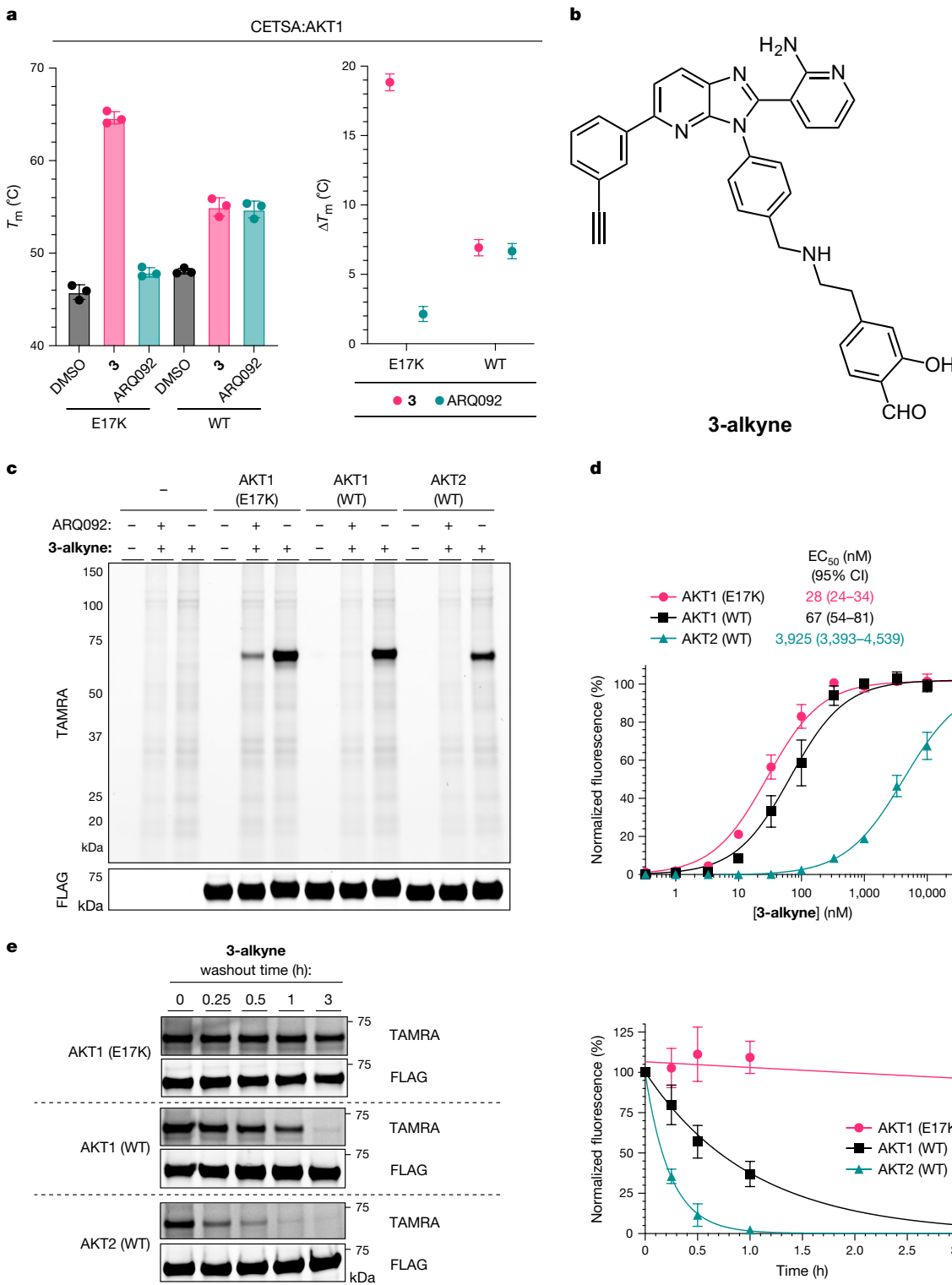
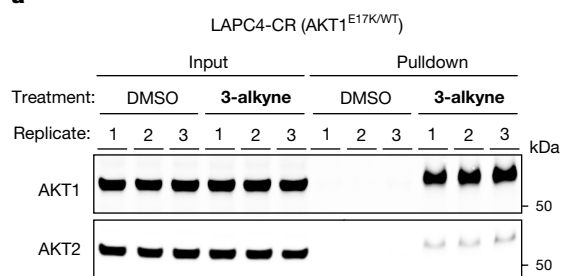


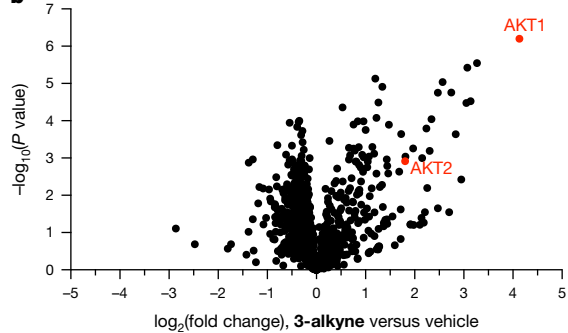
Fig. 2 | Cellular AKT engagement and residence-time-based selectivity. **a**, Cellular thermal shift assay of FLAG–AKT1 (E17K or WT) in BEAS-2B cells treated with DMSO, 3 (2 μ M) or ARQ092 (2 μ M) for 2 h. Cells were heat-challenged and lysed, and soluble FLAG–AKT1 levels were determined by dot blot. T_m values were determined by sigmoidal regression analysis ($n = 3$). ΔT_m was calculated relative to the DMSO control for each protein (mean \pm s.d.). **b**, Structure of 3-alkyne. **c**, BEAS-2B cells overexpressing the indicated FLAG–AKT constructs were treated with ARQ092 (5 μ M) or DMSO for 15 min and then with 3-alkyne (2 μ M) for 45 min. After cell lysis and reduction with NaBH₄ (10 mM), labelled proteins were conjugated to TAMRA-azide and visualized by in-gel fluorescence. **d**, The indicated BEAS-2B cell lines were treated with 3-alkyne for 6 h. After cell lysis and reduction

with NaBH₄ (10 mM), labelled proteins were conjugated to TAMRA-azide and visualized by in-gel fluorescence. Data were normalized to the maximum signal (mean \pm s.d., $n = 3$) and fitted with a sigmoidal regression. **e**, The indicated BEAS-2B cell lines were treated with 3-alkyne (2 μ M for E17K and WT FLAG–AKT1, 10 μ M for FLAG–AKT2) for 4 h. The medium was replaced with ARQ092-containing medium (5 μ M) to initiate competitive displacement. At the indicated time points, the cells were lysed and then reduced with NaBH₄ (10 mM). The labelled proteins were conjugated to TAMRA-picolyl-azide and visualized by in-gel fluorescence. Data were normalized to the 0 h time point (mean \pm s.d., $n = 3$) and fitted with an exponential decay. Missing errors bars indicate that the error was too small to be visualized.

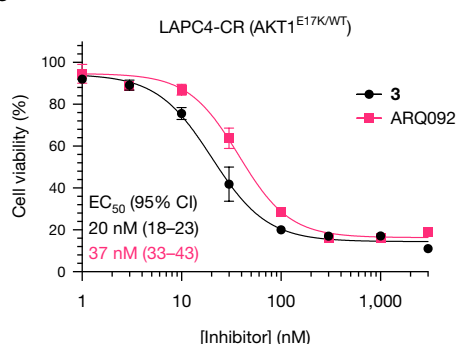
a



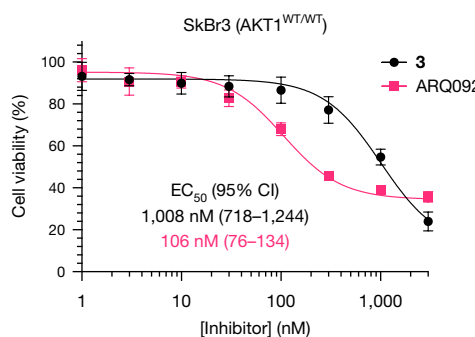
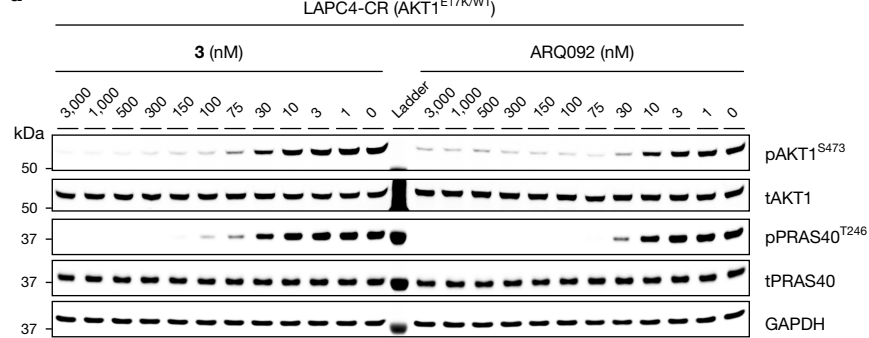
b



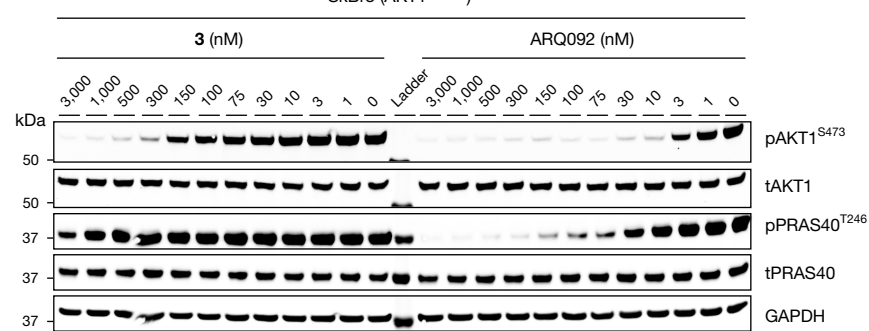
c



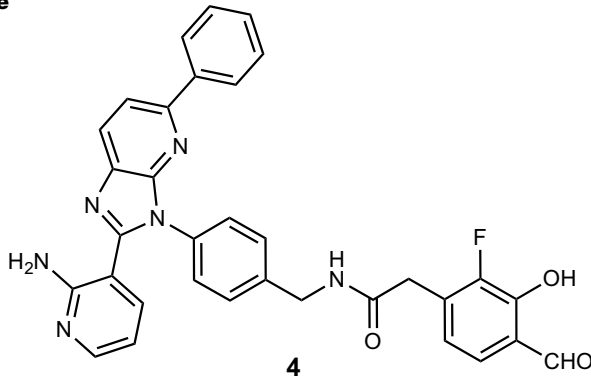
d



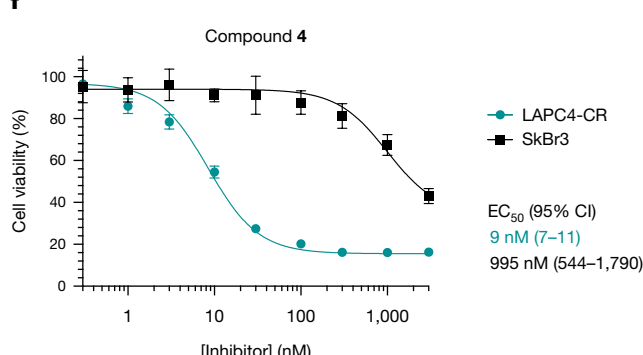
SkBr3 ($\text{AKT1}^{\text{WT}/\text{WT}}$)



e



f



corresponding P values (Student's t -test, two-tailed, unpaired, parametric).

c, LAPC4-CR or SkBr3 cells were treated with ARQ092 or compound 3 for 72 h, and cell viability was assessed. Data (mean \pm s.d., $n = 4$) were fitted with sigmoidal regression. **d**, LAPC4-CR and SkBr3 cells were treated with ARQ092 or compound 3 for 2 h, lysed and analysed by immunoblotting (loading controls: tAKT1, tPRAS40, GAPDH). This experiment was performed twice with similar results. **e**, Structure of compound 4. **f**, LAPC4-CR or SkBr3 cells were treated with compound 4 for 72 h, and cell viability was assessed. Data (mean \pm s.d., $n = 4$) were fitted with sigmoidal regression.

(and, by inference, the nearly identical compound **3**) selectively modifies endogenous AKT1 over AKT2 in LAPC4-CR prostate cancer cells expressing AKT1 (E17K). Treatment of LAPC4-CR tumour-bearing mice with **3**-alkyne (30 mg per kg body weight (30 mg kg⁻¹), intraperitoneal (i.p.) injection), followed by enrichment of modified proteins from tumour lysates, confirmed selective covalent engagement of AKT1 over AKT2 in vivo (Extended Data Fig. 4c).

Owing to a lack of mutant-selective inhibitors, it was not previously possible to test whether pharmacological blockade of endogenous AKT1 (E17K) is sufficient to abolish oncogenic signalling. We therefore compared the effects of compound **3** and ARQ092 on cell viability and AKT signalling in LAPC4-CR cells. As a control, we evaluated both inhibitors in SkBr3 breast cancer cells, which are WT for AKT1 and are known to be sensitive to pan-AKT inhibitors³⁴. Exposure of LAPC4-CR cells to compound **3** for 72 h potently reduced cell viability ($EC_{50} = 20$ nM), similar to the clinical pan-AKT inhibitor ARQ092 ($EC_{50} = 37$ nM) (Fig. 3c). By contrast, SkBr3 cells were 50-fold less sensitive to compound **3** ($EC_{50} = 1.0$ μ M) but only 3-fold less sensitive to ARQ092 ($EC_{50} = 106$ nM). Previous studies have shown that addition of a non-native myristylation sequence to AKT1 constitutively activates the kinase and is oncogenic³⁵. Consistent with an on-target mode of action, the effects of compound **3** (and, to a lesser extent, those of ARQ092) were abolished in LAPC4-CR cells transduced with a myristoylated AKT1 construct lacking the E17K mutation (Extended Data Fig. 4d,e).

The effects of compound **3** on LAPC4-CR cell viability were correlated with acute inhibition of AKT signalling readouts, including phospho-PRAS40 (Fig. 3d and Extended Data Fig. 5a), an AKT substrate that contributes to mTORC1 activation and cancer cell survival^{36,37}. Compound **3** also potently inhibited AKT signalling in E17K-mutant HBCx-2 breast cancer cells (Extended Data Fig. 5a). By contrast, the inhibitory effects on phospho-PRAS40 and other signalling readouts were reduced in AKT1 (WT)-expressing SkBr3 and MCF7 breast cancer cells (Fig. 3d and Extended Data Fig. 5a). The differential effects on AKT signalling were even more apparent when we measured the kinetics of phospho-PRAS40 recovery after compound **3** washout in LAPC4-CR and SkBr3 cells (Extended Data Fig. 5b,c). Overall, the increased potency of compound **3** towards E17K-mutant LAPC4-CR and HBCx-2 cells mirrored the increased thermal stability, potency and residence time towards E17K versus WT AKT1 and AKT2 (Fig. 2).

To enable in vivo studies, we developed fluorinated salicylaldehyde **4** (Fig. 3e), a derivative of compound **2** with improved pharmacokinetics and residence-time-based selectivity compared with both compounds **2** and **3** (Extended Data Fig. 6a–c). In a cellular nanoBRET assay using full-length AKT constructs³⁸, compound **4** bound to AKT1 (E17K) more potently than compound **3** and showed greater selectivity over WT AKT1 (2.5-fold) and AKT2 (24-fold) (Extended Data Fig. 6d). Strikingly, compound **4** dissociated from purified WT AKT1 18-fold faster than AKT1 (E17K) and showed greater potency towards E17K-mutant LAPC4-CR and HBCx-2 cells relative to SkBr3 and MCF7 cells (Fig. 3f and Extended Data Fig. 6b,e).

Treatment of LAPC4-CR tumour-bearing mice with a single dose of compound **4** (40 mg kg⁻¹, i.p. injection) reduced phospho-AKT1 and phospho-PRAS40 levels in tumours collected at 2 h and 7 h postdose (80–90% inhibition, Extended Data Fig. 6f,g). After 24 h, complete recovery of both biomarkers was observed, suggesting that more frequent dosing would be required to provide sustained inhibition of AKT1 (E17K) signalling in tumours. Twice-daily dosing with compound **4** (30 mg kg⁻¹) significantly blocked LAPC4-CR tumour growth (Fig. 4a and Extended Data Fig. 7a–c), confirming that covalent inhibition of AKT1 (E17K) (and possibly WT AKT1) could mediate antitumour effects in mice. Oral administration of ARQ092 (100 mg kg⁻¹)³⁰ was also efficacious in the LAPC4-CR xenograft model. However, ARQ092 was poorly tolerated relative to compound **4** and caused substantial weight loss (Extended Data Fig. 7d). Moreover, ARQ092 induced rapid

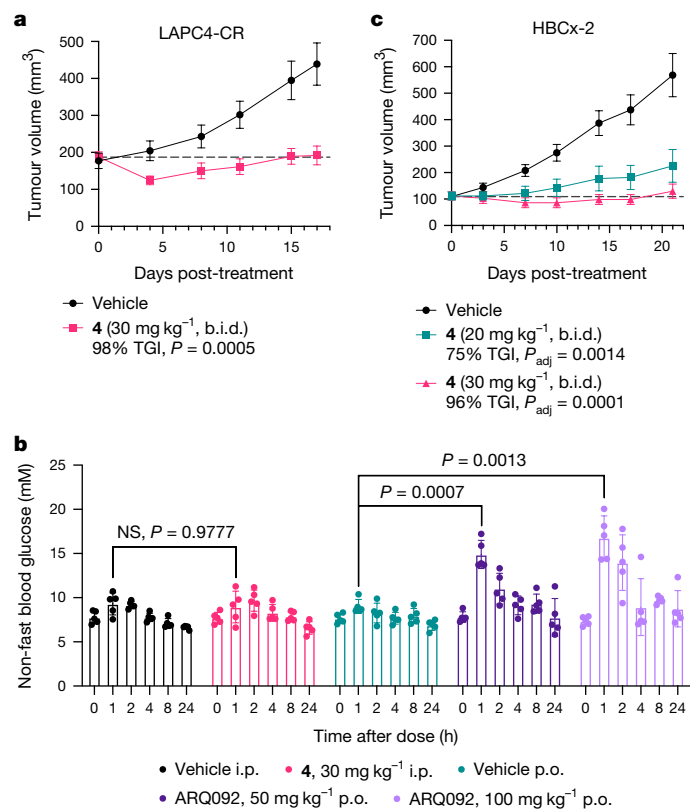


Fig. 4 | In vivo antitumour activity of compound **4.** **a**, LAPC4-CR tumour-bearing male mice were randomized to vehicle ($n = 10$) or compound **4** treatment (30 mg kg⁻¹, b.i.d., i.p. injection, $n = 12$). Tumour volumes (plotted as mean \pm s.e.m.) and TGI were determined as described in Methods. Student's *t*-test (two-tailed, unpaired, parametric) was used to calculate *P* values without adjustments for multiple comparison tests. **b**, Male athymic nude mice were treated with a single dose of vehicle (i.p. injection), compound **4** (30 mg kg⁻¹, i.p. injection), vehicle (p.o.) or ARQ092 (100 or 150 mg kg⁻¹, p.o.), and blood glucose levels measured at 0, 1, 2, 4, 8 and 24 h after treatment ($n = 5$, mean \pm s.d.). Adjusted *P* values were calculated relative to the appropriate vehicle using a two-way repeat-measurement analysis of variance (ANOVA) with Holm–Šídák's multiple comparisons test. NS, not significant. **c**, HBCx-2 tumour-bearing female mice were randomized to vehicle or compound **4** treatment (20 or 30 mg kg⁻¹, b.i.d., i.p. injection, $n = 8$). Tumour volumes (mean \pm s.e.m.) and TGI were determined as described in Methods. Adjusted *P* values were calculated relative to the vehicle using ordinary one-way ANOVA with Dunnett's multiple comparison test.

elevation in blood glucose levels when administered to tumour-free mice at either 50 or 100 mg kg⁻¹. By contrast, compound **4** (30 mg kg⁻¹) had no effect on blood glucose (Fig. 4b), consistent with its decreased potency towards AKT2 (Extended Data Fig. 6d). In a homozygous E17K-mutant breast cancer model (HBCx-2 patient-derived xenograft), compound **4** also showed significant, dose-dependent tumour growth inhibition (75% at 20 mg kg⁻¹; 96% at 30 mg kg⁻¹; Fig. 4c and Extended Data Fig. 7e). By contrast, a WT AKT1 breast cancer xenograft model (BT-474) was less sensitive to compound **4**, yet it was highly sensitive to pan-AKT inhibitors ARQ092 and capivasertib (Extended Data Fig. 7f,g).

We obtained a 2.2-Å-resolution crystal structure of AKT1 (E17K) in complex with compound **3**, which showed the anticipated imine bond between the salicylaldehyde and Lys17 (Extended Data Fig. 8a). Additional density suggested the presence of a tetravalent metal ion bound to the salicylaldimine through the phenol-O and the imine-N, along with Cys296 and Cys310 in the activation loop of the kinase domain. We tentatively identified the metal ion—which probably originated as a

trace contaminant in the crystallization buffer—as Zn²⁺ on the basis of its distinctive tetrahedral geometry and bond lengths³⁹. Indeed, simple salicylimines⁴⁰ have been shown to chelate Zn²⁺, which frequently coordinates cysteine and histidine in protein binding sites⁴¹. Crystallization in the presence of added ZnSO₄ (2 equivalents) provided a 2.1 Å structure that recapitulated the same binding configuration but with improved electron density and *B* factors for the metal and ligand, consistent with stoichiometric Zn²⁺ coordination (Fig. 5a and Extended Data Figs. 8b and 9a). Crystallization of AKT1 (E17K) in complex with compound 4 produced a 1.9 Å structure with a similar Zn²⁺ binding configuration (Extended Data Fig. 8c,d).

Our initial residence time measurements were performed in the presence of ethylenediaminetetraacetic acid (EDTA). Thus, a slowly dissociating covalent complex with AKT1 (E17K) could form even in the absence of Zn²⁺ coordination ($t_{1/2} \approx 124$ min; Fig. 1d). We determined the structure of the metal-free complex at 2.2 Å resolution after alkylation of Cys296 and Cys310 with iodoacetamide to prevent adventitious metal binding. This structure showed a similar binding pose for compound 3, albeit with the salicylaldehyde in a flipped orientation that maintained the imine bond with Lys17 (Fig. 5b and Extended Data Fig. 8e). The metal-free salicylaldimine exhibited a favourable coplanar geometry with an intramolecular hydrogen bond between the imine and the *ortho*-phenol (Fig. 5b), which probably contributes to its enhanced thermal stability and residence time⁴² relative to that of the complex with WT AKT1. A cocrystal structure of WT AKT1 in complex with compound 3 (2.0 Å resolution) confirmed covalent bond formation between the salicylaldehyde and Lys297, consistent with the results of the LC–MS/MS analysis (Extended Data Fig. 1f). However, in contrast to the Lys17-derived imine, the Lys297-derived imine in WT AKT1 was rotated out of plane and did not form an intramolecular hydrogen bond with the phenol (Fig. 5c and Extended Data Fig. 8f). Although we cannot exclude an effect of the crystallization conditions (cysteine alkylation was required to obtain a high-resolution dataset), our structure provides a plausible explanation for the decreased thermal stability and residence time of compound 3 bound to WT AKT1 compared with AKT1 (E17K). Finally, we solved a cocrystal structure of AKT2 in complex with compound 3 (2.0 Å resolution) in which electron density for the salicylaldehyde and Lys298 could not be resolved (Extended Data Fig. 8g,h), consistent with the formation of a conformationally dynamic or rapidly equilibrating imine conjugate. Collectively, our cocrystal structures support a model in which compound 3 binds to the AKT1 (E17K) allosteric site and positions the salicylaldehyde in proximity to both Lys17 and Lys297. Although reversible covalent bond formation may occur competitively with Lys297, the salicylaldimine–Lys17 conjugate is thermodynamically preferred.

Although the biological relevance of Zn²⁺ coordination was initially unclear, we considered that the formation of a tetravalent chelate containing the salicylaldimine–Lys17 conjugate would be stabilizing. Using DSF, we assessed the thermal stability of AKT1 (E17K) after treatment with compound 3 and found that adding Zn²⁺ (5 equivalents) stabilized the complex by a further 7.8 °C (Extended Data Fig. 9b). This stabilizing effect was abolished with an AKT1 mutant (E17K, C296/310A) lacking the two cysteines bound to Zn²⁺ in our crystal structure. Addition of Zn²⁺ likewise had no effect on the stability of WT AKT1 bound to compound 3. We assessed the effect of Zn²⁺ on residence time by diluting the preformed covalent complex of AKT1 (E17K)–compound 3 in the presence of excess ARQ092. The addition of ZnSO₄ rendered the covalent complex quasi-irreversible, whereas under metal-free conditions the complex dissociated with a half-time of 130 min (Fig. 5d). ZnSO₄ had no effect on the dissociation kinetics of compound 3 from AKT1 (E17K, C296/310A). Notably, the dissociation kinetics of AKT1 (E17K)–compound 3 in the presence of Zn²⁺ recapitulated the slow washout kinetics and enhanced thermal stability observed in cells (Fig. 2a,e and Extended Data Fig. 5b,c).

We used a cellular thermal shift assay (Fig. 2a) to test whether Zn²⁺ binding would stabilize the AKT1(E17K)–compound 3 complex in cells. Cotreatment of cells for 3 h with compound 3 and TPEN, a cell-permeable chelator that binds Zn²⁺ with femtomolar affinity⁴³, resulted in significantly reduced FLAG–AKT1 (E17K) stability relative to treatment with compound 3 alone (Fig. 5e and Extended Data Fig. 10a). A similar effect was observed in the absence of TPEN when we assessed the thermal stability of FLAG–AKT1 (E17K, C296/310A), which lacked the critical cysteines involved in Zn²⁺ chelation (Fig. 5e). Taken together, these data strongly suggest that metal chelation by Cys296 and Cys310 stabilizes the covalent complex formed by FLAG–AKT1 (E17K) and compound 3 in cells.

To identify the bound metal unambiguously, we purified the complex from cells with anti-FLAG beads, specifically eluted with excess FLAG peptide, and analysed the eluted material by inductively coupled plasma mass spectrometry (ICP-MS) to quantify five of the most abundant biologically relevant transition metals (Mn, Fe, Co, Cu and Zn). Using this protocol, we obtained FLAG–AKT1 (E17K) and FLAG–AKT1 (E17K, C296/310A) in >90% purity (Extended Data Fig. 10b) from cells treated with DMSO or compound 3 (2 µM for 2 h, in quadruplicate). Treatment of cells with compound 3 led to selective enrichment of Zn²⁺ with FLAG–AKT1 (E17K) but not the cysteine double mutant (Fig. 5f). Moreover, Zn²⁺ was not enriched with FLAG–AKT1 (E17K) purified from cells treated with DMSO instead of compound 3. Hence, covalent modification of Lys17 in AKT1 (E17K) by compound 3 in cells recruits Zn²⁺ in a Cys296/Cys310-dependent manner to form a stable chelate. Assembly of this ‘neo-zinc chelate’ results in prolonged inhibition of AKT1 (E17K) but not WT AKT1 or AKT2.

Discussion

This study reports covalent inhibitors that target the mutant oncprotein AKT1 (E17K), with improved selectivity over WT AKT paralogues driven by exceptionally long residence times. The E17K alteration constitutively activates AKT1 kinase signalling and has been identified in a variety of solid tumour types. Although pan-AKT inhibitors have shown encouraging preliminary activity in a subset of patients with AKT1 (E17K) mutant tumours^{2–4}, on-target toxicities (for instance, hyperglycaemia) have necessitated intermittent and/or reduced dosing, probably resulting in suboptimal AKT1 (E17K) engagement⁶. By creating a unique nucleophile for targeted covalent inhibitors, the E17K alteration offers the potential for sustained kinase inhibition and improved selectivity over WT AKT paralogues. This opportunity nevertheless comes with significant challenges intrinsic to the development of lysine-targeted covalent inhibitors, including the vastly reduced nucleophilicity and higher prevalence of lysine relative to cysteine⁴⁴.

To address these challenges, we used a structure-guided approach and exploited residence-time-based selectivity. The electrophilic salicylaldehyde in compound 3 preferentially forms a reversible imine conjugate with Lys17 in AKT1 (E17K), despite the presence of three other lysines within striking distance of the allosteric pocket, all of which are conserved in AKT1–3. The salicylaldehyde also efficiently modifies Lys297 in WT AKT1. However, the resulting covalent complex is thermally less stable and dissociates more than ten times faster than the AKT1 (E17K) complex, even in the absence of Zn²⁺ chelation. The relative hydrolytic stability of the imine adducts derived from Lys17 and Lys297, which approach the salicylaldehyde from different directions, can be rationalized on the basis of their structures. In the Zn²⁺-free cocrystal structure with AKT1 (E17K), the Lys17-derived salicylaldimine adopts an energetically favourable conformation with an intramolecular hydrogen bond between the imine and the phenol; notably, the imine bond is entirely shielded from solvent. By contrast, the Lys297-derived imine bond in WT AKT1 is more solvent-exposed and rotated out of plane, precluding intramolecular hydrogen bond formation. Our AKT1 (E17K) inhibitors show even greater

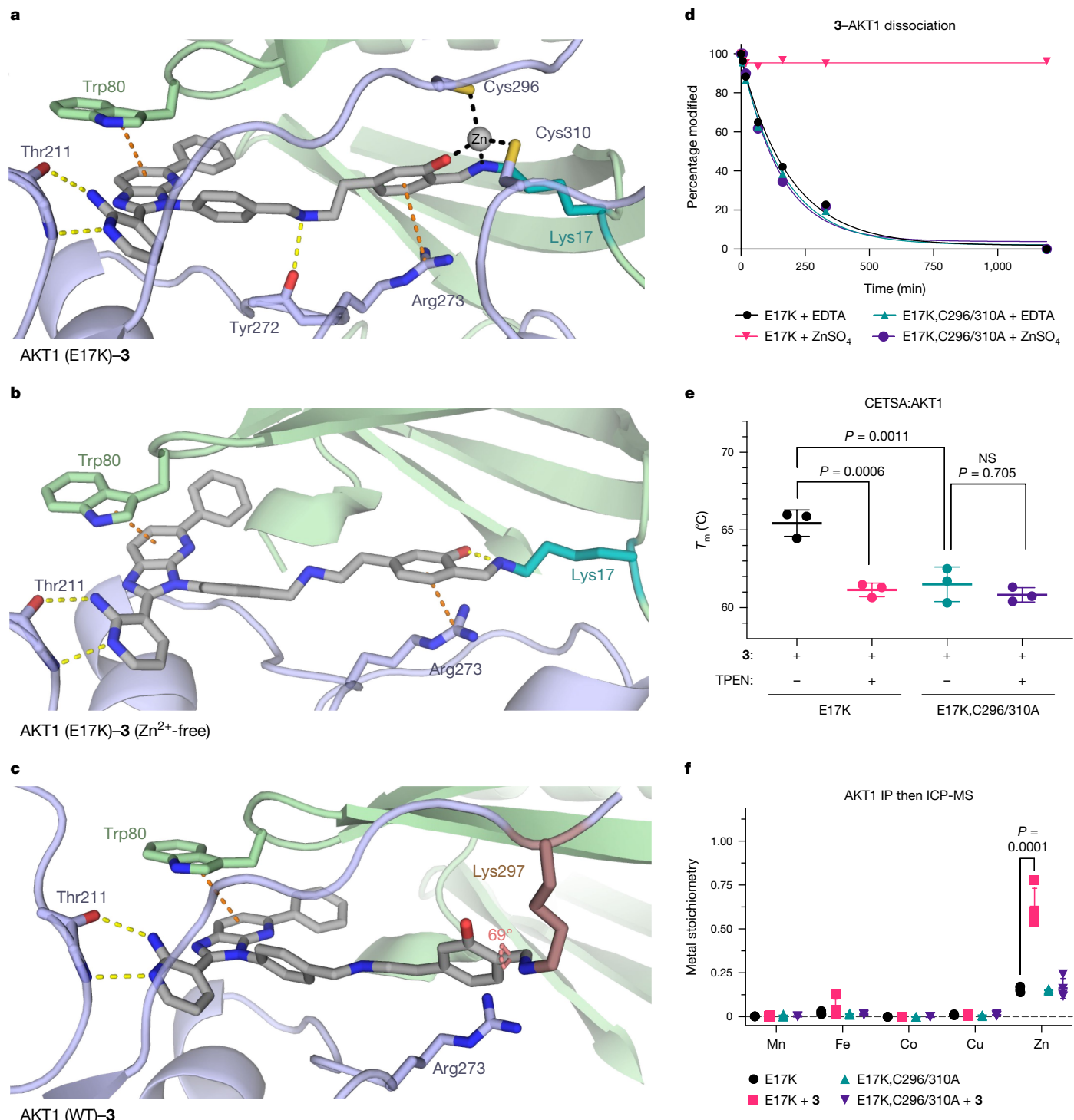


Fig. 5 | Structural analysis reveals a role of Zn^{2+} chelation in AKT1(E17K) inhibition. **a**, Cocrystal structure of AKT1(E17K) bound to salicylaldehyde **3** (grey) in the presence of Zn^{2+} at 2.2 Å resolution. Yellow dashes, H bonds; orange dashes, π -stacking; black dashes, Zn^{2+} chelate. **b**, Cocrystal structure of iodoacetamide-labelled AKT1(E17K) bound to salicylaldehyde **3** at 2.2 Å resolution (Zn^{2+} -free). **c**, Cocrystal structure of AKT1(WT) bound to salicylaldehyde **3** (grey) at 2.0 Å resolution. The dihedral angle (69°) for the aryl-imine C–C bond is indicated. **d**, Purified AKT1 mutants (1 μ M) were treated with compound **3** (5 μ M) in the presence of $ZnSO_4$ (5 μ M) or EDTA (5 mM) for 15 min. Dissociation of the covalent complex was initiated by adding ARQ092 (50 μ M) with continuous incubation at 37 °C, and the percentage of modified AKT1 was determined by mass spectrometry as described in Fig. 1d; $n=1$. **e**, BEAS-2B cells stably expressing FLAG-AKT1 mutants were treated for 3 h

with compound **3** (2 μ M) and DMSO or TPEN (10 μ M) and analysed by cellular thermal shift assay as in Fig. 2a. T_m values were determined by sigmoidal regression analysis (mean \pm s.d., $n=3$). Adjusted P values were calculated using ordinary one-way ANOVA with Tukey's multiple comparison test. **f**, BEAS-2B cells stably expressing FLAG-AKT1 mutants were treated with DMSO or compound **3** (2 μ M, 2 h). After cell lysis, FLAG-AKT1 was immunoprecipitated and eluted with FLAG peptide. Transition metals (Mn, Fe, Co, Cu and Zn) were quantified by ICP-MS using internal standards. Data are plotted as molar equivalents (mean \pm s.d., $n=4$) on the basis of estimated amounts of FLAG-AKT1 in each sample (Extended Data Fig. 10b). Missing errors bars indicate that the error was too small to be visualized. P values were calculated using Student's *t*-test (two-tailed, unpaired, parametric) without adjustments for multiple comparisons. IP, immunoprecipitation.

selectivity over AKT2, reflected by the absence of acute blood glucose elevation in mice treated with compound **4**. Applying the concept of residence-time-based selectivity to covalent inhibitor discovery—which requires an intrinsically reversible electrophile—may be especially advantageous for discriminating among the approximately 600,000 lysines in the proteome, as shown in this study and previous work aimed at selectively targeting the conserved catalytic lysine of protein kinases⁴⁵.

Several lines of evidence from structural, biophysical and cellular experiments indicate that the reversible AKT1(E17K)–salicylaldimine complex is further stabilized by engaging a Zn²⁺ ion. This produces a chelate in which the imine-*N* and phenol-*O* atoms occupy two positions of the Zn²⁺ coordination sphere. Completion of the tetravalent chelate requires Cys296 and Cys310, which are fortuitously located on a proximal segment of the kinase activation loop adjacent to the allosteric pocket. Notably, the prolonged residence time and TPEN-sensitive thermal stability of the intracellular AKT1(E17K)–**3** complex mirrors the effect of adding stoichiometric Zn²⁺ to the biochemically reconstituted complex. These results, along with our ICP-MS analysis of immunopurified AKT1(E17K), strongly suggest that the AKT1(E17K)–**3** complex is stabilized by endogenous Zn²⁺ chelation in cells. This chelation-enhanced stability translates to even greater selectivity over WT AKT1 and AKT2 in cells, potentially reducing the likelihood of on-target toxicities observed with pan-AKT inhibitors.

Here, we report the formation of a ‘neo-zinc chelate’ comprising a reversible covalent inhibitor and a protein that does not otherwise bind Zn²⁺. Chelation-enhanced binding has been reported for a class of non-covalent inhibitors that recruit adventitious Zn²⁺ to the catalytic site of trypsin-like serine proteases⁴⁶. More recently, endogenous Zn²⁺ chelation has been implicated in lactate binding to the SUMO hydrolase SENP1, which does not otherwise bind to transition metals⁴⁷. In principle, a ligand design strategy in which lysine modification by a salicylaldehyde moiety is coupled to Zn²⁺ recruitment by two proximal side chains (such as Cys or His) could be applied to other protein targets besides AKT1(E17K), leading to enhanced potency and selectivity. This strategy could also be used to target lysines near functional metal binding sites, such as metalloenzymes or even structural or regulatory domains (for instance, zinc fingers) in which metal binding is either intrinsically weak or compromised by a pathogenic mutation.

Although further optimization is required to develop an orally bioavailable salicylaldehyde inhibitor of AKT1(E17K), the recently approved salicylaldehyde-based drug voxelotor, which targets the amino-terminal amine of haemoglobin^{48,49}, suggests that this is an achievable goal. These challenges notwithstanding, our study demonstrates the feasibility of covalently targeting a mutant oncogenic lysine and inactivating the AKT1(E17K)-driven growth of malignant tumours, without inhibiting AKT2 or inducing hyperglycaemia.

Online content

Any methods, additional references, Nature Portfolio reporting summaries, source data, extended data, supplementary information, acknowledgements, peer review information; details of author contributions and competing interests; and statements of data and code availability are available at <https://doi.org/10.1038/s41586-024-08176-4>.

- Carpten, J. D. et al. A transforming mutation in the pleckstrin homology domain of AKT1 in cancer. *Nature* **448**, 439–444 (2007).
- Hyman, D. M. et al. AKT inhibition in solid tumors with AKT1 mutations. *J. Clin. Oncol.* **35**, 2251–2259 (2017).
- Kalinsky, K. et al. Effect of capivasertib in patients with an AKT1 E17K-mutated tumor. *JAMA Oncol.* **7**, 271 (2021).
- Kalinsky, K. et al. Ipatasertib in patients with tumors with AKT mutations: results from the NCI-MATCH ECOG-ACRIN trial (EAY131) sub-protocol Z1K. *Eur. J. Cancer* **174**, S8–S9 (2022).
- Smyth, L. M. et al. Capivasertib, an AKT kinase inhibitor, as monotherapy or in combination with fulvestrant in patients with AKT1 E17K-mutant, ER-positive metastatic breast cancer. *Clin. Cancer Res.* **26**, 3947–3957 (2020).
- Banerji, U. et al. A phase I open-label study to identify a dosing regimen of the pan-AKT inhibitor AZD5363 for evaluation in solid tumors and in PIK3CA-mutated breast and gynecologic cancers. *Clin. Cancer Res.* **24**, 2050–2059 (2018).
- Truebestein, L. et al. Structure of autoinhibited Akt1 reveals mechanism of PIP₃-mediated activation. *Proc. Natl. Acad. Sci. USA* **118**, e2101496118 (2021).
- Lučić, I. et al. Conformational sampling of membranes by Akt controls its activation and inactivation. *Proc. Natl. Acad. Sci. USA* **115**, E3940–E3949 (2018).
- Hoxhaj, G. & Manning, B. D. The PI3K-AKT network at the interface of oncogenic signalling and cancer metabolism. *Nat. Rev. Cancer* **20**, 74–88 (2020).
- Landgraf, K. E., Pilling, C. & Falke, J. J. Molecular mechanism of an oncogenic mutation that alters membrane targeting: Glu17Lys modifies the PIP lipid specificity of the AKT1 PH domain. *Biochemistry* **47**, 12260–12269 (2008).
- Bae, H. et al. PH domain-mediated autoinhibition and oncogenic activation of Akt. *eLife* **11**, e80148 (2022).
- Rudolph, M. et al. AKT1^{E17K} mutation profiling in breast cancer: prevalence, concurrent oncogenic alterations, and blood-based detection. *BMC Cancer* **16**, 622 (2016).
- Cohen, Y. et al. AKT1 pleckstrin homology domain E17K activating mutation in endometrial carcinoma. *Gynecol. Oncol.* **116**, 88–91 (2010).
- Yesilöz, Ü. et al. Frequent AKT1^{E17K} mutations in skull base meningiomas are associated with mTOR and ERK1/2 activation and reduced time to tumor recurrence. *Neuro. Oncol.* **19**, 1088–1096 (2017).
- Clark, V. E. et al. Genomic analysis of non-NF2 meningiomas reveals mutations in TRAF7, KLF4, AKT1, and SMO. *Science* **339**, 1077–1080 (2013).
- Varkaris, A. et al. Allosteric PI3Ka inhibition overcomes on-target resistance to orthosteric inhibitors mediated by secondary PIK3CA mutations. *Cancer Discov.* <https://doi.org/10.1158/2159-8290.CD-23-0704> (2023).
- Lindhurst, M. J. et al. Ubiquitous expression of Akt1 p.(E17K) results in vascular defects and embryonic lethality in mice. *Hum. Mol. Genet.* **29**, 3350–3360 (2020).
- Lindhurst, M. J. et al. A mosaic activating mutation in AKT1 associated with the proteus syndrome. *N. Engl. J. Med.* **365**, 611 (2011).
- Turner, N. C. et al. Capivasertib in hormone receptor-positive advanced breast cancer. *N. Engl. J. Med.* **388**, 2058–2070 (2023).
- Cho, H. et al. Insulin resistance and a diabetes mellitus-like syndrome in mice lacking the protein kinase Akt2 (PKBβ). *Science* **292**, 1728–1731 (2001).
- Dummler, B. et al. Life with a single isoform of Akt: mice lacking Akt2 and Akt3 are viable but display impaired glucose homeostasis and growth deficiencies. *Mol. Cell. Biol.* **26**, 8042–8051 (2006).
- George, S. et al. A family with severe insulin resistance and diabetes due to a mutation in AKT2. *Science* **304**, 1325–1328 (2004).
- Cho, H., Thorvaldsen, J. L., Chu, Q., Feng, F. & Birnbaum, M. J. Akt1/PKBα is required for normal growth but dispensable for maintenance of glucose homeostasis in mice. *J. Biol. Chem.* **276**, 38349–38352 (2001).
- Buzzi, F. et al. Differential effects of protein kinase B/Akt isoforms on glucose homeostasis and islet mass. *Mol. Cell. Biol.* **30**, 601–612 (2010).
- Chen, W. S. et al. Growth retardation and increased apoptosis in mice with homozygous disruption of the akt gene. *Genes Dev.* **15**, 2203–2208 (2001).
- Ostrem, J. M., Peters, U., Sos, M. L., Wells, J. A. & Shakat, K. M. K-Ras(G12C) inhibitors allosterically control GTP affinity and effector interactions. *Nature* **503**, 548–551 (2013).
- Skoulidis, F. et al. Sotorasib for lung cancers with KRAS p.G12C mutation. *N. Engl. J. Med.* **384**, 2371–2381 (2021).
- Jäne, P. A. et al. Adagrasib in non-small-cell lung cancer harboring a KRAS^{G12C} mutation. *N. Engl. J. Med.* **387**, 120–131 (2022).
- Lapierre, J. M. et al. Discovery of 3-(3-(4-(1-aminoacylobutyl)phenyl)-5-phenyl-3H-imidazo[4,5-b]pyridin-2-yl)pyridin-2-amine (ARQ 092): an orally bioavailable, selective, and potent allosteric AKT inhibitor. *J. Med. Chem.* **59**, 6455–6469 (2016).
- Yu, Y. et al. Targeting AKT1-E17K and the PI3K/AKT pathway with an allosteric AKT inhibitor, ARQ 092. *PLoS ONE* **10**, e0140479 (2015).
- Molina, D. M. et al. Monitoring drug target engagement in cells and tissues using the cellular thermal shift assay. *Science* **341**, 84–87 (2013).
- Parker, C. G. & Pratt, M. R. Click chemistry in proteomic investigations. *Cell* **180**, 605–632 (2020).
- Haffner, M. C. et al. Phenotypic characterization of two novel cell line models of castration-resistant prostate cancer. *Prostate* **81**, 1159–1171 (2021).
- Sangai, T. et al. Biomarkers of response to Akt inhibitor MK-2206 in breast cancer. *Clin. Cancer Res.* **18**, 5816–5828 (2012).
- Aoki, M., Batista, O., Bellacosa, A., Tschilis, P. & Vogt, P. K. The Akt kinase: molecular determinants of oncogenicity. *Proc. Natl. Acad. Sci. USA* **95**, 14950–14955 (1998).
- Kovacina, K. S. et al. Identification of a proline-rich Akt substrate as a 14-3-3 binding partner. *J. Biol. Chem.* **278**, 10189–10194 (2003).
- Oshiro, N. et al. The proline-rich Akt substrate of 40 kDa (PRAS40) is a physiological substrate of mammalian target of rapamycin complex 1. *J. Biol. Chem.* **282**, 20329–20339 (2007).
- Vasta, J. D. et al. Quantitative, wide-spectrum kinase profiling in live cells for assessing the effect of cellular ATP on target engagement. *Cell Chem. Biol.* **25**, 206–214 (2018).
- Tamames, B., Sousa, S. F., Tamames, J., Fernandes, P. A. & Ramos, M. J. Analysis of zinc-ligand bond lengths in metalloproteins: trends and patterns. *Proteins* **69**, 466–475 (2007).
- Leussing, D. L. & Leach, B. E. Stabilities, rates of formation, and rates of transimination in aqueous solutions of some zinc(II)-Schiff base complexes derived from salicylaldehyde. *J. Am. Chem. Soc.* **93**, 3377–3384 (1971).
- Laitaoja, M., Valjakka, J. & Jänis, J. Zinc coordination spheres in protein structures. *Inorg. Chem.* **52**, 10983–10991 (2013).

Article

42. Bruyneel, W., Charette, J. J. & De Hoffmann, E. Kinetics of hydrolysis of hydroxy and methoxy derivatives of N-benzylidene-2-aminopropane. *J. Am. Chem. Soc.* **88**, 3808–3813 (1966).
43. Arslan, P., Di Virgilio, F., Beltrame, M., Tsien, R. Y. & Pozzan, T. Cytosolic Ca^{2+} homeostasis in Ehrlich and Yoshida carcinomas. A new, membrane-permeant chelator of heavy metals reveals that these ascites tumor cell lines have normal cytosolic free Ca^{2+} . *J. Biol. Chem.* **260**, 2719–2727 (1985).
44. Cuesta, A. & Taunton, J. Lysine-targeted inhibitors and chemoproteomic probes. *Annu. Rev. Biochem.* **88**, 365–381 (2019).
45. Yang, T. et al. Reversible lysine-targeted probes reveal residence time-based kinase selectivity. *Nat. Chem. Biol.* **18**, 934–941 (2022).
46. Katz, B. A. et al. Design of potent selective zinc-mediated serine protease inhibitors. *Nature* **391**, 608–612 (1998).
47. Liu, W. et al. Lactate regulates cell cycle by remodelling the anaphase promoting complex. *Nature* **616**, 790–797 (2023).
48. Oksenberg, D. et al. GBT440 increases haemoglobin oxygen affinity, reduces sickling and prolongs RBC half-life in a murine model of sickle cell disease. *Br. J. Haematol.* **175**, 141–153 (2016).
49. Vichinsky, E. et al. A phase 3 randomized trial of voxelotor in sickle cell disease. *N. Engl. J. Med.* **381**, 509–519 (2019).

Publisher's note Springer Nature remains neutral with regard to jurisdictional claims in published maps and institutional affiliations.

Springer Nature or its licensor (e.g. a society or other partner) holds exclusive rights to this article under a publishing agreement with the author(s) or other rightsholder(s); author self-archiving of the accepted manuscript version of this article is solely governed by the terms of such publishing agreement and applicable law.

© The Author(s), under exclusive licence to Springer Nature Limited 2024

Methods

Cell culture

All cell lines (except LAPC4-CR, HBCx-2 and SF9) were obtained from ATCC, tested negative for mycoplasma contamination and were used without further authentication. BEAS-2B cells (ATCC, catalogue no. CRL-3588) were cultured in RPMI-1640 and GlutaMAX (Thermo Fisher Scientific, catalogue no. 61870036) supplemented with 10% fetal bovine serum (Axenia Biologix, catalogue no. F001). HEK293T cells (ATCC, catalogue no. CRL-3216) were cultured in Dulbecco's modified Eagle medium (DMEM) and GlutaMAX (Thermo Fisher Scientific, catalogue no. 10569069) supplemented with 10% fetal bovine serum (Axenia Biologix, catalogue no. F001). LAPC4-CR cells⁶ (gift from M. C. Haffner) were cultured in RPMI-1640 and GlutaMAX (Thermo Fisher Scientific, catalogue no. 61870036) supplemented with 10% fetal bovine serum (Axenia Biologix, catalogue no. F001). SKBr3 cells (ATCC, catalogue no. HTB-30) were cultured in McCoy's 5A and GlutaMAX (Thermo Fisher Scientific, catalogue no. 36600021) supplemented with 10% fetal bovine serum (Axenia Biologix, catalogue no. F001). HBCx-2 cells (XenTech) were cultured in Advanced DMEM/F12 (Thermo Fisher Scientific, catalogue no. 10569069) supplemented with 8% fetal bovine serum (Axenia Biologix, catalogue no. F001), 2 mM L-glutamine and 20 μM Rho-associated kinase inhibitor Y-27632. MCF7 cells (ATCC, catalogue no. HTB-22) were cultured in DMEM and GlutaMAX (Thermo Fisher Scientific, catalogue no. 10569069) supplemented with 10% fetal bovine serum (Axenia Biologix, catalogue no. F001). Cells were maintained in a humidified 37 °C incubator with 5% CO₂. SF9 insect cells (Expression Systems, catalogue no. 94-001S) were cultured in ESF 921 Insect Cell Culture Medium (Expression Systems, catalogue no. 96-001-01) at 27 °C with shaking (125 rpm).

Assessing AKT1 modification

For the results shown in Fig. 1c and Extended Data Fig. 1a, recombinant AKT1 (E17K), AKT1 (WT) or AKT2 (WT) (1 μM) was treated with DMSO or probes **1–3** (5 μM) in 25 mM HEPES (pH 8.0), 150 mM NaCl, 5 mM EDTA, 1 mM TCEP (Tris(2-carboxyethyl)phosphine) at 37 °C for 15 min and then reduced with NaBH₄ (10 mM, 5 min). The sample was diluted twofold with 50% MeCN, 0.5% trifluoroacetic acid (TFA) and analysed by intact-protein LC–MS (Waters Xevo G2-XS QToF). Data were acquired with an *m/z* scan range of 400–4,000, deconvoluted and quantified with Waters MassLynx (v.4.2) over a minimum of ten charge states, and plotted using GraphPad Prism (v.9.5.0).

For dissociation of preformed AKT–probe complexes (Fig. 1d and Extended Data Figs. 1b and 6c), AKT–probe complexes were preformed by incubating recombinant AKT1 (E17K), AKT1 (WT) or AKT2 (WT) (1 μM) with probes **1–4** (5 μM) in 25 mM HEPES (pH 8.0), 150 mM NaCl, 5 mM EDTA, 1 mM TCEP at 37 °C for 15 min. Dissociation was initiated by addition of ARQ092 (50 μM) with continuous incubation at 37 °C. Aliquots were removed at the indicated time points, quenched with NaBH₄ (10 mM, 5 min), diluted twofold in 50% MeCN, 0.5% TFA, and analysed by intact-protein LC–MS (Waters Xevo G2-XS QToF). Data were acquired with an *m/z* scan range of 400–4,000, deconvoluted and quantified with Waters MassLynx (v.4.2) over a minimum of ten charge states. The percentage modification was plotted versus time, and dissociation kinetics were determined using an exponential decay function in GraphPad Prism (v.9.5.0).

To determine the effects of Zn²⁺ on dissociation kinetics (Fig. 5d), the AKT1–**3** complex was preformed by incubating recombinant AKT1 (E17K or E17K, C296/310A, 1 μM) with **3** (5 μM) in 25 mM HEPES (pH 8.0), 150 mM NaCl, containing either 5 mM EDTA or 5 μM ZnSO₄ at 37 °C for 15 min. Dissociation was initiated by the addition of ARQ092 (50 μM) with continuous incubation at 37 °C. Aliquots were removed at the indicated time points and quenched with NaBH₄ (10 mM, 5 min) and then diluted

twofold in 50% MeCN, 0.5% TFA, and analysed by intact-protein LC–MS (Waters Xevo G2-XS QToF). Data were acquired with an *m/z* scan range of 400–4,000, deconvoluted and quantified with Waters MassLynx (v.4.2) over a minimum of ten charge states. The percentage modification was plotted versus time, and dissociation kinetics were determined using an exponential decay function in GraphPad Prism (v.9.5.0).

Modified site identification by tryptic LC–MS/MS

Recombinant AKT1 (WT or E17K, 2 μM, 40 μl) was treated with compound **3** (4 μM) in 25 mM HEPES (pH 8.0), 150 mM NaCl buffer at 37 °C for 15 min and then reduced with NaBH₄ (5 mM, 5 min). The solution was diluted with 40 μl of 20 mM Tris (pH 8.0) and 2 mM CaCl₂ buffer and sequentially incubated with dithiothreitol (DTT; 1 μl, 400 mM, 50 °C, 30 min), iodoacetamide (4 μl, 200 mM, room temperature, 15 min), DTT (2.1 μl, 400 mM, room temperature, 15 min) and then sequencing-grade trypsin/Lys-C mix (Thermo Fisher Scientific, catalogue no. A41007) (1 μl, 0.5 mg ml⁻¹, 37 °C, 18 h). The resulting peptides were acidified with 2 μl formic acid, desalted with C18 Omix Tips (Agilent, catalogue no. A57003100) and eluted with 50% MeCN, 0.1% formic acid. The samples were dried down by SpeedVac and then analysed by LC–MS/MS.

Tryptic peptides were reconstituted in 100 μl of 0.1% TFA in water and analysed with an Orbitrap Eclipse Tribrid Mass Spectrometer (Thermo Fisher Scientific) connected to an Ultimate 3000 RSLC nano system with 0.1% formic acid in H₂O as buffer A and 95% MeCN, 0.1% formic acid, as buffer B. Peptides (5 μl per injection) were separated on an EASY-Spray 3 mm, 75 μm × 15 cm C18 column (Thermo Fisher Scientific, catalogue no. ES800) with the following LC settings: flow rate of 0.3 μl min⁻¹, loading samples at 2% B for 12 min, then 2–31% B over 72 min and finally 31–53% B over 2 min. Data were acquired in a data-dependent mode. MS1 scans were acquired at a resolution of 120 K with a *m/z* scan range of 200–1,500, a maximum ion injection time of 50 ms, charge states of 2–7 and a 30 s dynamic exclusion time. MS2 spectra were acquired through higher-energy collisional dissociation at a collision energy of 30% in the orbitrap with an isolation width of 1.6 *m/z*.

The LC–MS/MS data were searched using FragPipe (v.19.1) with the MSFragger⁵⁰ (v.3.7) and IonQuant⁵¹ (v.1.8.10) modules against the AKT1 (E17K) and AKT1 (WT) sequences appended with decoy and common contaminant sequences. Methionine oxidation, protein N-terminal acetylation and lysine–compound **3** (+524.2324 Da) were set as variable modifications, whereas carbamidomethylation of cysteine was set as a static modification. Label-free quantification was applied, and ‘strictlytrypsin’ was selected as the digestion enzyme with a maximum of two missed cleavages. All other parameters were set as default.

Differential scanning fluorimetry

For the experiments shown in Fig. 1e and Extended Data Fig. 1c, recombinant AKT1 (E17K), AKT1 (WT) or AKT2 (WT) (2 μM) was treated with ARQ092 (10 μM), compound **3** (10 μM) or DMSO for 15 min in 25 mM HEPES (pH 8.0), 150 mM NaCl, 1 mM TCEP. After addition of SYPRO Orange (final concentration: 5×), the *T_m* was determined by measuring fluorescence (Bio-Rad C1000 Touch Thermal Cycler, FRET mode) over a temperature ramp (23–95 °C, 0.5 °C increments, 30 s per increment). The –d(fluorescence)/dT was plotted against *T*, and the minimum signal was used to define the *T_m*.

For the experiments shown in Extended Data Fig. 9b, recombinant AKT1 (WT, E17K or E17K, C296/310A) (2 μM) was treated with compound **3** (10 μM) or DMSO for 15 min in 25 mM HEPES (pH 8.0), 150 mM NaCl, 1 mM TCEP, in the presence or absence of ZnSO₄ (10 μM). After addition of SYPRO Orange (final concentration: 5×), the *T_m* was determined by measuring fluorescence (Bio-Rad C1000 Touch Thermal Cycler, FRET mode) over a temperature ramp (23–95 °C, 0.5 °C increments, 30 s per increment). The –d(fluorescence)/dT was plotted against temperature in GraphPad Prism (v.9.5.0), and the minimum signal was used to define the *T_m*.

Generation of BEAS-2B:FLAG–AKT stable cell lines

Plasmids for human AKT1 (residues 1–480) and AKT2 (residues 1–481) were obtained from Addgene (catalogue nos: 9021 and 86623, respectively). The E17K and C296/310A mutations were generated by site-directed mutagenesis. AKT1 and AKT2 were cloned by Gibson assembly⁵² into a pH lentiviral vector containing an CMV promoter, 3xFLAG tag and IRES-GFP. Lentivirus was generated by transfecting HEK293T cells in six-well dishes with lipid complexes containing 1.5 µg AKT plasmid, 1.35 µg pCMV-dR8.91, 165 ng pMD2-G and 7.5 µl Mirus TransIT-LT1 (VWR, catalogue no. 10767-118) diluted in OPTI-MEM. Virus-containing medium was collected after 48 h and used for infections without further processing. BEAS-2B cells at 70% confluence in 6 cm dishes were treated with 8 µg ml⁻¹ polybrene (Thermo Fisher Scientific, catalogue no. TR-1003-G) and 400 µl lentivirus. Forty-eight hours later, transduced cells were selected by addition of 2 µg ml⁻¹ puromycin (Invivogen, catalogue no. ant-pr-1) and incubated for 3 days. Afterwards, cells were trypsinized and passaged in complete growth medium.

Cellular thermal shift assay

For the experiments shown in Fig. 2a and Extended Data Fig. 2, a 15 cm dish containing confluent BEAS-2B cells (FLAG–AKT1 (E17K), FLAG–AKT1 (WT) or FLAG–AKT2 (WT)) was treated with DMSO, compound 3 (2 µM) or ARQ092 (2 µM), and incubated at 37 °C for 2 h. The medium was aspirated, and then the cells were trypsinized in 2 ml trypsin/EDTA. The trypsin was quenched with complete medium (8 ml), and the cells were pelleted and washed again with complete medium (8 ml). The medium was aspirated, and the cells (approximately 8 M) were resuspended in phosphate-buffered saline (PBS) 3 ml. The cells were aliquoted into PCR strips (100 µl per well) and heat-challenged for 3 min using a thermocycler (Eppendorf Nexus Gradient) at 12 temperatures from 35.0 to 77.5 °C. The cells were then freeze-thawed three times and clarified by centrifugation (21,000g, 15 min). The clarified lysates (60 µl) were mixed with 6X Laemmli sample buffer (20 µl) and heated at 95 °C for 5 min. Samples (2 µl) were loaded directly on to 0.45 µm nitrocellulose membranes (Bio-Rad, catalogue no. 1620115) for dot-blot analysis. The membranes were blocked with 2% bovine serum albumin (BSA) in Tris-buffered saline with Tween-20 (TBST) at room temperature for 30 min and then probed with anti-FLAG primary antibody (Sigma-Aldrich, catalogue no. F1804) at room temperature for 1 h and washed with TBST (3 × 5 min, room temperature). The secondary antibody (LI-COR, IRDye 800CW goat anti-mouse IgG, catalogue no. 926-32210) incubation was performed at room temperature for 1 h. The membranes were washed with TBST (3 × 5 min, room temperature), scanned on an Odyssey infrared imager (LI-COR Biosciences) and analysed with ImageJ (v.1.53k). The FLAG intensities were normalized against the 35.0 °C data point, plotted against temperature and fitted with a sigmoidal regression in GraphPad Prism (v.9.5.0) for derivation of the T_m .

For the experiments shown in Fig. 5e, a 15 cm dish containing confluent BEAS-2B cells (FLAG–AKT1 (E17K or E17K,C296/310A)) was cotreated with compound 3 (2 µM) and either TPEN (10 µM) or DMSO at 37 °C for 3 h. The medium was aspirated and the cells were trypsinized in 2 ml trypsin/EDTA. The trypsin was quenched with complete medium (8 ml), and the cells were pelleted and washed again with complete medium (8 ml). The medium was aspirated, and the cells (approximately 8 M) were resuspended in PBS (3 ml). The cells were aliquoted into PCR strips (100 µl per well) and heat-challenged for 3 min using a thermocycler (Eppendorf Nexus Gradient) over a temperature range (44.0–80.0 °C). The cells were then freeze-thawed three times and clarified by centrifugation (21,000g, 15 min). The clarified lysates (60 µl) were mixed with 6X Laemmli sample buffer (20 µl) and heated at 95 °C for 5 min. Samples (2 µl) were loaded directly on to 0.45 µm nitrocellulose membranes (Bio-Rad, catalogue no. 1620115) for dot-blot analysis. The membranes

were blocked with 2% BSA in TBST at room temperature for 30 min and then probed with anti-FLAG primary antibody (Sigma-Aldrich, catalogue no. F1804, 1:2500 dilution) at room temperature for 1 h before being washed with TBST (3 × 5 min, room temperature). The secondary antibody (LI-COR, IRDye 800CW goat anti-mouse IgG, catalogue no. 926-32210, 1:2500 dilution) incubation was performed at room temperature for 1 h. The membranes were washed with TBST (3 × 5 min, room temperature), scanned on an Odyssey infrared imager (LI-COR Biosciences) and analysed with ImageJ (v.1.53k). The FLAG intensities were plotted against temperature, fitted with a sigmoidal regression and normalized to the extrapolated upper plateau value in GraphPad Prism (v.9.5.0) for derivation of the T_m .

In-gel fluorescence analysis of 3-alkyne labelling

For the experiments shown in Fig. 2c, BEAS-2B cells (parental, FLAG–AKT1 (E17K), FLAG–AKT1 (WT) or FLAG–AKT2 (WT)) (in 1 ml medium, 12-well dish, 70% confluence) were pretreated with ARQ092 (5 µM) or DMSO for 15 min then treated with **3-alkyne** (2 µM) for 45 min (without washout of ARQ092 (5 µM) or DMSO). The medium was aspirated, and the cells were washed with PBS before being lysed in 100 µl of 0.1% NP-40, 50 mM HEPES (pH 8.0), 150 mM NaCl buffer. Freshly prepared NaBH₄ solution (5 µl, 100 mM) was added to each sample. The samples were clarified by centrifugation (21,000g, 20 min). A 20 µl aliquot of each sample was conjugated with TAMRA-azide for 1 h using 3.6 µl of click cocktail, resulting in a final concentration of 1 mM CuSO₄, 100 µM Tris((1-benzyl-4-triazolyl)methyl)amine (TBTA) (from a 2 mM stock prepared in 1:4 DMSO/t-butyl alcohol), 100 µM TAMRA-azide (Click Chemistry Tools, catalogue no. 1245-5), 1 mM TCEP and 1% sodium dodecyl sulfate (SDS). Each sample was treated with 6X Laemmli sample buffer (7 µl) and heated at 95 °C for 5 min. The samples were resolved by SDS polyacrylamide gel electrophoresis (SDS-PAGE) and scanned for TAMRA fluorescence (Typhoon Imaging System, Molecular Dynamics). The gels were then transferred to 0.45 µm nitrocellulose membranes (Bio-Rad, catalogue no. 1620115), followed by blocking with 2% BSA in TBST at room temperature for 30 min. Membranes were probed with anti-FLAG primary antibody (Sigma-Aldrich, catalogue no. F1804, 1:2500 dilution) at room temperature for 1 h and then washed with TBST (3 × 5 min, room temperature). The secondary antibody (LI-COR, IRDye 800CW goat anti-mouse IgG, catalogue no. 926-32210, 1:2500 dilution) incubation was performed at room temperature for 1 h. The membranes were washed with TBST (3 × 5 min, room temperature), scanned on an Odyssey infrared imager (LI-COR Biosciences) and visualized with ImageJ (v.1.53k).

For the experiments shown in Fig. 2d, BEAS-2B cells (FLAG–AKT1 (E17K), FLAG–AKT1 (WT) or FLAG–AKT2 (WT)) (in 1 ml media, 12-well dish, 70% confluence) were treated with increasing concentrations of **3-alkyne** for 6 h. The medium was aspirated, and the cells were washed with PBS before being lysed in 100 µl of 0.1% NP-40, 50 mM HEPES (pH 8.0), 150 mM NaCl buffer. Freshly prepared NaBH₄ solution (5 µl, 100 mM) was added to each sample. The samples were clarified by centrifugation (21,000g, 20 min). A 20 µl aliquot of each sample was clicked with TAMRA-azide for 1 h using 3.6 µl of click cocktail, resulting in a final concentration of 1 mM CuSO₄, 100 µM TBTA (from a 2 mM stock prepared in 1:4 DMSO/t-butyl alcohol), 100 µM TAMRA-azide (Click Chemistry Tools, catalogue no. 1245-5), 1 mM TCEP and 1% SDS. Each sample was treated with 6X Laemmli sample buffer (7 µl) and heated at 95 °C for 5 min. The samples were resolved by SDS-PAGE and scanned for TAMRA fluorescence (Typhoon Imaging System, Molecular Dynamics). The gels were then transferred to 0.45 µm nitrocellulose membranes (Bio-Rad, catalogue no. 1620115), followed by blocking with 2% BSA in TBST at room temperature for 30 min. Membranes were probed with anti-FLAG primary antibody (Sigma-Aldrich, catalogue no. F1804, 1:2500 dilution) at room temperature for 1 h and then washed with TBST (3 × 5 min, room temperature). The secondary antibody (LI-COR, IRDye 800CW goat anti-mouse IgG, catalogue no. 926-32210,

1:2500 dilution) incubation was performed at room temperature for 1 h. The membranes were washed with TBST (3×5 min, room temperature), scanned on an Odyssey infrared imager (LI-COR Biosciences) and quantified with ImageJ (v.1.53k). The fluorescence band intensity was normalized by the FLAG intensity, plotted against concentration and fitted with a sigmoidal regression in GraphPad Prism (v.9.5.0).

For the experiments shown in Fig. 2e, BEAS-2B cells (FLAG-AKT1(E17K), FLAG-AKT1(WT) or FLAG-AKT2(WT)) (in 1 ml media, 12-well dish, 70% confluence) were treated with **3-alkyne** (2 μ M for FLAG-AKT1(E17K) and FLAG-AKT1(WT), 10 μ M for FLAG-AKT2(WT)) for 4 h. The medium was aspirated and replaced with 1 ml medium containing 5 μ M ARQ092 to initiate washout. After 0, 0.25, 0.5, 1 or 3 h, the medium was aspirated, and the cells were washed with PBS before being lysed in 100 μ l of 0.1% NP-40, 50 mM HEPES (pH 8.0), 150 mM NaCl buffer. Freshly prepared NaBH₄ solution (5 μ l, 100 mM) was added to each sample. The samples were clarified by centrifugation (21,000g, 20 min). A 20 μ l aliquot of each sample was clicked with TAMRA-picolyl-azide for 1 h using 3.6 μ l of click cocktail, resulting in a final concentration of 1 mM CuSO₄, 100 μ M TBTA (from a 2 mM stock prepared in 1:4 DMSO/t-butyl alcohol), 100 μ M TAMRA-picolyl-azide (Click Chemistry Tools, catalogue no. 1254), 1 mM TCEP and 1% SDS. Each sample was treated with 6X Laemmli sample buffer (6 μ l) and heated at 95 °C for 5 min. The samples were resolved by SDS-PAGE and scanned for TAMRA fluorescence (Typhoon Imaging System, Molecular Dynamics). The gels were then transferred to 0.45 μ m nitrocellulose membranes (Bio-Rad, catalogue no. 1620115), followed by blocking with 2% BSA in TBST at room temperature for 30 min. Membranes were probed with anti-FLAG primary antibody (Sigma-Aldrich, catalogue no. F1804, 1:2500 dilution) at room temperature for 1 h and then washed with TBST (3×5 min, room temperature). The secondary antibody (LI-COR, IRDye800CW goat anti-mouse IgG, catalogue no. 926-32210, 1:2500 dilution) incubation was performed at room temperature for 1 h. The membranes were washed with TBST (3×5 min, room temperature), scanned on an Odyssey infrared imager (LI-COR Biosciences) and quantified with ImageJ (v.1.53k). The fluorescence band intensity was normalized by the FLAG intensity, plotted against time and fitted with an exponential decay in GraphPad Prism (v.9.5.0).

LAPC4-CR AKT1 (WT/E17K) zygosity determination

For genomic DNA isolation, amplicon PCR and sequencing (Extended Data Fig. 4a), a 35 mm dish of confluent LAPC4-CR cells was washed with PBS and lysed in 350 μ l QuickExtract DNA Extraction Solution (Lucigen, catalogue no. QE0905T). A 50 μ l aliquot of the extract was transferred into a PCR tube and heated sequentially to 65 °C (15 min), 68 °C (15 min) and 98 °C (10 min) on a thermocycler (Eppendorf Nexus Gradient), and the DNA concentration was measured to be 58 ng μ l⁻¹. An amplicon covering AKT1 exon 2 was generated by PCR using the following primers (forward: TGACCTCTAACTGTGGACGC; reverse: CAAGGGGATACTTACCGCGCC) using Phusion High-Fidelity DNA Polymerase (New England Biolabs) on a thermocycler (Eppendorf Nexus Gradient): 98 °C (130 s), 25× (98 °C (10 s), 58 °C (15 s), 72 °C (60 s)), 72 °C (5 min). The PCR product was purified using a QIAquick PCR Purification Kit (Qiagen, catalogue no. 28104), sequenced by QuintaraBio (sequencing primer: TCGCTGGCCCTAACGAAACAG) and analysed with SnapGene Viewer (v.6.2).

For RNA extraction, cDNA reverse transcription, transcript PCR and sequencing (Extended Data Fig. 4b), the RNA from a 35 mm dish of confluent LAPC4-CR cells was extracted using the RNeasy mini kit (Qiagen, catalogue no. 74104) protocol. In brief, the cells were washed with PBS, lysed in 250 μ l of RLT buffer and clarified by centrifugation (21,000g, 3 min), and the supernatant was treated with 300 μ l of 70% ethanol. The mixture was applied to an RNeasy column and washed sequentially with 700 μ l RWT buffer and 500 μ l RPE buffer. The RNA was eluted in 30 μ l of water to give 3.9 μ g of RNA. To generate cDNA from the RNA, a high-capacity cDNA Reverse Transcription Kit (Applied Biosystems, catalogue no. 4368814) was used. The transcription kit

reaction components were mixed with 1.3 μ g of RNA in a PCR tube (20 μ l final volume), and the transcription was performed on a thermocycler (Eppendorf Nexus Gradient) by heating sequentially to 25 °C (10 min), 37 °C (120 min) and 85 °C (5 min). An amplicon covering part of AKT1 transcript variant 4 was generated by PCR (forward primer: ATGGAC AGGGAGAGCAAACG; reverse primer: ACAGGTGGAAGAACAGCTCG) using Phusion High-Fidelity DNA Polymerase (New England Biolabs) on a thermocycler (Eppendorf Nexus Gradient): 98 °C (130 s), 25× (98 °C (10 s), 58 °C (15 s), 72 °C (60 s)), 72 °C (5 min). The PCR product was purified using a QIAquick PCR Purification Kit (Qiagen, catalogue no. 28104), sequenced by QuintaraBio (sequencing primer: TGCATCAGA GGCTGTGCCAG) and analysed with SnapGene Viewer (v.6.2).

3-alkyne target engagement in LAPC4-CR cells

LAPC4-CR cells (one confluent 10 cm dish per condition) were treated with DMSO or **3-alkyne** (1 μ M) at 37 °C for 2 h in triplicate. The cells were washed with PBS (Thermo Fisher Scientific, catalogue no. 10010049) and then lysed in 1 ml of 100 mM HEPES (pH 7.5), 150 mM NaCl, 0.1% NP-40 buffer containing the complete EDTA-free protease inhibitor cocktail (Sigma-Aldrich, catalogue no. 11873580001). Lysates were clarified by centrifugation (16,000g, 4 °C, 15 min), and then imine reduction was performed by adding 10 mM NaBH₄ for 30 min on ice. Protein concentrations were quantified by BCA assay (Thermo Fisher, catalogue no. 23225) and normalized to 1 mg ml⁻¹. For each sample, 1 ml of lysate was taken forward for pull-down western blot analysis (Fig. 3a), and another 1 ml of lysate was taken forward for pull-down tryptic mass spectrometry analysis (Fig. 3b).

For the pull-down western blot (Fig. 3a), lysates (1 ml) were incubated with 25 μ l of high-capacity NeutrAvidin agarose beads (Thermo Fisher Scientific, catalogue no. 29204) at 4 °C for 1 h to remove endogenous biotinylated proteins. Beads were removed by filtration using Mini Bio-Spin columns (Bio-Rad, catalogue no. 7326207). The supernatants were reacted with 102 μ l of click chemistry cocktail, resulting in a final concentration of 1% SDS, 100 μ M biotin-picolyl azide, 1 mM TCEP, 100 μ M TBTA (from a 2 mM stock prepared in 1:4 DMSO/t-butyl alcohol) and 1 mM CuSO₄. After incubation at room temperature for 90 min, the proteins were precipitated by addition of 10 ml of prechilled acetone and incubation overnight at -20 °C. The precipitated proteins were pelleted by centrifugation (4,000g, 4 °C, 20 min), resuspended in cold MeOH and repelleted. The pellets were solubilized in 10% SDS in PBS, diluted to a final detergent concentration of 0.6% SDS, 1.0% NP-40, in PBS and then incubated with 40 μ l of high-capacity NeutrAvidin agarose beads (Thermo Fisher Scientific, catalogue no. 29204) for 2 h at 4 °C. The beads were then transferred to Mini Bio-Spin columns (Bio-Rad, catalogue no. 7326207) and washed with 1% NP-40, 0.1% SDS in PBS (6 × 1 ml). The beads were transferred to microcentrifuge tubes and eluted by addition of 50 μ l of 6X Laemmli sample buffer with heating to 95 °C for 5 min. Samples were resolved by SDS-PAGE and transferred to 0.45 μ m nitrocellulose membranes (Bio-Rad, catalogue no. 1620115), followed by blocking with 2% BSA in TBST at room temperature for 30 min. Membranes were then incubated with primary antibodies (AKT1: Cell Signaling Technology, catalogue no. 2938, 1:1,000 dilution; AKT2: Cell Signaling Technology, catalogue no. 3063, 1:1,000 dilution) at 4 °C overnight and washed with TBST (3×5 min, room temperature). Secondary antibody (LI-COR, IRDye 800CW goat anti-rabbit IgG, catalogue no. 926-32211, 1:10,000 dilution) incubation was performed at room temperature for 1 h. Membranes were washed with TBST (3×5 min, room temperature), scanned on an Odyssey infrared imager (LI-COR Biosciences) and analysed with ImageJ (v.1.53k).

For the pull-down tryptic mass spectrometry (Fig. 3b), lysates (1 ml) were incubated with 25 μ l of settled high-capacity NeutrAvidin agarose beads (Thermo Fisher Scientific, catalogue no. 29204) at 4 °C for 1 h to remove endogenous biotinylated proteins. Beads were removed by filtration using Mini Bio-Spin columns (Bio-Rad, catalogue no. 7326207). The supernatants were reacted with 102 μ l of click chemistry cocktail,

Article

resulting in a final concentration of 1% SDS, 100 μ M biotin-picolyl azide, 1 mM TCEP, 100 μ M TBTA (from a 2 mM stock prepared in 1:4 DMSO/*t*-butyl alcohol) and 1 mM CuSO₄. After incubation at room temperature for 90 min, the proteins were precipitated by addition of 10 ml of prechilled acetone and incubation overnight at -20 °C. The precipitated proteins were pelleted by centrifugation (4,000g, 4 °C, 20 min), resuspended in cold MeOH and repelleted. The pellets were solubilized in 10% SDS in PBS, diluted to a final detergent concentration of 0.6% SDS, 1.0% NP-40, in PBS and then incubated with 40 μ l of settled high-capacity NeutrAvidin agarose beads (Thermo Fisher Scientific, catalogue no. 29204) for 2 h at 4 °C. The beads were then transferred to Mini Bio-Spin columns (Bio-Rad, catalogue no. 7326207) and washed sequentially with 1% NP-40, 0.1% SDS in PBS (6 \times 1 ml), PBS + 5 mM TCEP (3 \times 1 ml), PBS + 10 mM iodoacetamide (2 \times 1 ml), PBS + 5 mM TCEP (2 \times 1 ml), PBS (2 \times 1 ml) and finally digestion buffer (1 ml; 100 mM HEPES (pH 8.0), 2 mM CaCl₂). The beads were transferred to microcentrifuge tubes and resuspended in 50 μ l digestion buffer. On-bead digestion was performed at 37 °C overnight by adding 1 μ g sequencing-grade trypsin/Lys-C mix (Thermo Fisher Scientific, catalogue no. A41007). The beads were pelleted by centrifugation, and the supernatant was removed. The beads were further washed with 50 μ l digestion buffer, and the supernatants were combined. The resulting peptides were acidified with 2 μ l formic acid, desalted with C18 Omix Tips (Agilent, catalogue no. A57003100) and eluted with 50% MeCN, 0.1% formic acid. The samples were dried down by SpeedVac for TMT labelling. TMT labelling was performed with the TMT 6-plex kit (Thermo Scientific, catalogue no. 90061) according to the manufacturer's instructions with minor modifications. Briefly, peptides were reconstituted in 10 μ l of 30% MeCN in 200 mM HEPES buffer (pH 8.5). TMT reagents were reconstituted in 20 μ l of MeCN per vial, and 1.3 μ l of this stock solution was added to each sample for 1 h at room temperature. Reactions were quenched by adding 1.2 μ l of 5% hydroxylamine and incubated at room temperature for 15 min, followed by addition of 1.3 μ l of 5% TFA to acidify the solution. TMT-labelled samples were pooled, dried by SpeedVac and desalted using C18 Omix Tips (Agilent, catalogue no. A57003100). Peptides were eluted with 50% MeCN and 0.1% TFA and dried by SpeedVac. Samples were analysed by LC-MS/MS.

LC-MS/MS analysis of TMT-labelled samples

TMT-labelled tryptic peptides were reconstituted in 70 μ l of 5% DMSO, 0.1% TFA in water and analysed on a Orbitrap Eclipse Tribrid Mass Spectrometer (Thermo Fisher Scientific) connected to an Ultimate 3000 RSLC nano system with 0.1% formic acid in H₂O as buffer A and 95% MeCN, 0.1% formic acid as buffer B. Peptides (5 μ l per injection, two injections) were separated on an EASY-Spray 3 mm, 75 μ m \times 15 cm C18 column (Thermo Fisher Scientific, catalogue no. ES800) with the following LC settings: flow rate of 0.3 μ l min⁻¹, loading samples at 4% B for 20 min, then 4–7% B over 5 min, 7–35% B over 130 min, 35–95% B over 5 min and finally 95% B for 10 min. Data were acquired in a data-dependent mode. MS1 scans were acquired at a resolution of 120K with a *m/z* scan range of 400–1,600, a maximum ion injection time of 50 ms, charge states of 2–6, and a 60 s dynamic exclusion time. MS2 spectra were acquired through collision-induced dissociation at a collision energy of 35%, in the ion trap with an AGC target of 1e4, isolation width of 0.7 *m/z* and maximum ion injection time set to 'auto'. For real-time search, MS2 spectra were searched against the *Homo sapiens* reviewed Swiss-Prot FASTA database with the digestion enzyme set to trypsin. Methionine oxidation was set as a variable modification, whereas carbamidomethylation of cysteine and TMT modification were set as constant modifications. For MS3 acquisition, a synchronous precursor selection of ten fragments was acquired in the orbitrap for a maximum ion injection time of 105 ms with an AGC target of 1.5e5. MS3 spectra were collected at a resolution of 50K with higher-energy collisional dissociation collision energy of 55%.

The LC-MS/MS data were searched using MaxQuant⁵³ (v.1.6.7.0) against the HUMAN reviewed Swiss-Prot FASTA database. Under 'Group-specific parameters', 'type' was set as 'Reporter ion MS3', 'Isobaric labels' was set as '6plex TMT' and the reporter ion isotopic distributions were incorporated to correct for impurities during synthesis of the TMT reagents according to the manufacturer's specifications. Methionine oxidation and protein N-terminal acetylation were set as variable modifications, whereas carbamidomethylation of cysteine was set as a static modification. Trypsin was selected as the digestion enzyme with a maximum of two missed cleavages. All other parameters were set as default. Modified sites with localization probability \geq 0.75 were selected for further analysis. For TMT 6-plex samples, TMT intensities in each channel were normalized such that the median TMT intensity values (based on all modified sites) were equivalent across all six channels.

3-alkyne target engagement in LAPC4-CR xenografts

Specific-pathogen-free homozygous male athymic nude mice were used (Envigo). The animal study was approved by the Institutional Animal Care and Use Committee (IACUC) of Terremoto Biosciences. LAPC4-CR cells (1×10^6) were mixed with 70% Matrigel and subcutaneously implanted to the flank area of the animals (0.1 ml per mouse). Tumours were grown to a size of \geq 180 mm³ before dosing. Compound **3-alkyne** was formulated in a vehicle consisting of 5% (v/v) DMSO, 20% (v/v) PEG400, 20% (v/v) Cremophor EL and 55% (v/v) water immediately before dosing. A single dose of **3-alkyne** at 30 mg kg⁻¹ or vehicle was administered to mice by i.p. injection ($n = 4$). Mice were euthanized 4 h after administration, and tumours were subsequently collected and flash-frozen in liquid nitrogen.

Tumour tissues (75–125 mg) were homogenized using a Tissue-Tearor (BioSpec model 985370-395) on ice in 1 ml of buffer comprising 100 mM HEPES (pH 7.5), 150 mM NaCl, 0.1% NP-40 with phosphatase inhibitors (5 mM sodium fluoride, 1 mM sodium pyrophosphate, 1 mM β -glycerophosphate, 1 mM sodium orthovanadate) and complete EDTA-free protease inhibitor cocktail (Sigma-Aldrich, catalogue no. 11873580001). Proteins were clarified by centrifugation (21,000g, 4 °C, 10 min). Protein concentrations were quantified by BCA and normalized to 1 mg ml⁻¹. Tumour lysates (1 ml) were treated with 55 μ l of 100 mM NaBH₄ in PBS and further clarified by centrifugation (21,000g, 4 °C, 1 h). Each aliquot was treated with 180 μ l of click chemistry cocktail, resulting in a final concentration of 1% SDS, 100 μ M biotin-picolyl azide, 1 mM TCEP, 100 μ M TBTA (from a 2 mM stock prepared in 1:4 DMSO/*t*-butyl alcohol) and 1 mM CuSO₄. After incubation at room temperature for 90 min, the proteins were precipitated using acetone (10 ml) at -20 °C overnight. After centrifugation (21,000g, 4 °C, 15 min), the pellets were washed with cold methanol and repelleted. The pellets were solubilized by sonication in 20% SDS in PBS (75 μ l) at 37 °C, diluted to a final detergent concentration of 1% SDS, 1% NP-40 in PBS and clarified by centrifugation (21,000g, 4 °C, 30 min). The lysate (900 μ l) was incubated with 30 μ l of high-capacity NeutrAvidin agarose beads (Thermo Fisher Scientific, catalogue no. 29204) overnight at 4 °C. The beads were then transferred to Mini Bio-Spin columns (Bio-Rad, catalogue no. 7326207) and washed with 1% NP-40, 0.1% SDS in PBS (6 \times 0.5 ml). The beads were transferred to microcentrifuge tubes and eluted by addition of 70 μ l of 6X Laemmli sample buffer with heating to 95 °C for 5 min. Samples were resolved by SDS-PAGE and transferred to 0.45 μ m nitrocellulose membranes (Bio-Rad, catalogue no. 1620115) followed by blocking with 2% BSA in TBST at room temperature for 30 min. Membranes were then incubated with primary antibodies (AKT1: Cell Signalling Technology, catalogue no. 2938, 1:1,000 dilution; AKT2: Cell Signalling Technology, catalogue no. 3063, 1:1,000 dilution) at 4 °C overnight and washed with TBST (3 \times 5 min, room temperature). Secondary antibody (LI-COR, IRDye 800CW goat anti-rabbit IgG, catalogue no. 926-32211, 1:10,000 dilution) incubation was performed at room temperature for 1 h. Membranes were washed with TBST (3 \times 5 min, room temperature), scanned on

an Odyssey infrared imager (LI-COR Biosciences) and analysed with ImageJ (v.1.53k).

Generation of LAPC4-CR stable cell lines

AKT1 (WT) was cloned by Gibson assembly⁴ into a pHRLentiviral vector containing a CMV promoter, 3xFLAG tag and IRES-GFP (see ‘Generation of BEAS-2B: FLAG-AKT stable cell lines’). An N-terminal myristylation sequence (MGSSKSKPKDPSQR) was introduced by PCR. The ‘empty vector’ control comprised the pHRLentiviral vector containing a CMV promoter and GFP. Lentivirus was generated by transfecting HEK293T cells in six-well dishes with lipid complexes containing 1.5 µg pHRL plasmid, 1.35 µg pCMV-dR8.91, 165 ng pMD2-G and 7.5 µl of Mirus TransIT-LT1 (VWR, catalogue no. 10767-118) diluted in OPTI-MEM. Virus-containing medium was collected after 48 h and used for infections without further processing. LAPC4-CR cells at 70% confluence in 6 cm dishes were treated with 8 µg ml⁻¹ polybrene (Thermo Fisher Scientific, catalogue no. TR-1003-G) and 800 µl lentivirus and centrifuged for 30 min (840g, 37 °C). After 72 h incubation at 37 °C, transduced cells were selected by addition of 5 µg ml⁻¹ puromycin (Invivogen, catalogue no. ant-pr-1) and incubated for 7 days. Afterwards, cells were trypsinized and passaged in complete growth medium.

Cell viability assay

For experiments shown in Fig. 3c,f, Cells (10,000 LAPC4-CR cells per well, 5000 SkBr3 cells per well) were seeded into white 96-well plates (CELLSTAR, catalogue no. 655083) in 120 µl media and incubated overnight to adhere. Inhibitor dilutions were prepared at 10× in medium with 1% DMSO. Inhibitor dilutions (13.3 µl) were added to each well (final DMSO concentration: 0.1%) and incubated at 37 °C for 72 h. Alamar blue (14.8 µl, 1 mg ml⁻¹ in water) was added to each well, followed by incubation at 37 °C for 90 min. Fluorescence intensity (excitation/emission: 540/580 nm) was read using a CLARIOstar Plus plate-reader (BMG Labtech), and the percentage cell viability was derived by normalization against the maximum signal. The cell viability was plotted against inhibitor concentration, and the EC₅₀ value was determined using sigmoidal regression in GraphPad Prism (v.9.5.0).

Western blot biomarker analysis

For the dose–response experiments shown in Fig. 3d and Extended Data Fig. 5a, cells (0.5 M per well, SkBr3, LAPC4-CR, HBCx-2 and MCF7) were seeded in 12-well dishes. The adhered cells were treated with a dose of compound 3 or ARQ092 for 2 h at 37 °C. The cells were washed with PBS (Thermo Fisher Scientific, catalogue no. 10010049) and lysed in 0.1% NP-40, 50 mM HEPES (pH 8.0), 150 mM NaCl + phosphatase inhibitors (5 mM NaF, 1 mM sodium pyrophosphate, 1 mM β-glycerophosphate, 1 mM sodium orthovanadate). The lysates were clarified by centrifugation (21,000g, 4 °C, 20 min). The clarified lysates (60 µl) were mixed with 20 µl of 6X Laemmli sample buffer, heated to 95 °C for 5 min and analysed by western blotting.

For the washout shown in Extended Data Fig. 5b, cells (0.5 M per well, SkBr3 or LAPC4-CR) were seeded in 12-well dishes. The adhered cells were treated with compound 3 (2 µM) for 2 h at 37 °C. The medium was replaced with compound-free medium to initiate washout. After 0, 0.33, 1, 3, 8 or 24 h, the cells were washed with PBS (Thermo Fisher Scientific, catalogue no. 10010049) and lysed in 0.1% NP-40, 50 mM HEPES (pH 8.0), 150 mM NaCl + phosphatase inhibitors (5 mM NaF, 1 mM sodium pyrophosphate, 1 mM β-glycerophosphate, 1 mM sodium orthovanadate). The lysates were clarified by centrifugation (21,000g, 4 °C, 20 min). The clarified lysates (60 µl) were mixed with 20 µl of 6X Laemmli sample buffer, heated to 95 °C for 5 min and analysed by western blotting.

For the western blot analysis, samples were resolved by SDS-PAGE and transferred to 0.45 µm nitrocellulose membranes (Bio-Rad, catalogue no. 1620115), followed by blocking with 2% BSA in TBST at room temperature for 30 min. Membranes were then incubated with

primary antibodies (AKT1: Cell Signaling Technology, catalogue no. 2938, 1:1,000 dilution; pAKT1 (pS473): Cell Signaling Technology, catalogue no. 9018, 1:1,000 dilution; PRAS40: Cell Signaling Technology, catalogue no. 2691, 1:1,000 dilution; pPRAS40 (pT246): Cell Signaling Technology, catalogue no. 29971, 1:1,000 dilution; tS6RP: Cell Signaling Technology, catalogue no. 2317, 1:1,000 dilution; pS6RP (pS235/236): Cell Signaling Technology, catalogue no. 4858, 1:1,000 dilution; tGSK3b: Cell Signaling Technology, catalogue no. 12456, 1:1,000 dilution; pG3K3b (pS9): Cell Signaling Technology, catalogue no. 5558, 1:1,000 dilution; GAPDH: Santa Cruz Biotechnology, catalogue no. 32233, 1:1,000 dilution) at 4 °C overnight and washed with TBST (3 × 5 min, room temperature). Secondary antibody (LI-COR, IRDye 800CW goat anti-rabbit IgG, catalogue no. 926-32211, 1:10,000 dilution; LI-COR, IRDye 680RD goat anti-rabbit IgG, catalogue no. 926-68071, 1:10,000 dilution; LI-COR, IRDye 680RD goat anti-mouse IgG, catalogue no. 926-68070, 1:10,000 dilution) incubation was performed at room temperature for 1 h. Membranes were washed with TBST (3 × 5 min, room temperature), scanned on an Odyssey infrared imager (LI-COR Biosciences) and analysed with ImageJ (v.1.53k).

Pharmacokinetics

For the experiments shown in Extended Data Fig. 6c, all mouse manipulations were performed in accordance with the IACUC of Pharmaron. Male nude mice (nu/nu) were treated once with compound 3 or 4 (formulated in 5% (v/v) DMSO, 20% (v/v) PEG400, 20% (v/v) Cremophor EL and 55% (v/v) water), at a dose of 30 mg kg⁻¹ by i.p. injection (*n* = 3). Blood plasma was sampled at 0.25, 0.5, 1, 2, 4, 6, 8, 12 and 24 h postdose. To a 20 µl aliquot of plasma, 30 µl of 4% formic acid was added, followed by shaking for 20 s. The samples were incubated at 50 °C for 10 min and then mixed with 100 µl of 5 mM ammonium acetate in 90% acetonitrile with 0.1% acetic acid containing carbamazepine or dexamethasone as internal standard. The mixture was shaken for 15 min and subsequently centrifuged (3,220g, 15 min). The analyte concentration in the supernatant was determined by MRM (LC–MS/MS), and pharmacokinetic parameters were calculated (mean, *n* = 3). Analyte separation was performed using a DGU-20A5R HPLC (Shimadzu) equipped with a HALO 90A AQ-C18 (2 µm, 3 × 30 mm) column using a 5–95% gradient of MeCN in water (+0.1% FA). Mass analysis was performed using an API 4000 Triple Quad mass spectrometer (Applied Biosystems).

Cellular NanoBRET

Live cell target engagement assays were performed as described according to a published protocol³⁸ with minor modifications. HEK293 cells were transfected (Promega FuGene, catalogue no. E2311) with plasmids encoding full-length AKT1 (E17K), AKT1 (WT) and AKT2 (WT) kinase-NanoLuciferase fusion proteins (Promega, catalogue nos: NV2411, NV2421, NV1031). Cells were then treated with serial dilutions of compound and 300 nM (approximate EC₅₀ concentration) of fluorescently tagged ATP-competitive tracer (Promega, tracer K-10, catalogue no. N2840). After incubation for 2 h at 37 °C, luciferase substrate and extracellular luciferase inhibitor were added to all wells, and luminescent intensity at 460 nm and 600 nm were measured on a multimode plate-reader (PerkinElmer Envision). The E₆₀₀/E₄₆₀ ratio was calculated to give the tracer engagement signal (BRET). Half-maximal inhibitory concentration values were calculated by fitting BRET values to a log(inhibitor) versus response Hill equation.

LAPC4-CR tumour biomarker study

All mouse manipulations were performed in accordance with the IACUC of the University of California, San Francisco. LAPC4-CR cells (1 × 10⁶) were implanted into athymic male nude mice (nu/nu) at 8 weeks old. Tumours were grown to a size of ≥400 mm³ before dosing. Compound 4 was formulated in a vehicle consisting of 10% (v/v) DMSO, 20% (v/v) PEG400, 20% (v/v) Cremophor EL and 50% (v/v) water immediately before dosing. A single dose of compound 4 at 40 mg kg⁻¹ or vehicle was

Article

administered to mice by i.p. injection (dose volume: 10 ml kg⁻¹). Euthanasia was performed 2, 7 or 24 h after administration, and tumours were subsequently collected and flash-frozen in liquid nitrogen.

Tumour tissues (75–125 mg) were homogenized using a Tissue-Tearor (BioSpec model 985370-395) on ice in 1 ml of buffer comprising 100 mM HEPES (pH 7.5), 150 mM NaCl, 0.1% NP-40 with phosphatase inhibitors (5 mM sodium fluoride, 1 mM sodium pyrophosphate, 1 mM β-glycerophosphate, 1 mM sodium orthovanadate) and the EDTA-free complete EDTA-free protease inhibitor cocktail (Sigma-Aldrich, catalogue no. 11873580001). Proteins were clarified by centrifugation (21,000g, 4 °C, 30 min). Protein concentrations were quantified by BCA and normalized to 5 mg ml⁻¹. Aliquots (150 µl) of each lysate were mixed with 50 µl of 6X Laemmli sample buffer and heated to 95 °C for 5 min. Samples were resolved by SDS-PAGE and transferred to 0.45 µm nitrocellulose membranes (Bio-Rad, catalogue no. 1620115), followed by blocking with 2% BSA in TBST at room temperature for 30 min. Membranes were then incubated with primary antibodies (AKT1: Cell Signaling Technology, catalogue no. 2938, 1:1,000 dilution; pAKT1 (pS473): Cell Signaling Technology, catalogue no. 9018, 1:1,000 dilution; PRAS40: Cell Signaling Technology, catalogue no. 2691, 1:1,000 dilution; pPRAS40 (pT246): Cell Signaling Technology, catalogue no. 2997, 1:1,000 dilution; GAPDH: Santa Cruz Biotechnology, catalogue no. 32233, 1:1,000 dilution) at 4 °C overnight and washed with TBST (3 × 5 min, room temperature). Secondary antibody (LI-COR, IRDye 800CW goat anti-rabbit IgG, catalogue no. 926-32211:10,000 dilution; LI-COR, IRDye 680RD goat anti-rabbit IgG, catalogue no. 926-68071, 1:10,000 dilution; LI-COR, IRDye 680RD goat anti-mouse IgG, catalogue no. 926-68070, 1:10,000 dilution) incubation was performed at room temperature for 1 h. Membranes were washed with TBST (3 × 5 min, room temperature), scanned on an Odyssey infrared imager (LI-COR Biosciences) and analysed with ImageJ (v.1.53k).

Tumour growth inhibition studies

LAPC4-CR CDX model. Specific-pathogen-free homozygous male athymic nude mice were used (Envigo). Mice were given food and water ad libitum and housed in microisolator cages under specific-pathogen-free conditions with a controlled light–dark cycle (12 h circadian cycle of artificial light) and controlled room temperature and humidity (30–70%). Animals (6 to 8 weeks old) were tagged with microchips (RapID Lab) for identification. The animal study was approved by the IACUC of Terremoto Biosciences. LAPC4-CR cells were mixed with 70% Matrigel and subcutaneously implanted into the flank area of the animals (0.1 ml per mouse). Tumour growth and body weight were measured twice per week after cell implantation. For experiments shown in Fig. 4a, when the tumour size reached approximately 180 mm³, mice were randomized into two groups. Compound 4, formulated in 5% (v/v) DMSO, 20% (v/v) PEG400, 20% (v/v) Cremophor EL and 55% (v/v) water, was administered by i.p. injection at a dose of 30 mg kg⁻¹ to 12 mice, and a vehicle control was administered to ten mice, using a twice-daily regimen for 5 days per week over the course of 3 weeks, with a dosing volume of 10 ml kg⁻¹. For experiments shown in Extended Data Fig. 7d, when the tumour size reached approximately 180 mm³, mice were randomized into two groups: ARQ092 (ten mice) or vehicle control (ten mice). ARQ092, formulated in 10% (v/v) N,N-dimethylacetamide (DMA) and 90% (v/v) water, at a dose of 100 mg kg⁻¹ or a vehicle control was administered orally (p.o.) using a once-daily regimen. The humane end point was 20% body weight loss, and the entire ARQ092 arm was terminated when 50% of the animals in the group reached this threshold.

HBCx-2 PDX model. Specific-pathogen-free homozygous female athymic nude mice were used (Envigo). Mice were given food and water ad libitum and housed in individually ventilated cages under specific-pathogen-free conditions with a controlled light–dark cycle (12 h circadian cycle of artificial light) and controlled room temperature and humidity (30–70%). All animals were identified by a unique pattern

using an RFID chip numbering system. The animal study was performed in accordance with French legislation concerning the protection of laboratory animals and in accordance with a valid license for experiments on vertebrate animals, issued by the French Ministry of Higher Education, Research and Innovation (APAFIS#29136-2020121415204532v1). The HBCx-2 triple-negative breast cancer patient-derived xenograft model (homozygous AKT1 E17K mutation)⁵⁴ was passaged from donor tumours when tumours reached 1800 mm³. Tumours were cut into fragments of approximately 20 mm³ and implanted into the interscapular area of the animals at 6 weeks of age. Mice were randomized into three groups with eight mice per group. Compound 4, formulated in 5% (v/v) DMSO, 20% (v/v) PEG400, 20% (v/v) Cremophor EL and 55% (v/v) water, was administered by i.p. injection at a dose of 20 or 30 mg kg⁻¹, along with a vehicle control, using a twice-daily regimen for 21 consecutive days, with a dosing volume of 10 ml kg⁻¹.

BT-474 CDX model. Specific-pathogen-free female BALB/c nude mice 6–8 weeks old (Vital River) were used. Mice were given food and water ad libitum and housed in individually ventilated cages under specific-pathogen-free conditions with a controlled light–dark cycle (12 h circadian cycle of artificial light) and controlled room temperature and humidity (30–70%). Animals were identified with cage cards and ear tags. This animal study was approved by the IACUC of GenenDesign. BT-474 cells were cultured in DMEM with 10% fetal bovine serum. Each mouse received 5 × 10⁶ cells in medium mixed 1:1 with Matrigel at a total volume of 100 µl. Three days before cell implantation, 17β-estradiol pellets (0.25 mg, 60-day release, made in-house with Beewax) were implanted into mice subcutaneously at the back/neck area. When tumours reached 155–219 mm³ in volume, mice were randomized into four groups with ten mice in each group and treated as follows: vehicle (5% (v/v) DMSO, 20% (v/v) PEG400, 20% (v/v) Cremophor EL and 55% (v/v) water), twice daily (b.i.d.), i.p.; compound 4, formulated in 5% (v/v) DMSO, 20% (v/v) PEG400, 20% (v/v) Cremophor EL and 55% (v/v) water at 30 mg kg⁻¹, b.i.d., i.p.; ARQ092, formulated in 10% (v/v) DMA, 90% (v/v) water at 100 mg kg⁻¹, p.o., every day; or capivasertib, formulated in 10% (v/v) DMSO, 22.5% (w/w) (2-hydroxypropyl)-β-cyclodextrin, 67.5% (v/v) water at 150 mg kg⁻¹, b.i.d., p.o. All treatments were administered for 21 consecutive days.

Antitumour activity was assessed by tumour growth inhibition (TGI). TGI was defined as $(1 - \Delta T/\Delta C) \times 100$, where $\Delta T/\Delta C$ is the ratio of the change in mean tumour volume of the treated group (ΔT) and that of the control group (ΔC). TGI was determined on the basis of the last measurement when all the animals in the vehicle group still survived.

The maximal tumour size end point permitted by the IACUC protocols was when tumour size exceeded 20 mm in any one direction, when tumours interfered with normal behaviour, or when ulceration or necrosis occurred (these limits were not exceeded in any of the experiments). Animals were euthanized if their body weight loss reached 20% or they reached a body condition score of 2 or less.

Blood glucose study

Eight-week-old male athymic nude mice (Envigo) were used to assess blood glucose levels. Before the study, animals were quarantined for at least 7 days and had free access to a normal diet throughout the study period. Five mice per group were treated once with the i.p. vehicle (5% (v/v) DMSO, 20% (v/v) PEG400, 20% (v/v) Cremophor EL and 55% (v/v) water), p.o. vehicle (10% (v/v) DMA, 90% (v/v) water), compound 4 at a dose of 30 mg kg⁻¹ (i.p.) or ARQ092 at a dose of 50 or 100 mg kg⁻¹ (p.o.). Blood samples were collected by tail vein lancet puncture at various time points: 0, 1, 2, 4, 8 and 24 h post-treatment. Blood glucose concentrations were measured using an Accu-Chek Guide (Roche).

Data are reported as mean ± s.d. To calculate the statistical significance of differences between the treatment group and corresponding vehicle group, a two-way repeat-measurement analysis of variance with

Holm–Šídák's multiple comparisons test was used. All animal studies were approved by the IACUC of Terremoto Biosciences.

FLAG–AKT1 immunoprecipitation for ICP–MS analysis

FLAG–AKT1 Immunoprecipitation. BEAS-2B cells (FLAG–AKT1 (E17K) or FLAG–AKT1 (E17K,C296/310 A); 2× confluent 15 cm dishes of cells per condition) were treated with DMSO or compound 3 (2 μM, 2 h) (four replicates per condition). All buffers were pretreated with Chelex 100 resin (Bio-Rad, catalogue no. 1421253, 20 g l⁻¹) and then filtered to remove trace metal impurities. After probe treatment, the cells were washed with PBS (Thermo Fisher Scientific, catalogue no. 10010049) and then lysed in 1.6 ml of 0.1% NP-40, 50 mM HEPES (pH 8.0), 150 mM NaCl buffer. The lysates were clarified by centrifugation (20,000g, 4 °C, 10 min), transferred to clean microcentrifuge tubes and incubated with 35 μl settled anti-FLAG-agarose (GenScript, catalogue no. L00432S) for 1 h at 4 °C. The beads were transferred to Mini Bio-Spin columns (Bio-Rad, catalogue no. 7326207) and then washed six times with 1 ml of 30 mM HEPES (pH 7.5), 150 mM NaCl buffer. FLAG–AKT1 was eluted by incubating the beads three times with 3xFLAG peptide (50 μl, 1.0 mg ml⁻¹, 15 min, 30 °C) (ApexBio, catalogue no. A6001). The eluates (150 μl total) were incubated with 2.5 mg of Chelex 100 resin (Bio-Rad, catalogue no. 1421253) and incubated for 15 min at room temperature. The resin was removed by filtration using Mini Bio-Spin columns (Bio-Rad, catalogue no. 7326207), and the flow-through was concentrated to approximately 56 μl using Amicon Ultra-0.5 10 kDa MWCO Centrifugal Filter Units (Millipore, catalogue no. UFC501096). A 6 μl aliquot was treated with 6 μl 2X Laemmli sample buffer and heated to 95 °C for 5 min, and the concentration of AKT1 was determined by SDS–PAGE with Flamingo staining. The remaining 50 μl was frozen and stored at –80 °C for analysis by ICP–MS.

AKT1 concentration determination. Recombinant AKT1 (E17K) was titrated from 9.6–0.04 μM (concentration determined by Nanodrop A280) in 25 mM HEPES (pH 8.0), 150 mM NaCl buffer. A 6 μl aliquot of each standard was treated with 6 μl 2X Laemmli sample buffer and heated to 95 °C for 5 min. Samples (10 μl) and standards (10 μl) were resolved by SDS–PAGE and fixed in a solution of 40% EtOH, 10% acetic acid at room temperature for 2 h. The gel was stained with Flamingo fluorescent gel stain (Bio-Rad, catalogue no. 161-0491) at room temperature for 3 h and then scanned for Flamingo fluorescence (Typhoon Imaging System, Molecular Dynamics). The relative band intensities were analysed with ImageJ (v.1.53k) and used to determine FLAG–AKT1 concentrations.

ICP–MS analysis

Sample preparation. Samples (50 μl) were transferred to 15 ml metal-free polypropylene tubes (VWR, catalogue no. 89049-170) and diluted with 1,650 μl of 1% HNO₃ (trace metal grade, Thermo Fisher Scientific, catalogue no. A509P500).

Control/standard preparation. A National Institute of Standards and Technology (NIST) standard reference material (SRM) 1683f was prepared at 8× dilution (3.5 ml of 1% HNO₃ + 500 μl of NIST SRM 1683f) to ensure the accuracy of the calibration curve.

Measurement. ICP–MS analysis was performed using an Agilent 8900 Triple Quad equipped with a synchronous precursor selection autosampler. The system was operated at a radio frequency power of 1,550 W, argon plasma gas flow rate of 15 l min⁻¹, and argon carrier gas flow rate of 0.9 l min⁻¹. Elemental concentrations were acquired in kinetic energy discrimination mode (Mn, Fe, Co, Cu and Zn) using He gas (at 5 ml min⁻¹) or in mass-on-mass mode (Fe) using O₂. Data were quantified using weighed, serial dilutions of a multielement standard (CEM 2, (VHG Labs, VHG-SM70B-100) Mn, Fe, Co, Cu, Zn). For each sample, data were acquired in triplicate and averaged. A coefficient of variance

was determined from frequent measurements of a sample containing approximately 10 ppb of Mn, Fe, Co, Cu and Zn. An internal standard (Ge, Bi) continuously introduced with the sample was used to correct for detector fluctuations and to monitor plasma stability. Results for the NIST water SRM were measured within 98–105%. ICP–MS measurements were performed in the Oregon Health & Science University Elemental Analysis Core.

Analysis. The absolute concentration of each metal was normalized against the FLAG–AKT concentration (estimated by SDS–PAGE with Flamingo staining) to estimate the metal stoichiometry.

Recombinant AKT constructs

AKT for in vitro assays. The following human AKT constructs (AKT1, amino acids 2–446; AKT2, amino acids 2–447) containing a TEV cleavable N-terminal His₈ tag were gene synthesized, cloned into the pFastBac vector by Gibson assembly⁴, expressed in insect cells and used to assess AKT modification through intact-protein mass spectrometry, modified site identification by tryptic LC–MS/MS and DSF.

AKT1 (WT) sequence: MSHHHHHHHHGSENLYFQSDVAIVKEGW LHKRGEYIKTWRPRYFLLKNDGTFIGYKERPDVDQREAPLNNFSVAQC QLMKTERPRPNTFIIRCLQWTTVIERTFHVTPEEREEWTTAIQTVADGLK KQEEEEMDFRSGSPSDNSGAEEEMEVSLAKPKHRVTMNEFEYLKLLGKGT FGKVILVKEKATGRYYAMKILKKEVIVAKDEVAHTLTENRVLQNSRHPFLT ALKYSFQTHDRLCFVMEYANGGELFFHLSRERVFSEDRAFYGAIEIVSAL DYHLSEKNVVYRDLKLENLMLDKDGHIKITDFGLCKEGIKDGATMKTFC GTPEYLAPEVLEDNDYGRAWDWWGLGVVMYEMMCGRLPFYNQDHEK FELILMEEIRFPRTLGPEAKSLLSGLLKDPKQRLGGGSEDAKEIMQHRRF AGIVWQHQVYEKKLSPPFKPQVTSETDTRYFDEEFTAQM.

AKT 1(E17K) sequence: MSHHHHHHHHGSENLYFQSDVAIVKEGWL HKRGKYIKTWRPRYFLLKNDGTFIGYKERPDVDQREAPLNNFSVAQC QLMKTERPRPNTFIIRCLQWTTVIERTFHVTPEEREEWTTAIQTVADGLK KQEEEEMDFRSGSPSDNSGAEEEMEVSLAKPKHRVTMNEFEYLKLLGKGT FGKVILVKEKATGRYYAMKILKKEVIVAKDEVAHTLTENRVLQNSRHPFLT ALKYSFQTHDRLCFVMEYANGGELFFHLSRERVFSEDRAFYGAIEIVSAL DYHLSEKNVVYRDLKLENLMLDKDGHIKITDFGLCKEGIKDGATMKTFC GTPEYLAPEVLEDNDYGRAWDWWGLGVVMYEMMCGRLPFYNQDHEK LFELILMEEIRFPRTLGPEAKSLLSGLLKDPKQRLGGGSEDAKEIMQHRRF AGIVWQHQVYEKKLSPPFKPQVTSETDTRYFDEEFTAQM.

AKT1 (E17K, C296/310A) sequence: MSHHHHHHHHGSENLYFQS DVAIVKEGWLHKRGKYIKTWRPRYFLLKNDGTFIGYKERPDVDQREAPLNNFSVAQCQLMKTERPRPNTFIIRCLQWTTVIERTFHVTPEEREEWTTAIQTVADGLKQEEEEMDFRSGSPSDNSGAEEEMEVSLAKPKHRVTMNEFEYLKLLGKGT FGKVILVKEKATGRYYAMKILKKEVIVAKDEVAHTLTENRVLQNSRHPFLTALKYSFQTHDRLCFVMEYANGGELFFHLSRERVFSEDRAFYGAIEIVSAL DYHLSEKNVVYRDLKLENLMLDKDGHIKITDFGLCKEGIKDGATMKTFC GTPEYLAPEVLEDNDYGRAWDWWGLGVVMYEMMCGRLPFYNQDHEK LFELILMEEIRFPRTLGPEAKSLLSGLLKDPKQRLGGGSEDAKEIMQHRRF AGIVWQHQVYEKKLSPPFKPQVTSETDTRYFDEEFTAQM.

AKT2 (WT) sequence: MSHHHHHHHHGSENLYFQSNEVSVIKEWLHKRGYEYIKTWRPRYFLLKSDGSFIGYKERPEAPDQTLPPLNNFSVAEC QLMKTERPRPNTFIVRCLQWTTVIERTFHVDSPDEREEWMRAIQMVANS LKQRAPGEDPMYKCGSPSDSSTTEEMEVASKARAKVTMNDFDYLKLL GKGTGKVILVREKATGRYYAMKILKEVIIAKDEVAHTVTESRVLQNLTRHP FLTALKYAFQTHDRLCFVMEYANGGELFFHLSRERVFTEERARFYGAIEIVSALEYLHSRDVVYRDIKLENLMLDKDGHIKITDFGLCKEGISDGMATMKTFC CGTPEYLAPEVLEDNDYGRAWDWWGLGVVMYEMMCGRLPFYNQDHER LFELILMEEIRFPRTLSPEAKSLLAGLKKDPKQRLGGGPSDAKEVMERHF FLSINWQDVVKQKLLPPFKPQVTSEVDTRYFDDFTAQS.

AKT1^{DrLink} for crystallography. The following human AKT1 constructs (amino acids 2–446) contain a shortened interdomain linker based on the *Drosophila* AKT sequence (DrLink) and a TEV cleavable N-terminal His₈ tag. The *Drosophila* linker binds to nanobody-41

Article

(NB41), which enhances AKT1 crystallization⁷. The sequences were gene synthesized, cloned into the pFastBac vector by Gibson assembly⁴, expressed in insect cells and used for crystallography as described below.

AKT1^{Drlink}(WT) sequence: MSHHHHHHHHGSENLYFQSDVAIVKEGWLHKRGEYIKTWRPRYFLLKNDGTFIGYKERPQDVQREAPLNNFSVAQCQLMKTERPRPNTFIIRCLQWTTVIERTFHVETPEEREEWTTAIQTVADGLKKQEEEMDASAEHTDMEVSLAKPKHRVTMNEFEYLKLLGKGTFGKVILVKEKATGRYYAMKILKKEVIVAKDEVAHTLTENRLQNSRHPFLTALKYSFQTHDRLCFVMEYANGGELFFHLSRERVFSEDRARFYGAIEVSALDYLHSEKNVVYRDLKLENLMLDKDGHKITDFGLCKEGIKDGATMKTFCGTPEYLAPEVLEDNDYGRAVDWWGLGVVMMYEMMCGRLPFYNQDHEKLFELILMEEIRFPRTLGPEAKSLLSGLLKDPKQRLGGGSEDAKEIMQHRRFFAGIVWQHVYEKKLSPPFKPQVTSETDTRYFDEEFTAQM.

AKT1^{Drlink}(E17K) sequence: MSHHHHHHHHGSENLYFQSDVAIVKEGWLHKRGKYIKTWRPRYFLLKNDGTFIGYKERPQDVQREAPLNNFSVAQCQLMKTERPRPNTFIIRCLQWTTVIERTFHVETPEEREEWTTAIQTVADGLKKQEEEMDASAEHTDMEVSLAKPKHRVTMNEFEYLKLLGKGTFGKVILVKEKATGRYYAMKILKKEVIVAKDEVAHTLTENRLQNSRHPFLTALKYSFQTHDRLCFVMEYANGGELFFHLSRERVFSEDRARFYGAIEVSALDYLHS EKNVYRDLKLENLMLDKDGHKITDFGLCKEGIKDGATMKTFCGTPEYLAPEVLEDNDYGRAVDWWGLGVVMMYEMMCGRLPFYNQDHEKLFELILMEEIRFPRTLGPEAKSLLSGLLKDPKQRLGGGSEDAKEIMQHRRFFAGIVWQHVYEKKLSPPFKPQVTSETDTRYFDEEFTAQM.

AKT2 (P115A/G116A) for crystallography sequence: HHHHHHENLYFQGNEVSVIKEGWLHKRGEYIKTWRPRYFLLKSDGSFIGYKERPEAPDQTLPPLNNFSVAECQLMKTERPRPNTFIRCLQWTTVIERTFHVDSPDEREEWMRAIQMVANSLKQRAAAEDPMYDYGCGSPSDSSTTEEMEAVSKARAKVTMNDFDYLKLLGKGTFGKVILVREKATGRYYAMKILRKVEIIAKDEV AHTVTESRVLQNTRHPFLTALKYAFQTHDRLCFVMEYANGGELFFHLSRERVFTEERARFYGAIEVSALEYLHSRVDVYRDIKLENLMLDKDGHKITDFGLCKEGISDGMKTCGTPEYLAPEVLEDNDYGRAVDWWGLGVVMMYEMMCGRLPFYNQDHERLFEILMEEIRFPRTLSPEAKSLLAGLKKDPKQRLGGPSDAKEVMEHRRFLSINWQDVVKKLLPPFKPQVTSEVDTRYFDDEFTAQS.

Protein expression and purification of AKT1

The pFastBac plasmids encoding AKT1 or AKT2 were transformed into DH10Bac cells (Thermo Fisher Scientific, catalogue no. 10361012), and the recombinant bacmid was isolated and used to generate baculovirus in Sf9 cells. Expression of AKT1 constructs was induced in Sf9 cells by infection of cultured cells (1.1 M ml⁻¹) with baculovirus solution (20 ml virus per 1 l culture) and incubation for 72 h. The cells were collected by centrifugation (8,000g, 10 min), and the pellets were resuspended in 50 ml lysis buffer per 1 l culture (25 mM HEPES (pH 8.0), 150 mM NaCl, 1.0 mM TCEP) supplemented with EDTA-free protease inhibitor cocktail (Roche, catalogue no. 04693132001). The cells were then lysed by sonication and the cell debris pelleted by centrifugation (48,380g, 30 min). The clarified lysate was incubated with Ni-NTA resin (Thermo Scientific, catalogue no. 88222, 3.0 ml per 1 l culture) at 4 °C for 1 h. The resin was washed with lysis buffer (3 × 20 ml) and then 10 ml wash buffer (40 mM imidazole, 25 mM HEPES (pH 8.0), 150 mM NaCl, 1.0 mM TCEP). AKT1 was eluted in 6 ml of elution buffer (400 mM imidazole, 25 mM HEPES (pH 8.0), 150 mM NaCl, 1.0 mM TCEP). The eluted protein was then incubated with 1.5 mg TEV protease per 1 l culture. After 1 h at room temperature, the resulting solution was diluted to 60 ml with 20 mM Tris (pH 8.0), 150 mM NaCl buffer and then passed through Ni-NTA resin (1 ml per 1 l culture), and the flow-through was collected. The resin was further washed with 5 ml of 25 mM Tris (pH 7.5), 100 mM NaCl, 40 mM imidazole buffer to recover the remaining AKT1, which was combined with the flow-through. The protein was buffer-exchanged into 20 mM Tris (pH 8.0), 20 mM NaCl, and purified by ion exchange chromatography (Q HiTrap, gradient from 20 to 250 mM NaCl). The resulting protein was purified further by gel filtration on a Superdex 200 Increase (10/300 GL) column (gel filtration buffer: 25 mM HEPES

(pH 8.0), 150 mM NaCl, 1 mM TCEP). The protein was then concentrated to approximately 5 mg ml⁻¹, flash-frozen in liquid nitrogen and stored at -80 °C.

AKT2 (P115A/G116A) purification for crystallography

The cell paste from 5 l of baculovirus-infected Sf9 cells was lysed in 50 mM Tris, 500 mM NaCl, 1 mM TCEP, 10% glycerol, 0.1% Triton X-100, pH 8.0 buffer supplemented with cComplete EDTA-free protease inhibitors (Roche). Purification was performed by Ni-NTA capture of the His-tagged protein in lysis buffer; washing with 50 mM Tris, 500 mM NaCl, 1 mM TCEP, 10% glycerol, pH 8.0, 20 mM imidazole; and elution in two steps with 50 and 250 mM imidazole in 50 mM Tris, 500 mM NaCl, 1 mM TCEP, 10% glycerol, pH 8.0. Fractions eluted with 20 and 50 mM imidazole were dialysed against 4 l of buffer (50 mM Tris, 200 mM NaCl, 1 mM DTT, 10% glycerol, pH 8.0) and digested with His-tagged TEV (TEV/protein ratio of 1:15) at 4 °C overnight and then loaded onto a second Ni-NTA column. The flow-through was pooled and then purified by anion exchange chromatography using a HiTrap Q HP column (Cytiva, catalogue no. 17115401). The elution gradient (0–100% B) was generated using buffer A (25 mM Tris, 50 mM NaCl, 1 mM DTT, 10% glycerol, pH 8.0) and buffer B (25 mM Tris, 1 M NaCl, 1 mM DTT, 10% glycerol, pH 8.0). This produced two distinct peaks, representing non-phosphorylated and monophosphorylated species. The two pools of AKT2 (2–447, P115A/G116A) were separately concentrated and purified by size-exclusion chromatography (SEC) using a Superdex 75 100/300 GL column, with SEC buffer (25 mM Tris, 100 mM NaCl, 5 mM DTT, 10% glycerol, pH 7.5); both forms were monomeric. The monophosphorylated form was concentrated to 6 mg ml⁻¹ in SEC buffer, flash-frozen in liquid nitrogen and stored at -80 °C.

NB41 construct, expression and purification

NB41 construct. NB41 was gene synthesized and cloned by Gibson assembly⁴ into a PET26b vector containing an N-terminal PelB signal sequence.

NB41 sequence: QVQLQESGGGLVQAGGSLRLSCAASGIDVRIKTMAWYRQAPGKQRELLASVLVSGSTNYADPVKGRTISRDNAKNTVYLQMNKLIPDDTAVYYCNYGRLRRDVWGPCTQVTSSHHHHHEPEA.

NB41 expression and purification. BL21 (DE3) cells were transformed with the NB41 PET26b plasmid. The transformed bacteria were grown in 21TB + kanamycin at 37 °C until the culture reached an optical density at 600 nm of 0.66. The culture was cooled to 18 °C, induced with 0.25 mM isopropyl β-D-thiogalactopyranoside and incubated overnight at 18 °C. Bacteria were harvested (10,000g, 10 min), and the resulting pellet was frozen.

The pellet was warmed to 4 °C and lysed in 15 ml of 200 mM Tris (pH 8.0), 500 mM sucrose buffer with rotation. After 1 h, 30 ml of 50 mM Tris (pH 8.0), 125 mM sucrose, was added. After a further 45 min rotation at 4 °C, the sample was centrifuged for 30 min at 7,500g. The supernatant was collected and passed over 3 ml Ni-NTA resin (Thermo Scientific, catalogue no. 88222). The resin was washed with 3 × 10 ml wash buffer (40 mM imidazole, 25 mM HEPES (pH 8.0), 150 mM NaCl). NB41 was eluted in 6 ml of elution buffer (400 mM imidazole, 25 mM HEPES (pH 8.0), 150 mM NaCl). The resulting protein was purified further by gel filtration on a Superdex 75 Increase (10/300 GL) column (gel filtration buffer: 20 mM Tris pH 7.5, 100 mM NaCl, 1 mM TCEP). The protein was then concentrated to 5 mg ml⁻¹, flash-frozen in liquid nitrogen and stored at -80 °C.

AKT1 crystallography

AKT1^{Drlink}-inhibitor-NB41 complex formation. Compound 3 or 4 (200 µl, 0.5 mM stock in DMSO) was added to 1 mg of AKT1^{Drlink} (WT or E17K) in 10 ml of 20 mM HEPES (pH 8.0), 150 mM NaCl and 1 mM TCEP buffer to give a final concentration of 10 µM. After 10 min, the sample was concentrated to 1 ml; then, NB41 (0.55 mg) was added, followed by incubation for 15 min. The resulting complex was purified by gel

filtration on a Superdex 200 Increase (10/300 GL) column (gel filtration buffer: 20 mM HEPES (pH 8.0), 20 mM NaCl, 1 mM TCEP). The protein was then concentrated to 2.5–7.5 mg ml⁻¹ and used directly for crystal formation. Crystallization was performed by hanging-drop vapour diffusion. The protein and reservoir solution were mixed in a 1:1 ratio (150 + 150 nl), and the crystals grew overnight and were cryoprotected in a reservoir solution containing 25% ethylene glycol. Conditions for each structure are provided below.

AKT1^{DrLink} (E17K)-3-NB41-Zn²⁺. Protein solution: AKT1^{DrLink} (E17K)-3-NB41 (2.5 mg ml⁻¹) in 20 mM HEPES (pH 8.0), 20 mM NaCl, 1 mM TCEP, 0.2 mM ZnSO₄. Reservoir solution: 29% PEG3350, 200 mM Li₂SO₄, 100 mM bis-tris propane pH 8.5, 10% ethylene glycol. Data are from Protein Data Bank (PDB) 8UVY.

AKT1^{DrLink} (E17K)-3-NB41, Zn²⁺-free. Protein solution: AKT1^{DrLink} (E17K)-3-NB41 (6.5 mg ml⁻¹) in 20 mM HEPES (pH 8.0), 20 mM NaCl, 1 mM TCEP, 1.2 mM iodoacetamide. Reservoir solution: 19% PEG3350, 200 mM Li₂SO₄, 100 mM bis-tris propane pH 8.5, 10% ethylene glycol. Data are from PDB 8UW2.

AKT1^{DrLink} (WT)-3-NB41. Protein solution: AKT1^{DrLink} (WT)-3-NB41 (7.5 mg ml⁻¹) in 20 mM HEPES (pH 8.0), 20 mM NaCl, 1 mM TCEP, 1.2 mM iodoacetamide. Reservoir solution: 19% PEG3350, 200 mM Na₂SO₄, 100 mM bis-tris propane pH 7.2, 10% ethylene glycol. Data are from PDB 8UW7.

AKT1^{DrLink} (E17K)-4-NB41-Zn²⁺. Protein solution: AKT1^{DrLink} (E17K)-4-NB41 (6.5 mg ml⁻¹) in 20 mM HEPES (pH 8.0), 20 mM NaCl, 1 mM TCEP. Reservoir solution: 15% PEG3350, 200 mM Li₂SO₄, 100 mM bis-tris propane pH 6.5, 10% ethylene glycol. Data are from PDB 8UW9.

AKT1 X-ray data and structure determination

Diffraction data were collected at beamlines 2.0.1 and 8.3.1 of the Advanced Light Source (Lawrence Berkeley National Laboratory), indexed and integrated using XDS⁵⁵, scaled with AIMLESS⁵⁶ and solved by molecular replacement using Phaser⁵⁷. The structures were manually refined with Coot⁵⁸ and PHENIX⁵⁹. Data collection and refinement statistics are reported in Extended Data Fig. 9a. The structures have been deposited in the PDB. Crystal structures and maps were visualized using PyMOL v.2.5.0 (Schrödinger).

AKT2 crystallography

Monophosphorylated AKT2(P115A/G116A) (6 mg ml⁻¹) was incubated with compound **3** (1:5 molar ratio) on ice for 1 h. Crystals were obtained by the vapour diffusion method after mixing an equal volume of the complex with reservoir solution containing 0.1 M HEPES pH 7.5, 20% (w/v) PEG 8000 at 4 °C. Crystals were cryoprotected in mother liquor supplemented with 10% ethylene glycol and flash-cooled in liquid nitrogen for storage and data collection.

AKT2 X-ray data and structure determination

Diffraction data were obtained at Beamline 05 A at Taiwan Photon Source using a Rayonix MX300HS detector. This dataset was processed with xia2 (ref. 60) and solved by molecular replacement using Phaser (with PDB 8Q61 as a search model). The structures were manually refined with Coot and PHENIX. Data collection and refinement statistics are reported in Extended Data Fig. 9a. The structure has been deposited in the PDB. Crystal structures and maps were visualized using PyMOL v.2.5.0 (Schrödinger).

Reporting summary

Further information on research design is available in the Nature Portfolio Reporting Summary linked to this article.

Data availability

The reported crystal structures have been deposited in the PDB with accession numbers 8UVY, 8UW2, 8UW7, 8UW9 and 9C1W. The raw proteomic data have been deposited to MassIVE with accession number MSV000093542, including the *Homo sapiens* reviewed Swiss-Prot FASTA database file used for searches. Source data are provided with this paper. Statistical tests, descriptive statistics and associated graphical data are included in source data files.

50. Kong, A. T., Leprevost, F. V., Avtonomov, D. M., Mellacheruvu, D. & Nesvizhskii, A. I. MSFragger: ultrafast and comprehensive peptide identification in mass spectrometry-based proteomics. *Nat. Methods* **14**, 513–520 (2017).
51. Yu, F., Haynes, S. E. & Nesvizhskii, A. I. IonQuant enables accurate and sensitive label-free quantification with FDR-controlled match-between-runs. *Mol. Cell. Proteomics* **20**, 100077 (2021).
52. Gibson, D. G. et al. Enzymatic assembly of DNA molecules up to several hundred kilobases. *Nat. Methods* **6**, 343–345 (2009).
53. Cox, J. & Mann, M. MaxQuant enables high peptide identification rates, individualized p.p.b.-range mass accuracies and proteome-wide protein quantification. *Nat. Biotechnol.* **26**, 1367–1372 (2008).
54. Davies, B. R. et al. Tumors with AKT1^{E17K} mutations are rational targets for single agent or combination therapy with AKT inhibitors. *Mol. Cancer Ther.* **14**, 2441–2451 (2015).
55. Kabsch, W. XDS. *Acta Crystallogr. Sect. D: Biol. Crystallogr.* **66**, 125–132 (2010).
56. Evans, P. R. & Murshudov, G. N. How good are my data and what is the resolution? *Acta Crystallogr. Sect. D: Biol. Crystallogr.* **69**, 1204–1214 (2013).
57. McCoy, A. J. et al. Phaser crystallographic software. *J. Appl. Crystallogr.* **40**, 658–674 (2007).
58. Emsley, P., Lohkamp, B., Scott, W. G. & Cowtan, K. Features and development of Coot. *Acta Crystallogr. Sect. D: Biol. Crystallogr.* **66**, 486–501 (2010).
59. Adams, P. D. et al. PHENIX: a comprehensive Python-based system for macromolecular structure solution. *Acta Crystallogr. Sect. D: Biol. Crystallogr.* **66**, 213–221 (2010).
60. Winter, G. xia2: an expert system for macromolecular crystallography data reduction. *J. Appl. Crystallogr.* **43**, 186–190 (2010).

Acknowledgements Funding for this study was provided by the Ono Pharma Foundation (J.T.), the Tobacco-Related Disease Research Program Postdoctoral Fellowship Award (T32FT4880 to G.B.C.) and Terremoto Biosciences. We thank the UCSF Preclinical Therapeutics Core and V. Steri for research assistance and M. Haffner (FHCC) for providing the LAPC4-CR cells. ICP-MS measurements were performed by the Oregon Health & Science University Elemental Analysis Core with partial support from the US National Institutes of Health (NIH) (S10OD028492). The Berkeley Center for Structural Biology is supported by the Howard Hughes Medical Institute, participating research team members and the NIH National Institute of General Medical Sciences, ALS-ENABLE grant P30 GM24169. The Advanced Light Source is a Department of Energy Office of Science User Facility under contract no. DE-AC02-05CH11231. The Pilatus detector on beamline 2.0.1 was funded under NIH grant S10OD021832. Beamline 8.3.1 is supported with NIH grants (R01 GM124149 and P30 GM124169).

Author contributions G.B.C. and J.T. conceived the project, analysed data and wrote the paper. G.B.C. designed, performed and analysed biochemical, cellular, chemoproteomic and X-ray crystallographic experiments. G.B.C., H. Chu. and H. Chen designed, synthesized and characterized the compounds. J.D.S., B.C., S.D. and W.K. designed, performed and analysed in vivo experiments. X.M. designed and analysed X-ray crystallographic experiments. J.D.C. designed and analysed nanoBRET experiments. Y.C., A.D.Z., K.S.Y., S.H.R., J.R.L. and P.A.T. assisted with data analysis and provided key scientific input.

Competing interests H. Chu., J.D.S., J.D.C., B.C., X.M., S.D., W.K., A.D.Z., K.S.Y., S.H.R., P.A.T. and J.R.L. are current or former employees of Terremoto Biosciences. J.T. is a cofounder of Kezar Life Sciences and Terremoto Biosciences and is a scientific advisor to Lambic Therapeutics. J.T., G.B.C., S.H.R., K.S.Y., H.C., J.D.C. and P.A.T. are inventors on a patent application filed by the University of California and Terremoto Biosciences (WO2023168291A1). The remaining authors declare no competing interests.

Additional information

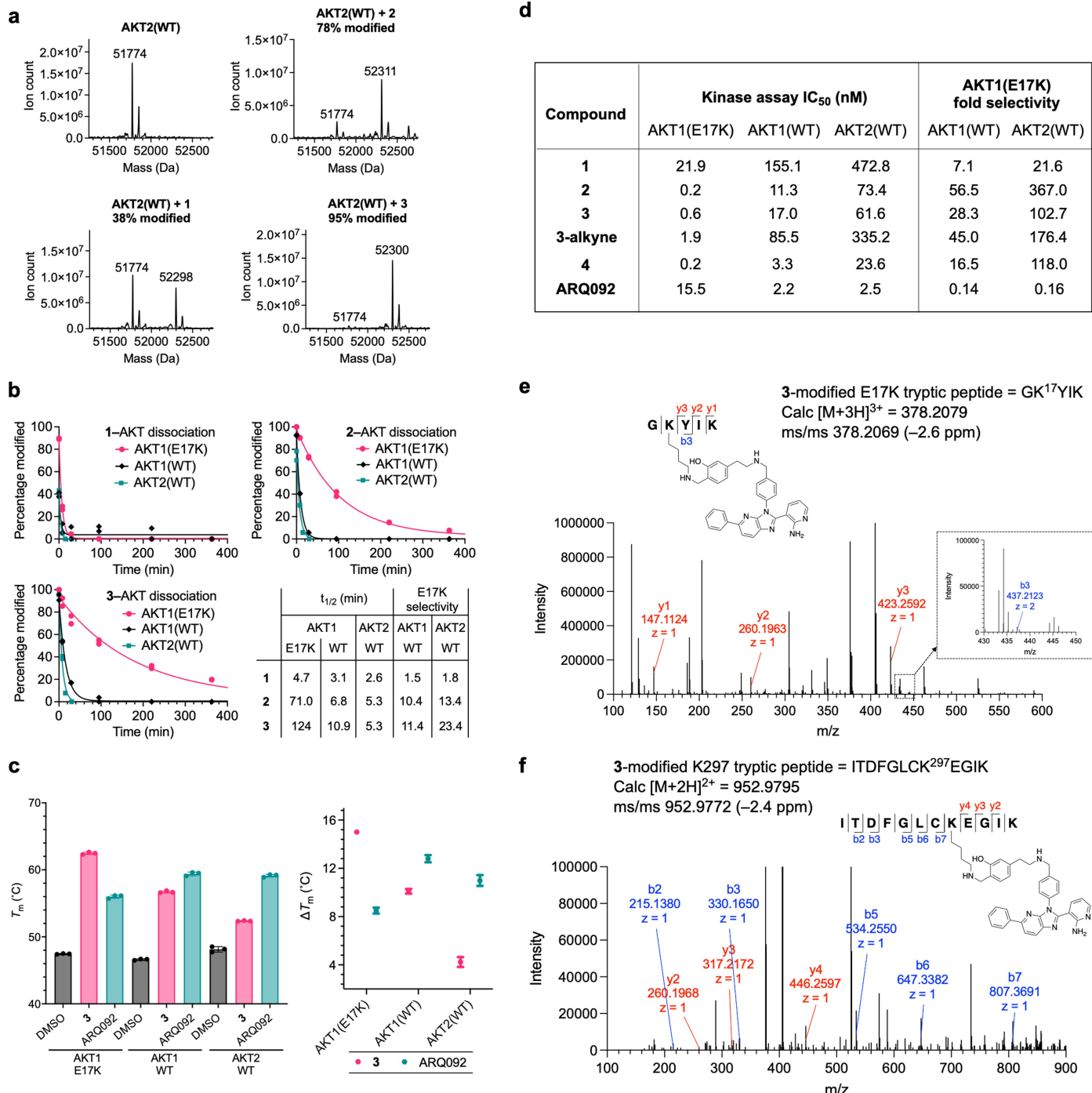
Supplementary information The online version contains supplementary material available at <https://doi.org/10.1038/s41586-024-08176-4>.

Correspondence and requests for materials should be addressed to Jack Taunton.

Peer review information *Nature* thanks Elena De Vita, Derek Lowe and the other, anonymous reviewer(s) for their contribution to the peer review of this work.

Reprints and permissions information is available at <http://www.nature.com/reprints>.

Article



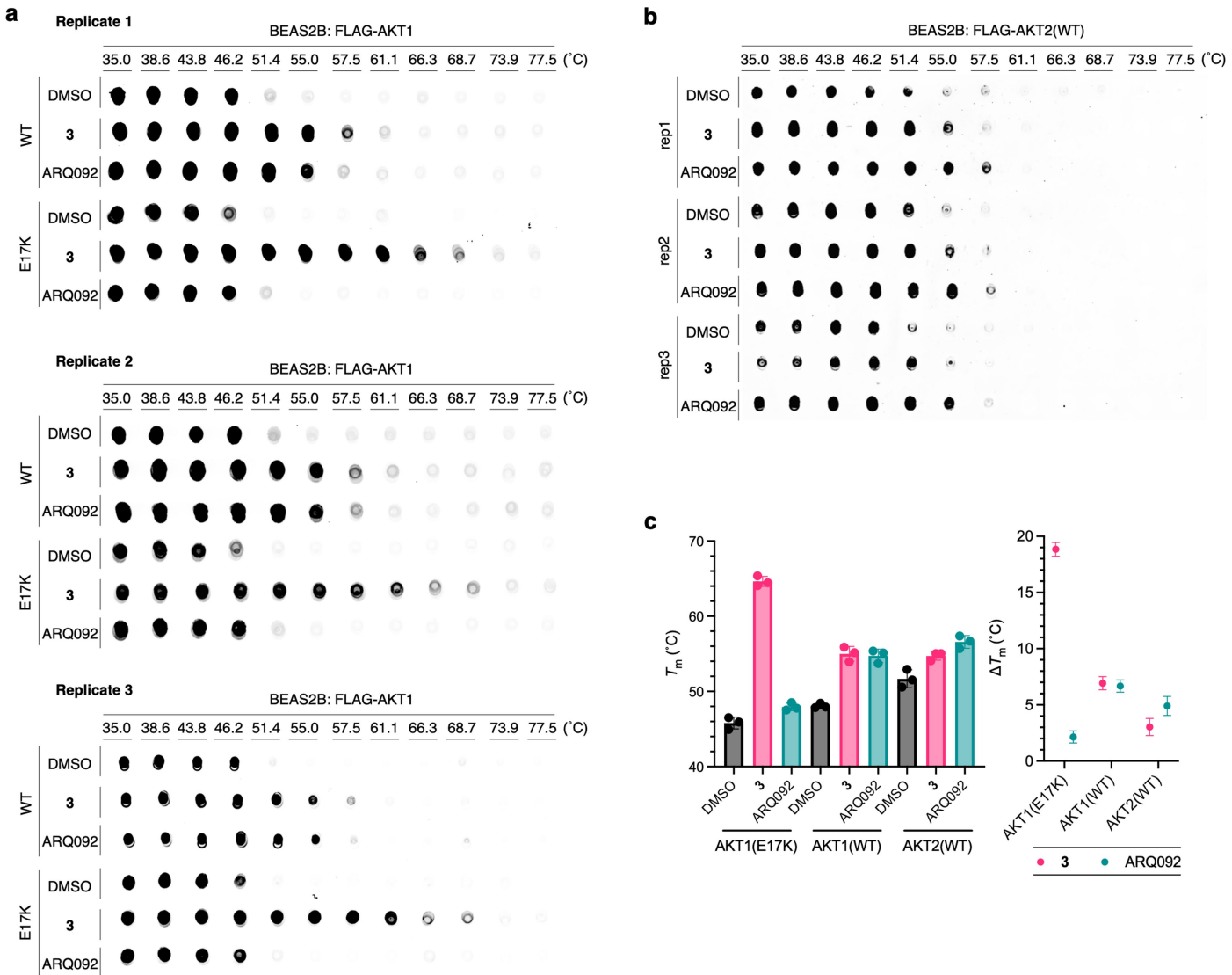
Extended Data Fig. 1 | Additional in vitro characterization of compound 3.

a, Deconvoluted intact-protein mass spectra of AKT2(WT) (1 μ M) treated with vehicle or 1–3 (5 μ M, 37 °C, 15 min) and then reduced with NaBH₄ (10 mM, 5 min).

b, Dissociation of preformed AKT2(WT)-ligand complexes (1 μ M AKT2(WT), 5 μ M ligand) was initiated by the addition of excess ARQ092 (50 μ M) with continuous incubation at 37 °C. At the indicated time points, the percentage of covalently modified AKT2(WT) was determined by intact-protein MS after quenching with NaBH₄ (10 mM, 5 min). Duplicate measurements for each time point were plotted, and dissociation half-times were determined using an exponential decay function. Kinetics of AKT1 dissociation are reproduced from Fig. 1d.

c, The melting temperature (T_m) of AKT2(WT) (2 μ M) treated with DMSO, 3 (10 μ M), or ARQ092 (10 μ M) was assessed by differential scanning fluorimetry (DSF, mean \pm s.d., $n = 3$). ΔT_m was calculated relative to the DMSO

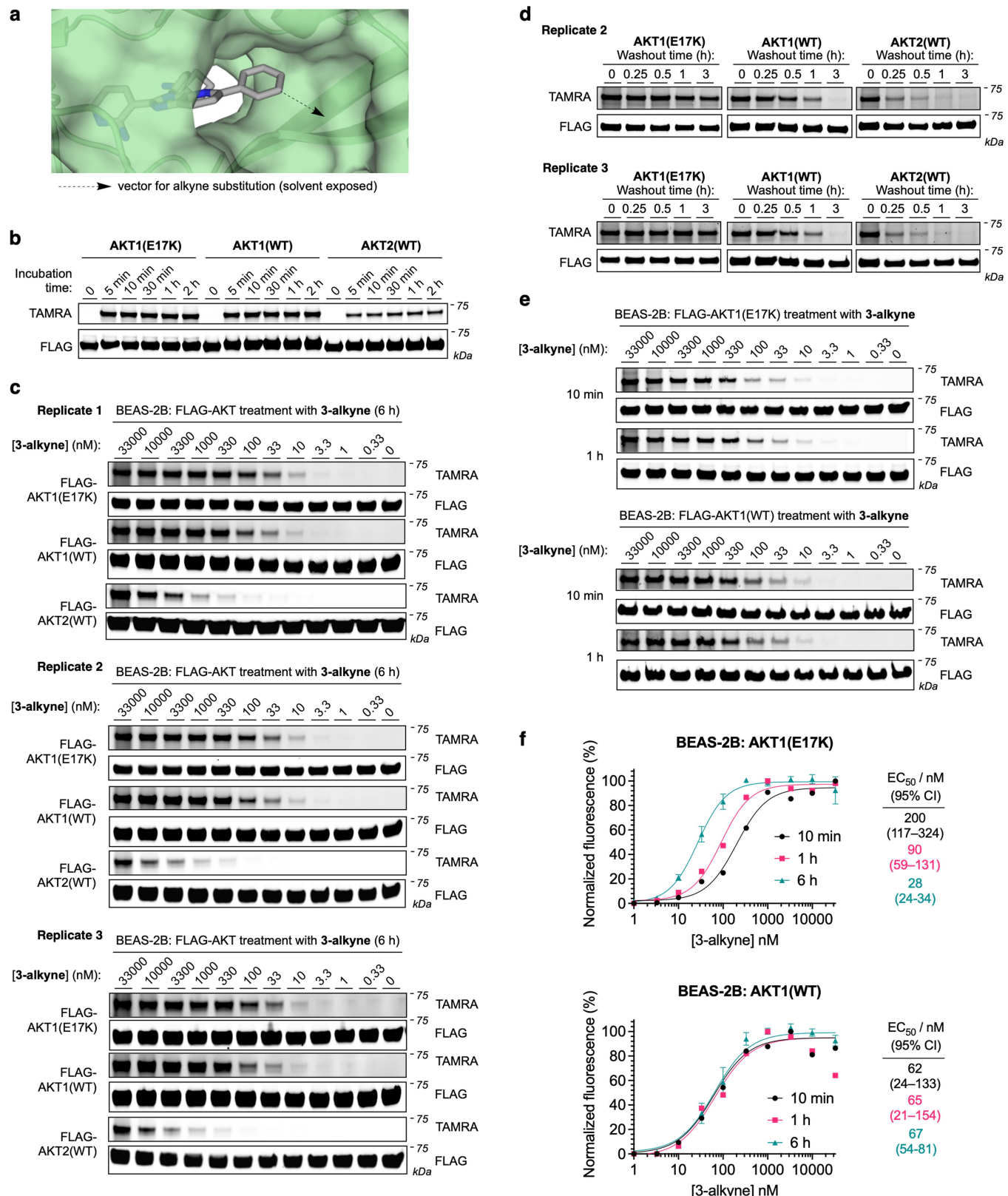
control (mean \pm s.d.). Apparently missing error bars indicate that the error is too small to be visualized. Data for AKT1 are reproduced from Fig. 1e. **d**, IC₅₀ values from biochemical AKT kinase activity assays (10 μ M ATP, radioisotope filter binding, 10-pt dose response, Reaction Biology). **e**, Modified site identification by tryptic LC-MS/MS. Purified recombinant AKT1(E17K) or AKT1(WT) (**f**), was treated with compound 3 (4 μ M, 15 min) and reduced with NaBH₄ (5 mM). The sample was reduced with DTT, alkylated with iodoacetamide and then digested with trypsin. The tryptic peptides were analysed by LC-MS/MS and modified sites identified using MSFragger. The modified sites with the greatest MS1 intensity were Lys17 for AKT1(E17K) (**e**) and Lys297 for AKT1(WT) (**f**). The annotated MS2 spectra with b- and y-ions for the relevant modified peptides are shown.



Extended Data Fig. 2 | Dot blot images and CETSA data related to Fig. 2.
a, Dot blot images related to Fig. 2a. **b**, Dot blot images related to Extended Data Fig. 2c. **c**, Cellular thermal shift assay (CETSA) data reproduced from Fig. 2a with the addition of AKT2(WT) data. Melting temperatures (T_m) were

determined by sigmoidal regression analysis ($n = 3$). ΔT_m was calculated relative to the DMSO control for each protein (mean \pm s.d.). Apparently missing errors bars indicate that the error is too small to be visualized.

Article

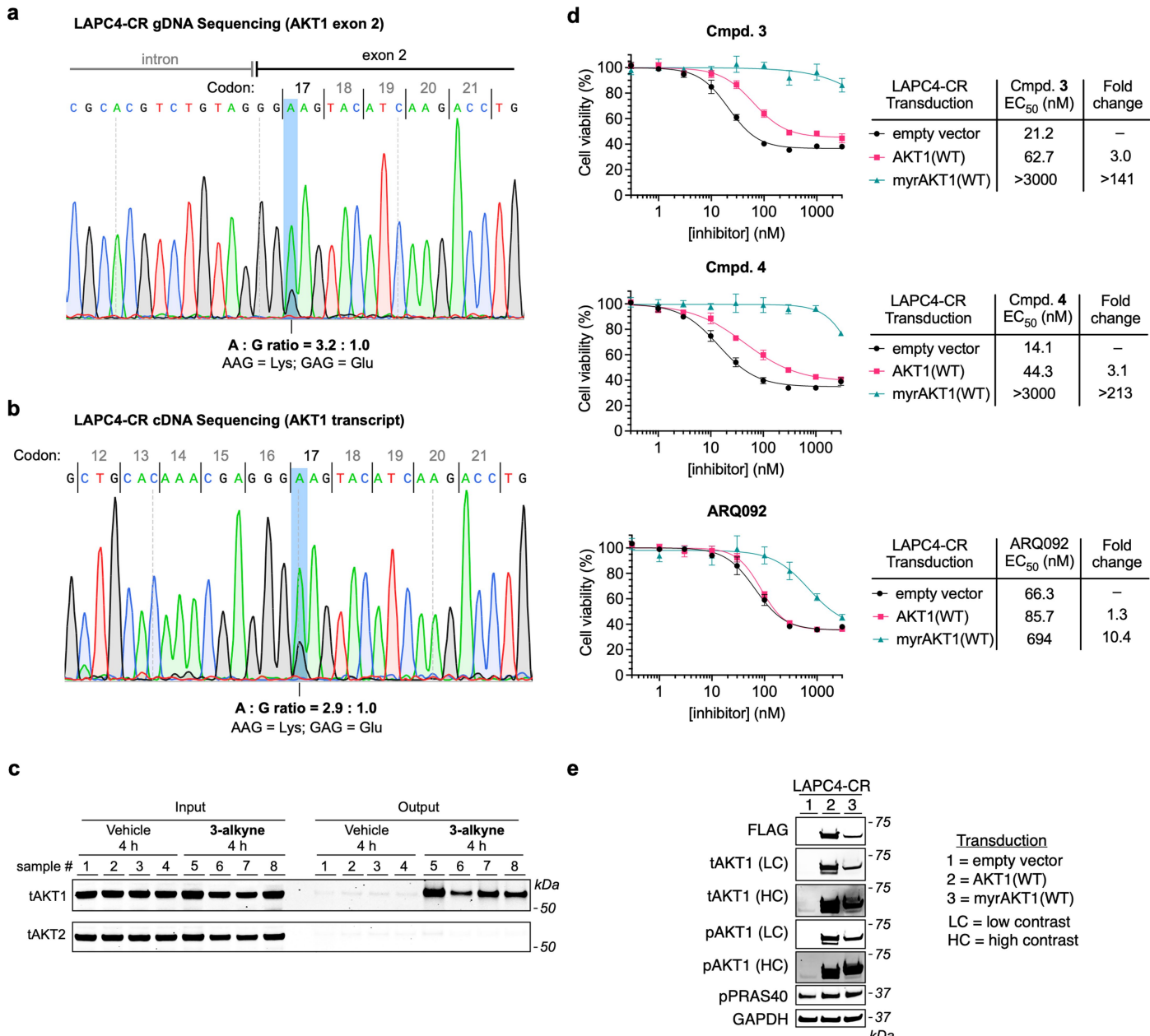


Extended Data Fig. 3 | See next page for caption.

Extended Data Fig. 3 | In-gel fluorescence data related to Fig. 2. **a**, Crystal structure of ARQ092 (grey) with AKT1(WT) (green) (PBD: 5kcv) illustrating the solvent-exposed vector that informed the design of **3-alkyne**. **b**, BEAS-2B cells (FLAG-AKT1(E17K), FLAG-AKT1(WT) or FLAG-AKT2(WT)) were treated with **3-alkyne** (2 μ M) for 0, 5, 10, 30, 60 or 120 min. After cell lysis and reduction with NaBH₄ (10 mM), the labelled proteins were conjugated to TAMRA-azide and visualized by in-gel fluorescence. **c**, In-gel fluorescence images related to Fig. 2d. **d**, In-gel fluorescence images related to Fig. 2e. Replicate 1 is shown in Fig. 2e. **e**, BEAS-2B cells (FLAG-AKT1(E17K) or FLAG-AKT1(WT)), were treated

with increasing concentrations of **3-alkyne** for 10 or 60 min. The cells were lysed and reduced with NaBH₄ (10 mM). The labelled proteins were conjugated to TAMRA-azide and visualized by in-gel fluorescence. **f**, Normalized in-gel fluorescence data reproduced from Fig. 2d (6 h dose-response, n = 3) with the addition of the 10 and 60 min dose responses (n = 1) from Extended Data Fig. 3e. Apparently missing errors bars indicate that the error is too small to be visualized. The experiments in (**b-d**) were performed twice with similar results. The experiment in (**e**) was performed once.

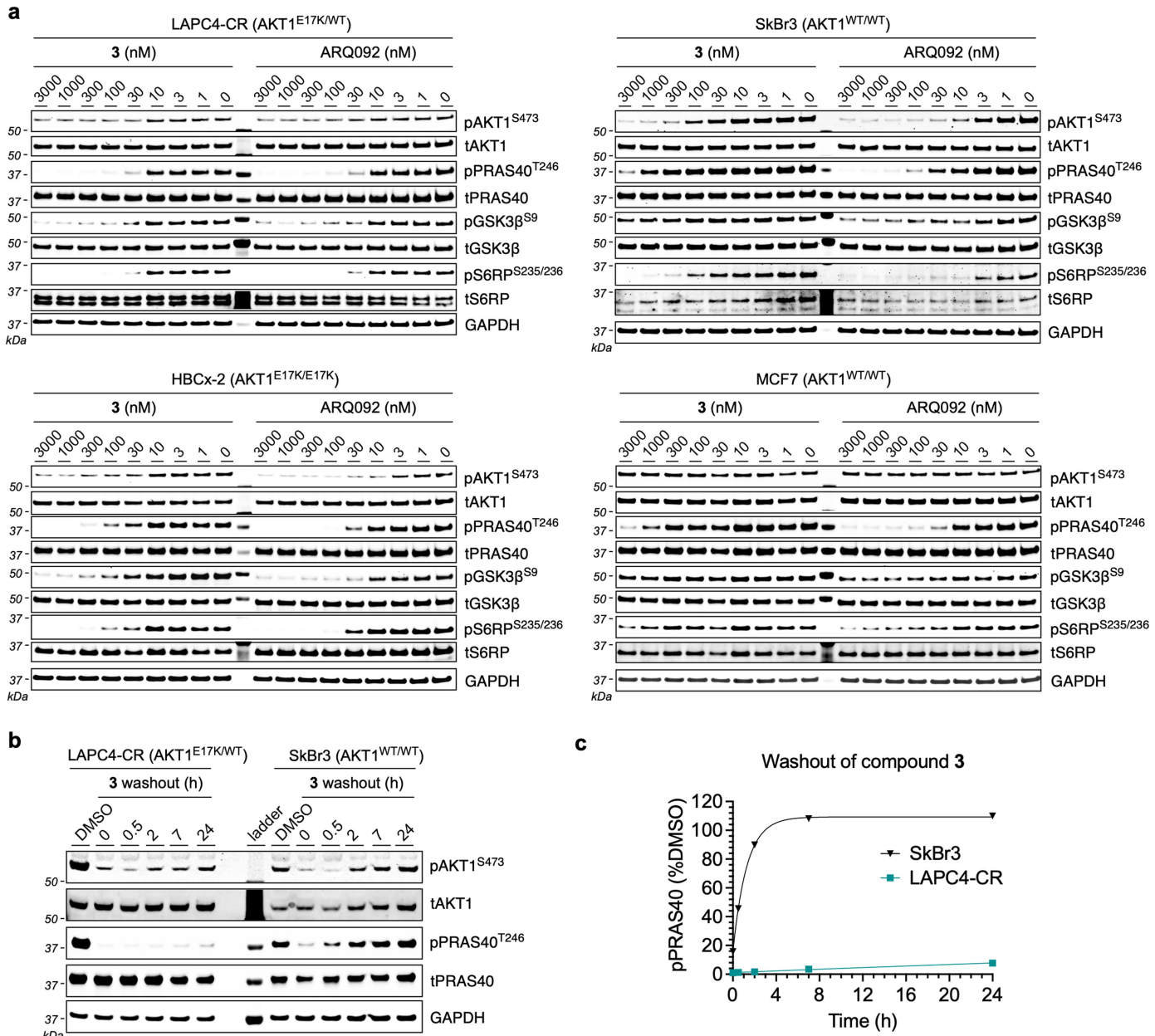
Article



Extended Data Fig. 4 | AKT1(WT/E17K) selectivity in LAPC4-CR cells and tumors. LAPC4-CR AKT1(WT/E17K) zygosity determination (a) and (b)

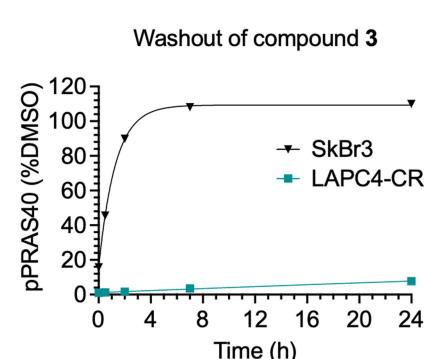
a, Sequencing of AKT1 exon 2 amplicon derived from LAPC4-CR gDNA. Amplicon primers: f = TGACCTCTAACTGTGGACCC; r = CAAGGGGATACTTACCGCGC. Sequencing primer = TCGCTGGCCCTAAGAACAGC. **b**, Sequencing of AKT1 transcript amplicon derived from LAPC4-CR cDNA. Amplicon primers: f = ATG GACAGGGAGAGCAAACG; r = ACAGGTGGAAGAACAGCTCG. Sequencing primer = TGCATCAGAGGCTGTGCCAG. **c**, LAPC4-CR tumor bearing mice were dosed with vehicle or **3-alkyne** (30 mg kg⁻¹, IP injection) (n = 4). Tumors were harvested after 4 h and lysed. Tumor lysate was reduced with NaBH₄ (10 µM), and conjugated with biotin-picolyl azide. Biotinylated proteins were pulled

down with neutravidin agarose, eluted, and analyzed by immunoblotting. **d**, LAPC4-CR cells were transduced with empty vector, AKT1(WT) or myrAKT1(WT) and selected with puromycin. Transduced cells were treated with the indicated concentrations of ARQ092, compound **3** or **4** for 72 h, and cell viability was determined by the Alamar Blue assay. Data (mean \pm s.d., n = 4) were fitted with sigmoidal regression. Apparently missing errors bars indicate that the error is too small to be visualized. **e**, Transduced LAPC4-CR cells relating to (**d**) were lysed and analyzed by immunoblotting for FLAG, tAKT1, pAKT1^{S473} and pPRAS40^{T246} (loading control: GAPDH). This experiment was performed twice with similar results.

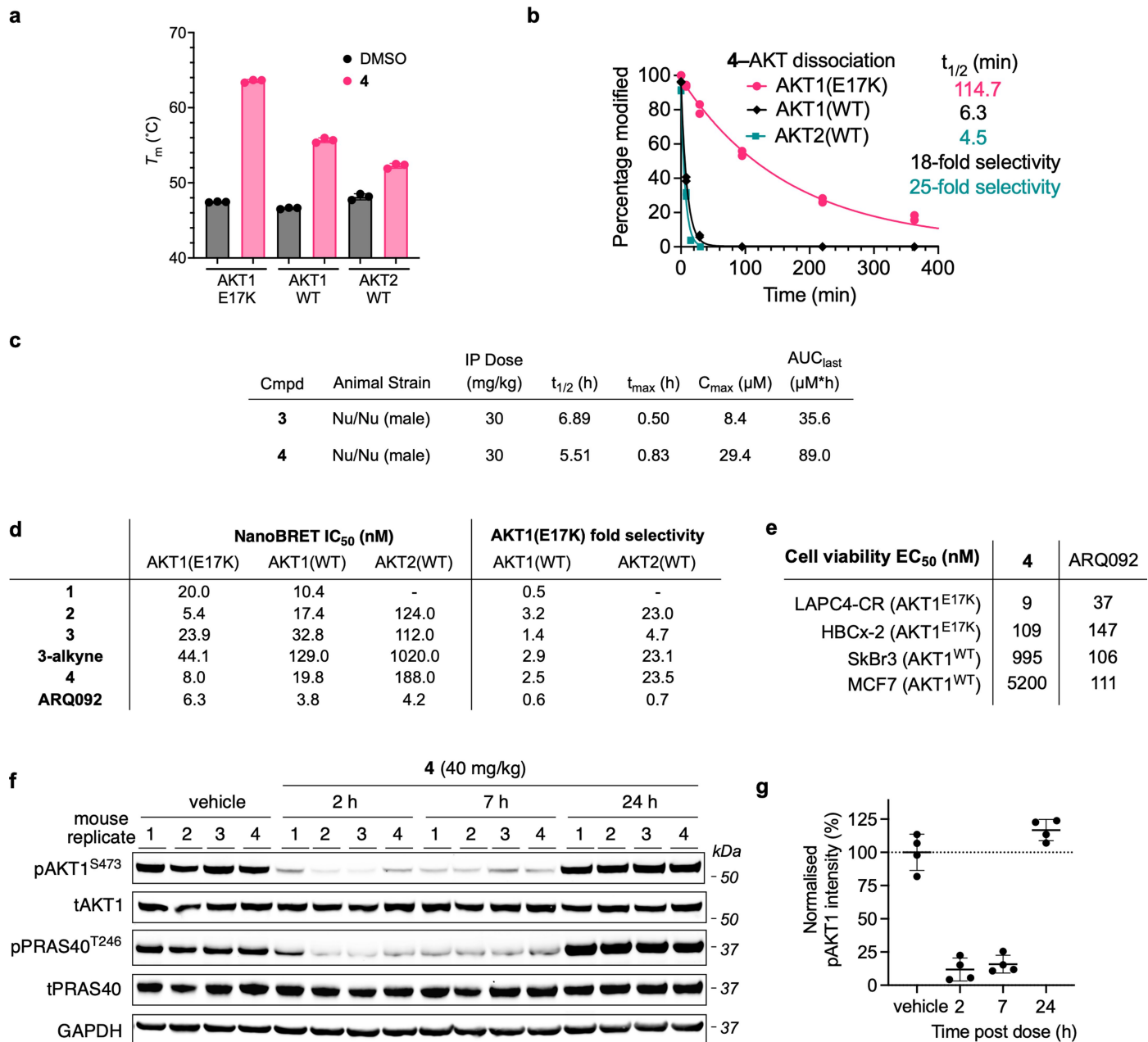


Extended Data Fig. 5 | Inhibition of AKT signaling in cancer cells, related to Fig. 3d. **a**, LAPC4-CR, HBCx-2, SkBr3 and MCF7 cells were treated with increasing concentrations of ARQ092 or compound **3** for 2 h, lysed, and analyzed by immunoblotting for pAKT1^{S473}, pPRAS40^{T246}, pS6RP^{S235/236}, pGSK3^{βS9} (loading controls: tAKT1, tPRAS40, tS6RP, tGSK3^β and GAPDH). **b**, Washout of compound **3** in LAPC4-CR and SkBr3 cells. LAPC4-CR or SkBr3 cells were

treated with 2 μ M compound **3** for 2 h. The media was aspirated and replaced with compound-free media. After 0, 0.5, 2, 7, or 24 h, the cells were lysed and then probed for pAKT1^{S473} and pPRAS40^{T246} by immunoblotting (loading controls: tAKT1, tPRAS40, GAPDH). **c**, The pPRAS40 signal (**b**) was normalized to the DMSO control and fitted with an exponential regression. The experiments in (**a**, **b**) were performed twice with similar results.



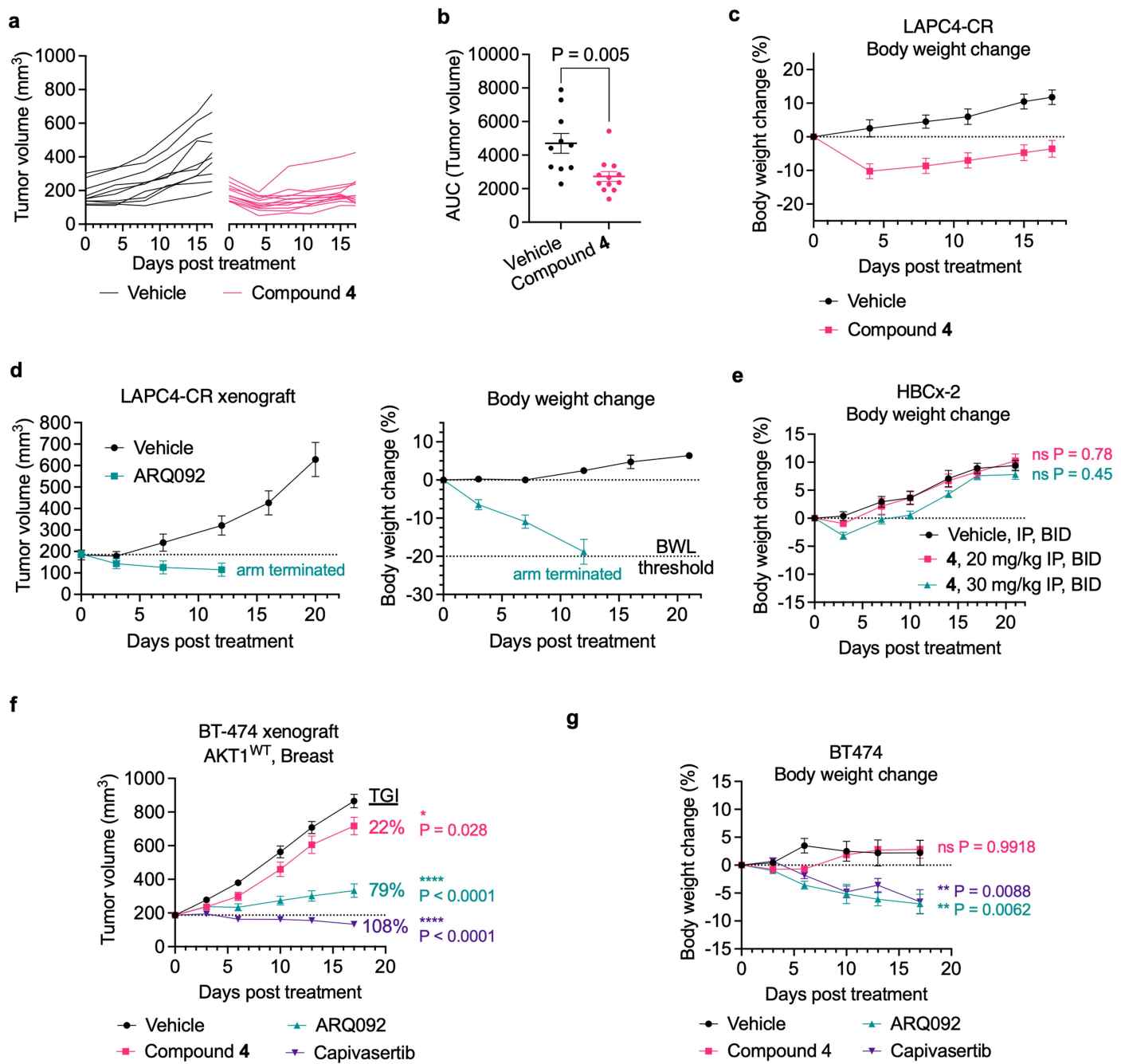
Article



Extended Data Fig. 6 | In vitro and in vivo characterization of compound 4.

a, The melting temperature (T_m) of AKT1(E17K), AKT1(WT) and AKT2(WT) (2 μ M) treated with DMSO or **4** (10 μ M) was assessed by differential scanning fluorimetry (DSF, mean \pm s.d., n = 3). Apparently missing errors bars indicate that the error is too small to be visualized. **b**, Dissociation of the preformed complex of AKT1(E17K), AKT1(WT) or AKT2(WT) (1 μ M) bound to compound **4** (5 μ M) was initiated by the addition of excess ARQ092 (50 μ M) with continuous incubation at 37 °C. The percentage of modified AKT at the indicated time points was determined by intact-protein mass spectrometry after quenching aliquots with NaBH₄ (10 mM, 5 min). Duplicate measurements for each time point were plotted, and dissociation half-times were determined using an exponential decay function. Dissociation kinetics were determined using an exponential decay function. **c**, Pharmacokinetic data for compounds **3** and **4**

(mean, n = 3). **d**, Target engagement of full-length AKT1(E17K), AKT1(WT), and AKT2(WT) fused to NanoLuc was determined in HEK293 cells using the NanoBRET assay kit (Promega). IC₅₀s were calculated by sigmoidal regression and presented as the geometric mean. **e**, Cell viability EC₅₀s (72 h incubation) for compound **4** and ARQ092 in LAPC4-CR, HBCx-2, SkBr3 and MCF7 cells. **f**, Athymic male nude mice (nu/nu) bearing LAPC4-CR-derived xenografts were dosed with vehicle or 40 mg kg⁻¹ compound **4** by IP injection (n = 4). Euthanasia was performed 2, 7, or 24 h after dosing with compound **4** (vehicle = 2 h) and tumors were collected, homogenized, and analyzed by immunoblotting (loading controls: tAKT1, tPRAS40, GAPDH). **g**, Tumor pAKT1 intensities were determined by immunoblotting (**f**) and normalized to the mean intensity from vehicle-treated mice. Data are mean \pm s.d., n = 4.

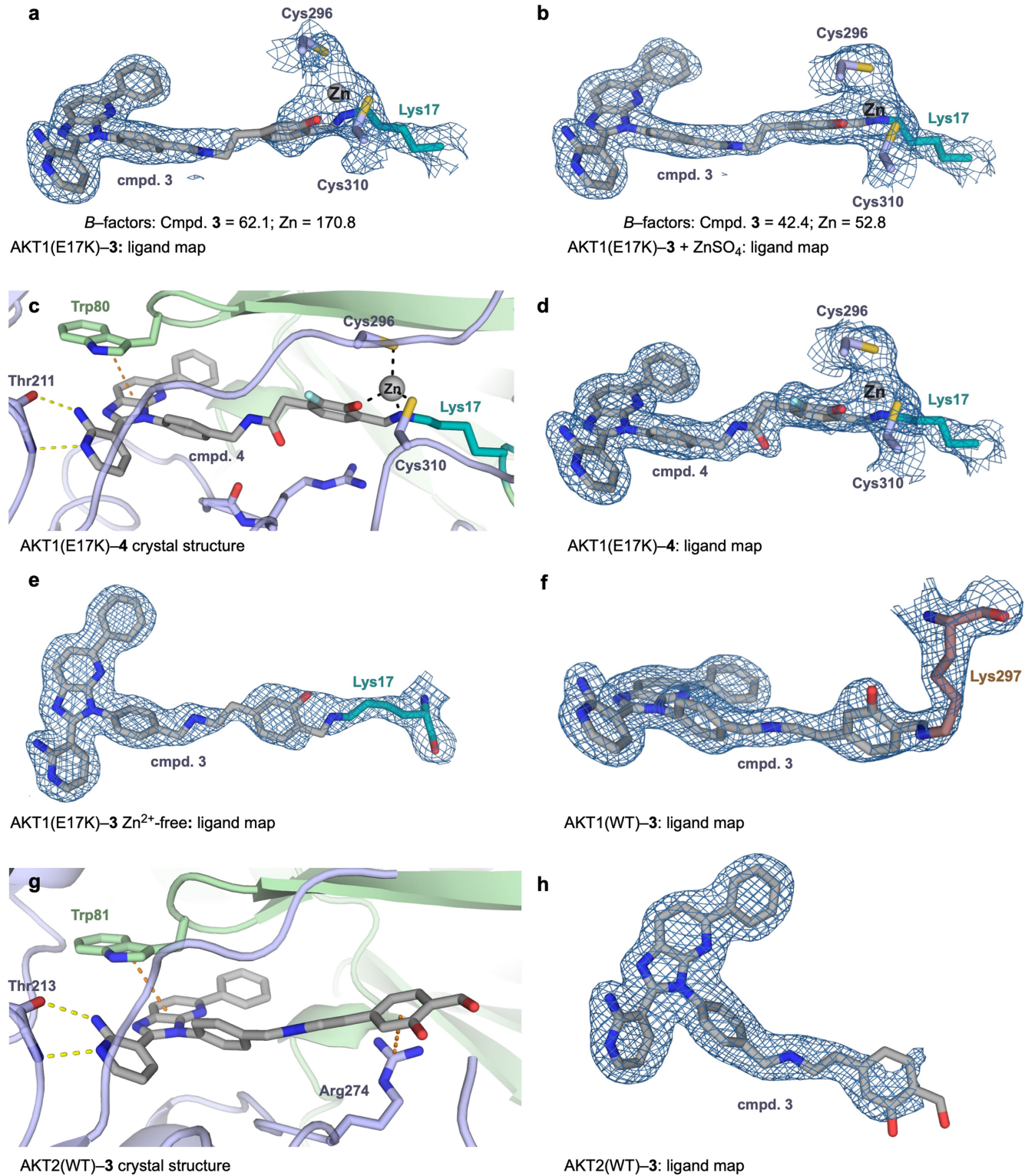


Extended Data Fig. 7 | Further in vivo characterization of compound 4.

a, Individual growth curves of LAPC4-CR xenografts related to Fig. 4a. LAPC4-CR tumor-bearing mice (athymic nu/nu) were randomized to vehicle ($n=10$) or compound 4 treatment groups (30 mg kg^{-1} , BID, IP, $n=12$). **b**, Individual tumor growth curves (**a**) were integrated (AUC, mm^3) over the 18 day study. Vehicle, $n=10$; compound 4, $n=12$ (mean \pm s.e.m.). Student's t-test (two-tailed, unpaired, parametric) was used to calculate the P value without adjustments for multiple comparison tests. **c**, Percentage change in mouse body weights during the LAPC4-CR tumor growth inhibition study. Vehicle, $n=10$; compound 4, $n=12$ (mean \pm s.e.m.). **d**, LAPC4-CR tumor-bearing mice (athymic nu/nu) were randomized to vehicle or ARQ092 treatment groups (100 mg kg^{-1} , PO, QD), $n=10$. Tumor volumes (mean \pm s.e.m.) and body weights (mean \pm s.e.m.) were measured on the indicated days. The humane endpoint was 20% body weight loss and the ARQ092 arm was terminated when 50% of the animals in the group reached this threshold. **e**, Percentage change in mouse body

weights during the HBCx-2 tumor growth inhibition study (see Fig. 4c). $n=8$, mean \pm s.e.m., ns = not significant. Adjusted P values were calculated for the final day measurements relative to the vehicle using an ordinary one-way ANOVA with Dunnett's multiple comparison test. **f**, BT-474 tumor-bearing mice (athymic nude) were randomized to vethicle (BID, IP injection), compound 4 (30 mg kg^{-1} , BID, IP injection), ARQ092 (100 mg kg^{-1} , QD, PO) or capivasertib (150 mg kg^{-1} , BID, PO) treatment groups ($n=10$). Tumor volumes (mean \pm s.e.m.) were measured on the indicated days. Adjusted P values were calculated for the final day measurements relative to the vehicle using an ordinary one-way ANOVA with Dunnett's multiple comparison test. **g**, Percentage change in mouse body weights during the BT-474 tumor growth inhibition study. $n=10$, mean \pm s.e.m. Adjusted P values were calculated for the final day measurements relative to the vehicle using an ordinary one-way ANOVA with Dunnett's multiple comparison test. Apparently missing errors bars indicate that the error is too small to be visualized.

Article



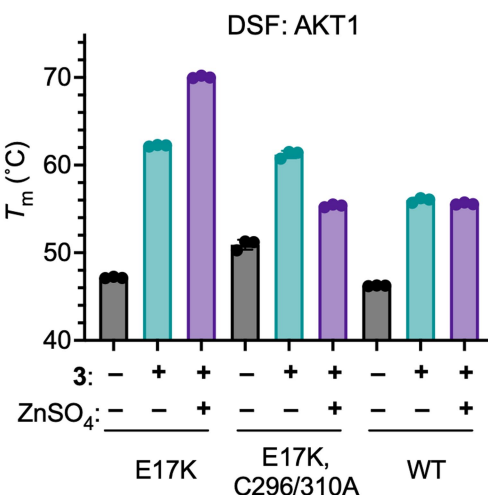
Extended Data Fig. 8 | Supplementary crystal structures and electron density maps. **a**, Ligand electron density map (2Fo-Fc, 1.0 σ) for AKT1(E17K)-3 cocrystallized without added Zn²⁺. **b**, Ligand electron density map (2Fo-Fc, 1.0 σ) for AKT1(E17K)-3 with added ZnSO₄ (2 equiv). **c**, Cocrystal structure of AKT1(E17K) bound to salicylaldehyde 4 (grey) at 1.9 Å resolution. Yellow dashes, hydrogen bonds; orange dashes, π-stacking; black dashes, Zn²⁺-chelate interactions. **d**, Ligand electron density map (2Fo-Fc, 1.0 σ) for AKT1(E17K)-4.

e, Ligand electron density map (2Fo-Fc, 1.0 σ) for AKT1(E17K) labelled with iodoacetamide and cocrystallized with compound 3 (Zn²⁺-free). **f**, Ligand electron density map (2Fo-Fc, 1.0 σ) for AKT1(WT)-3. **g**, Cocrystal structure of AKT2(WT) bound to salicylaldehyde 3 (grey) at 2.0 Å resolution. Yellow dashes, hydrogen bonds; orange dashes, π-stacking. **h**, Ligand electron density map (2Fo-Fc, 1.0 σ) for AKT2(WT)-3.

a		AKT1(E17K)-3-Zn	AKT1(E17K)-3	AKT1(WT)-3	AKT1(E17K)-4-Zn	AKT2(WT)-3
	PDB Code	8UVY	8UW2	8UW7	8UW9	9C1W
Data collection						
	Space group	C 2 2 21	P 3 2 2 1			
Cell dimensions	a, b, c (Å)	75.84, 87.38, 197.43	76.01, 87.63, 197.25	76.31, 87.71, 198.50	76.22, 87.21, 198.10	76.14, 76.14, 153.31
	a, b, g (°)	90, 90, 90	90, 90, 90	90, 90, 90	90, 90, 90	90, 90, 120
Resolution (Å)		49.54–2.11 (2.19–2.11)*	43.82–2.20 (2.28–2.20)*	57.57–1.97 (2.04–1.97)*	36.39–1.90 (1.97–1.90)*	27.01–2.00 (2.07–2.00)*
	R_{merge}	0.051 (0.930)	0.082 (0.385)	0.016 (0.628)	0.033 (0.507)	0.116 (2.452)
$I / \sigma I$		8.13 (0.81)	15.02 (3.35)	24.74 (1.11)	10.89 (1.53)	17.10 (1.96)
	Completeness (%)	99.90 (99.92)	99.03 (99.10)	99.18 (92.04)	99.73 (99.65)	99.91 (99.97)
Redundancy		2.0 (2.0)	2.0 (2.0)	2.0 (2.0)	2.0 (2.0)	19.9 (21.0)
	Refinement					
Resolution (Å)		49.54–2.11	43.82–2.20	57.57–1.97	36.39–1.90	27.01–2.00
	No. reflections	38125 (3751)	33544 (3288)	46975 (4310)	52258 (5167)	35506 (3474)
$R_{\text{work}} / R_{\text{free}}$		0.207 / 0.256	0.220 / 0.279	0.217 / 0.267	0.205 / 0.245	0.205 / 0.242
	Protein	4152	4111	4165	4119	3191
No. atoms	Ligand/ion	75	84	88	94	129
	Water	92	106	104	155	133
B-factors (Å ²)	Protein	54.16	49.78	58.2	48.3	48.8
	Ligand/ion	58.52	57.11	60.68	50.11	50.2
R.m.s. deviations	Water	50.13	46.56	52.36	48.7	50.04
	Bond lengths (Å)	0.008	0.008	0.009	0.008	0.008
E17K	Bond angles (°)	0.98	0.95	1.07	1.04	0.92

*Highest-resolution shell is shown in parentheses.

b

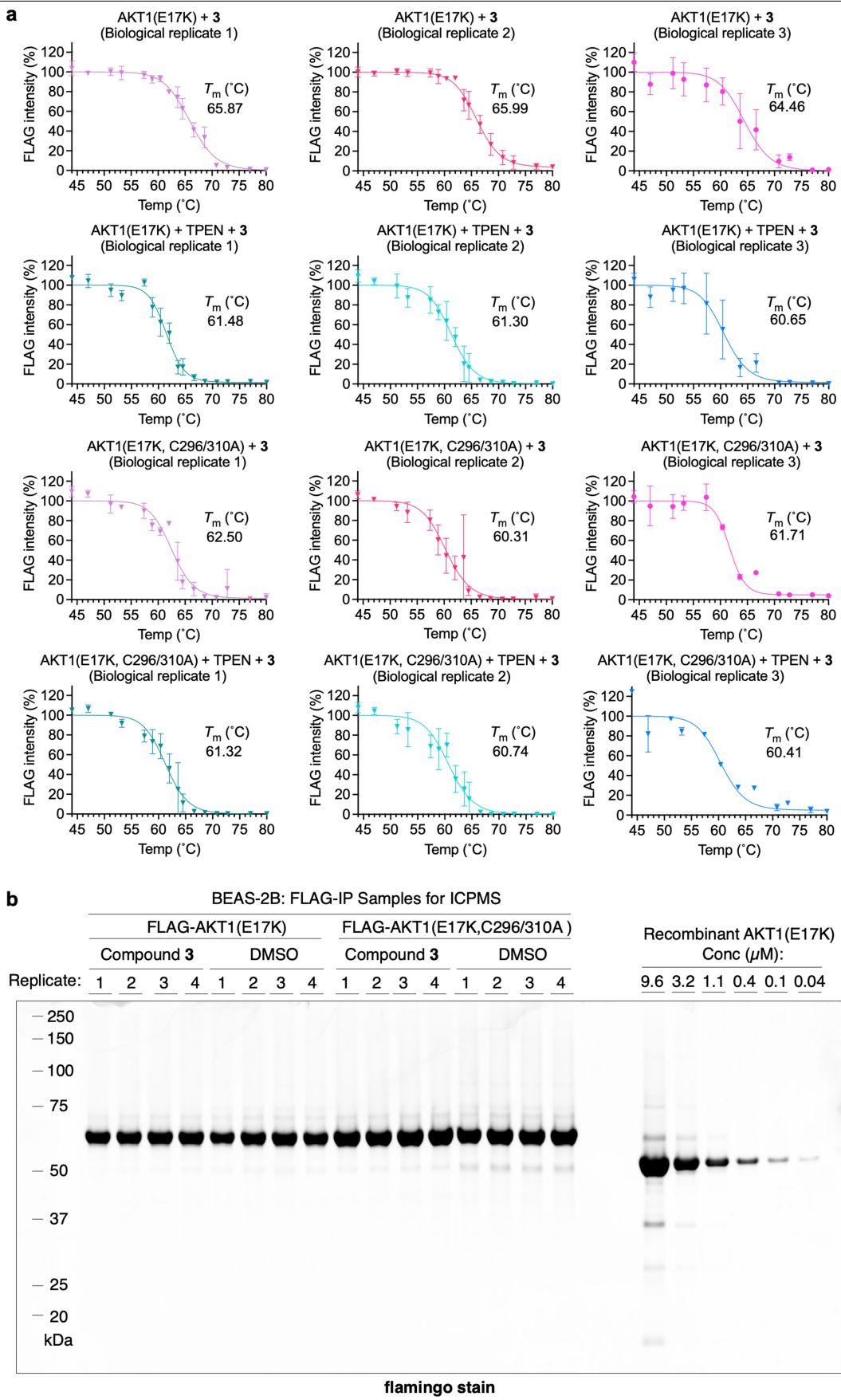


Extended Data Fig. 9 | Crystallographic data and effect of Zn²⁺ on thermal stability. a, Crystallographic data collection and refinement statistics.

b, Purified WT or mutant AKT1 (2 μM) was treated with DMSO or compound 3 (10 μM) in the presence or absence of ZnSO₄ (10 μM) for 15 min. Thermal

stability (melting temperature, T_m) was assessed by differential scanning fluorimetry (mean ± s.d., n = 3). Apparently missing errors bars indicate that the error is too small to be visualized.

Article



Extended Data Fig. 10 | See next page for caption.

Extended Data Fig. 10 | Further characterization of Zn²⁺ binding in cells.

a, CETSA data related to Fig. 5e. BEAS-2B cells stably expressing FLAG-AKT1(E17K or E17K/C296A/C310A) were treated for 3 h with compound **3** (2 μ M) and DMSO or TPEN (10 μ M). Thermal stability of FLAG-AKT1 was determined by CETSA with three biological replicates. After treatment with compounds, cells were heat-challenged at the indicated temperatures for 3 min and lysed. Levels of soluble FLAG-AKT1 were determined by dot blot (Biological replicates 1 and 2: plotted as mean \pm s.d., three technical replicates. Biological replicate 3: plotted as mean \pm s.d., two technical replicates). Apparently missing errors bars indicate that the error is too small to be visualized. Melt temperatures (T_m) were determined by sigmoidal regression analysis. **b**, BEAS-2B cells stably expressing FLAG-AKT1(E17K) or AKT1(E17K/C296A/C310A) were treated with

DMSO or 2 μ M compound **3** for 2 h ($n = 4$). The cells were washed with PBS, lysed, and incubated with anti-FLAG agarose beads for 1 h at 4 °C. The agarose resin was washed 6 times and then FLAG-AKT1 was eluted from the beads with 3xFLAG peptide. Samples were incubated with Chelex 100 resin (15 min), filtered, and concentrated to 57 μ L by spin filtration. Samples were analysed by SDS-PAGE with Flamingo dye staining and in-gel fluorescence. Equal volumes of the immunopurified FLAG-AKT1 samples and dilutions of purified recombinant AKT1(E17K) were loaded on the gel. The extrapolated concentrations of immunopurified and eluted FLAG-AKT1 were used to estimate the molar equivalents of transition metals quantified by ICP-MS analysis (Fig. 5f).

Reporting Summary

Nature Portfolio wishes to improve the reproducibility of the work that we publish. This form provides structure for consistency and transparency in reporting. For further information on Nature Portfolio policies, see our [Editorial Policies](#) and the [Editorial Policy Checklist](#).

Statistics

For all statistical analyses, confirm that the following items are present in the figure legend, table legend, main text, or Methods section.

n/a Confirmed

- The exact sample size (n) for each experimental group/condition, given as a discrete number and unit of measurement
- A statement on whether measurements were taken from distinct samples or whether the same sample was measured repeatedly
- The statistical test(s) used AND whether they are one- or two-sided
 - Only common tests should be described solely by name; describe more complex techniques in the Methods section.*
- A description of all covariates tested
- A description of any assumptions or corrections, such as tests of normality and adjustment for multiple comparisons
- A full description of the statistical parameters including central tendency (e.g. means) or other basic estimates (e.g. regression coefficient) AND variation (e.g. standard deviation) or associated estimates of uncertainty (e.g. confidence intervals)
- For null hypothesis testing, the test statistic (e.g. F , t , r) with confidence intervals, effect sizes, degrees of freedom and P value noted
 - Give P values as exact values whenever suitable.*
- For Bayesian analysis, information on the choice of priors and Markov chain Monte Carlo settings
- For hierarchical and complex designs, identification of the appropriate level for tests and full reporting of outcomes
- Estimates of effect sizes (e.g. Cohen's d , Pearson's r), indicating how they were calculated

Our web collection on [statistics for biologists](#) contains articles on many of the points above.

Software and code

Policy information about [availability of computer code](#)

Data collection

In-gel fluorescence data were collected on Typhoon Imaging System (Molecular Dynamics). Western blots were scanned on an Odyssey infrared imager (LI-COR Biosciences). The LC-MS/MS data were collected on a Orbitrap Eclipse Tribrid Mass Spectrometer (Thermo) connected to an Ultimate 3000 RSLnano system. Intact protein MS data were collected on a Xevo G2-XS QToF Spectrometer (Waters). ICP-MS analysis was performed using an Agilent 8900 triple-quad mass spectrometer. CLARIOstar Plus (BMG Labtech) and Envision (PerkinElmer) multimode platereaders were used for plate-based fluorescence and luminescence assays. DSF measurements were taken on a Bio-Rad C1000 Touch Thermal Cycler. X-ray diffraction data were collected at beamline 2.0.1 or 8.3.1 of the Advanced Light Source (Lawrence Berkeley National Laboratory) or Beamline 05A at Taiwan Photon Source.

Data analysis

In-gel fluorescence images and immunoblots were analysed with ImageJ v1.53k. Data plotting and regression analysis was performed using Prism v9.5.0 (GraphPad). LC-MS/MS data was processed with MaxQuant v1.6.7.0 or FragPipe v19.1, including MSFragger v3.7 and IonQuant3 v1.8.10. Sequencing data was analyzed with SnapGeneViewer v6.2. Crystallographic data was processed with XDS v20220110, xia2 v0.3.8.0, AIMLESS v0.7.7 and Phaser v2.7.16, and modeled and refined with coot v0.9.8.5 and PHENIX v1.20.1. Crystal structures were visualized using Pymol v2.5.0 (Schrödinger).

For manuscripts utilizing custom algorithms or software that are central to the research but not yet described in published literature, software must be made available to editors and reviewers. We strongly encourage code deposition in a community repository (e.g. GitHub). See the Nature Portfolio [guidelines for submitting code & software](#) for further information.

Data

Policy information about [availability of data](#)

All manuscripts must include a [data availability statement](#). This statement should provide the following information, where applicable:

- Accession codes, unique identifiers, or web links for publicly available datasets
- A description of any restrictions on data availability
- For clinical datasets or third party data, please ensure that the statement adheres to our [policy](#)

The reported crystal structures have been deposited to the Protein Data Bank (PDB) with accession numbers 8UVY, 8UW2, 8UW7, 8UW9, and 9C1W. The raw proteomic data have been deposited to MassIVE with the accession number MSV000093542, including the Homo sapiens reviewed Swiss-Prot FASTA database used for searches. Statistical tests, descriptive statistics, and associated graphical data are included in source data files.

Research involving human participants, their data, or biological material

Policy information about studies with [human participants or human data](#). See also policy information about [sex, gender \(identity/presentation\), and sexual orientation](#) and [race, ethnicity and racism](#).

Reporting on sex and gender

N/A

Reporting on race, ethnicity, or other socially relevant groupings

N/A

Population characteristics

N/A

Recruitment

N/A

Ethics oversight

N/A

Note that full information on the approval of the study protocol must also be provided in the manuscript.

Field-specific reporting

Please select the one below that is the best fit for your research. If you are not sure, read the appropriate sections before making your selection.

Life sciences

Behavioural & social sciences

Ecological, evolutionary & environmental sciences

For a reference copy of the document with all sections, see nature.com/documents/nr-reporting-summary-flat.pdf

Life sciences study design

All studies must disclose on these points even when the disclosure is negative.

Sample size

The sample sizes were guided by previous studies of panAKT inhibitors (PMID: 26469692 and PMID: 26351323) as well as our experimental observations and experience, in which a particular sample size was found to provide reliable and reproducible results.

Data exclusions

No data were excluded.

Replication

The experimental replicates are stated in the figure legends. Replicates are biological replicates unless stated otherwise.

Randomization

Mice for tumor growth inhibition studies were randomized into vehicle or drug-treated groups based on tumor size and body weight. For other experiments, randomization was not necessary as all input samples were prepared from the same stocks and handled identically.

Blinding

In the tumor growth inhibition studies, mice were randomized into treatment groups in a blinded manner by the in vivo study management software. Mice were dosed by a technician who was blinded to the treatment, and tumor volume measurements were performed by a technician who was blinded to the previous measurements. For other experiments, samples were handled and analyzed identically and therefore blinding was not necessary.

Reporting for specific materials, systems and methods

We require information from authors about some types of materials, experimental systems and methods used in many studies. Here, indicate whether each material, system or method listed is relevant to your study. If you are not sure if a list item applies to your research, read the appropriate section before selecting a response.

Materials & experimental systems

n/a	Involved in the study
<input type="checkbox"/>	<input checked="" type="checkbox"/> Antibodies
<input type="checkbox"/>	<input checked="" type="checkbox"/> Eukaryotic cell lines
<input checked="" type="checkbox"/>	<input type="checkbox"/> Palaeontology and archaeology
<input type="checkbox"/>	<input checked="" type="checkbox"/> Animals and other organisms
<input checked="" type="checkbox"/>	<input type="checkbox"/> Clinical data
<input checked="" type="checkbox"/>	<input type="checkbox"/> Dual use research of concern
<input checked="" type="checkbox"/>	<input type="checkbox"/> Plants

Methods

n/a	Involved in the study
<input checked="" type="checkbox"/>	<input type="checkbox"/> ChIP-seq
<input checked="" type="checkbox"/>	<input type="checkbox"/> Flow cytometry
<input checked="" type="checkbox"/>	<input type="checkbox"/> MRI-based neuroimaging

Antibodies

Antibodies used

Primary: FLAG (Sigma-Aldrich, F1804), AKT1 (Cell Signaling Technology, 2938), AKT2 (Cell Signaling Technology, 3063), pAKT1(pS473) (Cell Signaling Technology, 9018), PRAS40 (Cell Signaling Technology, 2691), pPRAS40(pT246) (Cell Signaling Technology, 2997), GAPDH (Santa Cruz Biotechnology, 32233), tS6RP (Cell Signaling Technology, 2317), pS6RP(pS235/236) (Cell Signaling Technology, Cat 4858), tGSK3b (Cell Signaling Technology, 12456), pG3K3b(pS9) (Cell Signaling Technology, 5558). Secondary: IRDye 800CW goat anti-mouse IgG (LI-COR, 926-32210), IRDye 800CW goat rabbit IgG (LI-COR, 926-32211), IRDye 680RD goat anti-rabbit IgG (LI-COR, 926-68071), IRDye 680RD goat anti-mouse IgG (LI-COR, 926-68070). Antibody dilutions are noted in the methods.

Validation

The antibodies used in this study have all been validated by the manufacturers. Manufacturer validation statements are as follows:
 FLAG (Sigma-Aldrich, F1804): The antibody recognizes the FLAG peptide sequence at the N-terminus, Met-N-terminus, C-terminus, and internal sites of the fusion protein.
 AKT1 (Cell Signaling Technology, 2938): Akt1 (C73H10) Rabbit mAb detects endogenous levels of total Akt1 protein. This antibody does not cross-react with Akt2 or Akt3.
 AKT2 (Cell Signaling Technology, 3063): Akt2 (D6G4) Rabbit mAb detects endogenous levels of total Akt2 protein. It does not cross-react with Akt1 or Akt3.
 pAKT1(pS473) (Cell Signaling Technology, 9018): Phospho-Akt1 (Ser473) (D7F10) XP Rabbit mAb recognizes endogenous levels of Akt1 protein only when phosphorylated at Ser473. It does not detect Akt2 protein when phosphorylated at Ser474.
 PRAS40 (Cell Signaling Technology, 2691): PRAS40 (D23C7) XP Rabbit mAb detects endogenous levels of total PRAS40 protein.
 pPRAS40(pT246) (Cell Signaling Technology, 2997): Phospho-PRAS40 (Thr246) (C77D7) Rabbit mAb detects endogenous levels of PRAS40 protein only when phosphorylated at Thr246.
 GAPDH (Santa Cruz Biotechnology, 32233): GAPDH Antibody (6C5) is an IgG1 κ mouse monoclonal GAPDH antibody that detects GAPDH of mouse, rat and human origin by WB, IP and IF.
 tS6RP (Cell Signaling Technology, 2317): S6 Ribosomal Protein (54D2) Mouse mAb detects endogenous levels of total S6 ribosomal protein independent of phosphorylation.
 pS6RP(pS235/236) (Cell Signaling Technology, Cat 4858): Phospho-S6 Ribosomal Protein (Ser235/236) (D57.2.2E) XP Rabbit mAb detects endogenous levels of ribosomal protein S6 only when phosphorylated at Ser235 and 236. Non-specific labeling in pancreatic islets has been observed by immunofluorescence in fixed frozen mouse tissue post-processed with λ phosphatase.
 tGSK3b (Cell Signaling Technology, 12456): GSK-3β (D5C5Z) XP Rabbit mAb recognizes endogenous levels of total GSK-3β protein. This antibody does not cross-react with GSK-3α protein.
 pG3K3b(pS9) (Cell Signaling Technology, 5558): Phospho-GSK-3β (Ser9) (D85E12) XP Rabbit mAb detects endogenous levels of GSK-3β only when phosphorylated at Ser9. This antibody reacts with denatured components of bovine serum, including BSA.

Eukaryotic cell lines

Policy information about [cell lines](#) and [Sex and Gender in Research](#)

Cell line source(s)

BEAS-2B cells (ATCC, Cat #: CRL-3588), HEK293T cells (ATCC, Cat #: CRL-3216), MCF7 (ATCC, Cat #: HTB-22) and SkBr3 cells (ATCC, Cat #: HTB-30) were sourced from American Type Culture Collection (ATCC). LAPC4-CR cells were a gift from Michael C. Haffner. HBCx-2 cells were acquired from XenTech. Sf9 insect cells were sourced from Expression Systems, Cat #: 94-0015.

Authentication

The cell lines were used as supplied by the vendor without further verification. Sequencing of the LAPC4-CR cells was conducted (Extended Data Fig. 4) to confirm the presence of the AKT1(E17K) mutation.

Mycoplasma contamination

The cell lines used in this study were tested negative for mycoplasma.

Commonly misidentified lines (See [ICLAC](#) register)

No commonly misidentified lines were used in this study.

Animals and other research organisms

Policy information about [studies involving animals](#); [ARRIVE guidelines](#) recommended for reporting animal research, and [Sex and Gender in Research](#)

Laboratory animals

Homozygous athymic nude mice (6–8 weeks old) were used for pharmacokinetic studies (male), and LAPC4-CR CDX (male) and

Laboratory animals	HBCx-2 PDX (female) models as described in the methods. Female BALB/c nude mice (6–8 weeks old) were used for the BT-474 CDX model as described in the methods. Information on housing conditions for the mice is described in the methods.
Wild animals	The study did not involve wild animals.
Reporting on sex	Male nude mice are the standard host for the LAPC4-CR (prostate cancer) xenograft model. Female nude mice are the standard host for the HBCx-2 (breast cancer) xenograft model. Female BALB/c nude mice are the standard host for the BT-474 (breast cancer) xenograft model.
Field-collected samples	The study did not involve samples collected from the field.
Ethics oversight	All mouse manipulations were performed in accordance with the Institutional Animal Care and Use Committee (IACUC) of or under the approval of University of California, San Francisco, Terremoto Biosciences, Pharmaron, XenTech or GenenDesign as described in the methods.

Note that full information on the approval of the study protocol must also be provided in the manuscript.

Plants

Seed stocks	<i>Report on the source of all seed stocks or other plant material used. If applicable, state the seed stock centre and catalogue number. If plant specimens were collected from the field, describe the collection location, date and sampling procedures.</i>
Novel plant genotypes	<i>Describe the methods by which all novel plant genotypes were produced. This includes those generated by transgenic approaches, gene editing, chemical/radiation-based mutagenesis and hybridization. For transgenic lines, describe the transformation method, the number of independent lines analyzed and the generation upon which experiments were performed. For gene-edited lines, describe the editor used, the endogenous sequence targeted for editing, the targeting guide RNA sequence (if applicable) and how the editor was applied.</i>
Authentication	<i>Describe any authentication procedures for each seed stock used or novel genotype generated. Describe any experiments used to assess the effect of a mutation and, where applicable, how potential secondary effects (e.g. second site T-DNA insertions, mosaicism, off-target gene editing) were examined.</i>